Galaxy Morphology[1]

Ronald J. Buta

Department of Physics and Astronomy, University of Alabama, Box 870324, Tuscaloosa, AL 35487

Received _____; accepted _____

[1]To be published in Planets, Stars, and Stellar Systems, Vol. 6, Series Editor T. D. Oswalt, Volume editor W. C. Keel, Springer Reference, 2011

ABSTRACT

Galaxy morphology is a product of how galaxies formed, how they interacted with their environment, how they were influenced by internal perturbations, AGN, and dark matter, and of their varied star formation histories. This article reviews the phenomenology of galaxy morphology and classification with a view to delineating as many types as possible and how they relate to physical interpretations. The old classification systems are refined, and new types introduced, as the explosion in available morphological data has modified our views on the structure and evolution of galaxies.

Subject headings: galaxies: spiral; galaxies: elliptical; galaxies: S0s; galaxies: structure; galaxies: high redshift; galaxies: classification; galaxies: peculiar; galaxies: dwarfs; galaxies: clusters; galaxies: active; galaxies: isolated; galaxies: Galaxy Zoo project

Index terms: Hubble-Sandage-de Vaucouleurs classification; spiral galaxies; elliptical galaxies; S0 galaxies; irregular galaxies; resonance ring galaxies; outer rings; inner rings; nuclear rings; secondary bars; nuclear bars; pseudorings; grand design spirals; flocculent spirals; merger morphologies; tidal tails; collisional ring galaxies; polar ring galaxies; barred galaxies; lens galaxies; spiral arm classes; counter-winding spiral galaxies; anemic spiral galaxies; spiral arm multiplicity; dust lanes; pseudobulges; classical bulges; dust-lane elliptical galaxies; shell/ripple galaxies; ultra-luminous infrared galaxies; bar ansae; brightest cluster members; low surface brightness galaxies; dwarf galaxies; dwarf spiral galaxies; dwarf spheroidal galaxies; Galaxy Zoo project; isolated galaxies; blue compact dwarf galaxies; star-forming galaxy morphologies; warped disks; stellar mass morphology; luminosity classes; boxy ellipticals; disky ellipticals; late-type galaxies; early-type galaxies;

Magellanic barred galaxies; color galaxy morphology; atomic and molecular gas galaxy morphology

Contents

1. Introduction

In the nearly 100 years since galaxy morphology became a topic of research, much has been learned about galactic structure and dynamics. Known only as "nebulae" at that time, galaxies were found to have a wide range of largely inexplicable forms whose relations to one another were a mystery. As data accumulated, it became clear that galaxies are fundamental units of matter in space, and an understanding of how they formed and evolved became one of the major goals of extragalactic studies. Even in the era of space observations, galaxy morphology continues to be the backbone of extragalactic research as modern instruments provide information on galactic structure across a wide range of distances and lookback times.

In spite of the advances in instrumentation and the explosion of data, classical galaxy morphology (i. e., the visual morphological classification in the style of Hubble and others) has not lost its relevance. The reasons for this are as follows:

1. Morphology is still a logical starting point for understanding galaxies. Sorting galaxies into their morphological categories is similar to sorting stars into spectral types, and can lead to important astrophysical insights. Any theory of galaxy formation and evolution will have to, at some point, account for the bewildering array of galactic forms.

2. Galaxy morphology is strongly correlated with galactic star formation history. Galaxies where star formation ceased gigayears ago tend to look very different from those where star formation continues at the present time. Classical morphology recognizes these differences in an ordered way.

3. Information on galaxy morphology, in the form of new types of galaxies, multi-wavelength views of previously known galaxy types, and higher resolution views of all or part of some galaxies, has exploded as modern instrumentation has superceded the old photographic

plates that were once used exclusively for galaxy classification.

4. Galaxy classification has gone beyond the realm of a few thousand galaxies to that of a *million* galaxies through the Galaxy Zoo project. Not only this, but GalaxyZoo has taken morphology from the exclusive practice of a few experts to the public at large, thus facilitating citizen science at its best. Galaxy Zoo images are also in *color*, thus allowing the recognition of special galaxy types and features based on stellar populations or gaseous emission.

5. Finally, deep surveys with the Hubble Space Telescope have extended morphological studies well beyond the realm of the nearby galaxies that dominated early catalogues, allowing detailed morphology to be distinguished at unprecedented redshifts.

Now, more than ever, galaxy morphology is a vibrant subject that continues to provide surprises as more galaxies are studied for their morphological characteristics across the electromagnetic spectrum. It is clear that a variety of effects are behind observed morphologies, including environmental density and merger/interaction history, internal perturbations, gas accretions, nuclear activity, secular evolution, as well as the diversity in star formation histories, and that a global perspective based on large numbers of galaxies will improve theoretical models and give a more reliable picture of galactic evolution.

The goal of this article is to present the phenomenology of galaxy morphology in an organized way, and highlight recent advances in understanding what factors influence morphology and how various galaxy types are interpreted. The article is a natural follow-up to the excellent review of galaxy morphology and classification by Sandage (1975) in Volume IX of the classic *Stars and Stellar Systems* series. It also complements the recently published *de Vaucouleurs Atlas of Galaxies* (Buta, Corwin, & Odewahn 2007, hereafter the dVA), which provided a detailed review of the state and technique of galaxy classification up to about the year 2005. Illustrations are very important in a review of this nature,

and the article draws on a large number of sources of images. For this purpose, the Sloan Digital Sky Survey (SDSS), the NASA/IPAC Extragalactic Database (NED), and the dVA have been most useful.

2. Overview

As extended objects rather than point sources, galaxies show a wide variety of forms, some due to intrinsic structures, others due to the way the galaxy is oriented to the line of sight. The random orientations, and the wide spread of distances, are the principal factors that can complicate interpretations of galaxy morphology. If we could view every galaxy along its principal axis of rotation, and from the same distance, then fairer comparisons would be possible. Nevertheless, morphologies seen in face-on galaxies can also often be recognized in more inclined galaxies (Figure 1). It is only for the highest inclinations that morphology switches from face-on radial structure to vertical structure. In general we either know the planar structure in a galaxy, or we know its vertical structure, but we usually cannot know both well from analysis of images alone.

Galaxy morphology began to get interesting when the "Leviathan of Parsonstown", the 72-inch meridian-based telescope built in the 1840s by William Parsons, Third Earl of Rosse, on the grounds of Birr Castle in Ireland, revealed spiral patterns in many of the brighter Herschel and Messier "nebulae." The nature of these nebulae as galaxies wasn't fully known at the time, but the general suspicion was that they were star systems ("island universes") like the Milky Way, only too distant to be easily resolved into their individual stars. In fact, one of Parsons' motivations for building the "Leviathan" was to try and resolve the nebulae to prove this idea. The telescope did not convincingly do this, but the discovery of spiral structure itself was very important because such structure added to the mystique of the nebulae. The spiral form was not a random pattern and had

to be significant in what it meant. The telescope was not capable of photography, and observers were only able to render what they saw with it in the form of sketches. The most famous sketch, that of M51 and its companion NGC 5195, has been widely reproduced in introductory astronomy textbooks.

While visual observations could reveal some important aspects of galaxy morphology, early galaxy classification was based on photographic plates taken in the blue region of the spectrum. Silver bromide dry emulsion plates were the staple of astronomy beginning in the 1870s and were relatively more sensitive to blue light than to red light. Later, photographs taken with Kodak 103a-O and IIa-O plates became the standard for galaxy classification. In this part of the spectrum, massive star clusters, dominated by spectral class O and B stars, are prominent and often seen to line the spiral arms of galaxies. These clusters, together with extinction due to interstellar dust, can give blue light images a great deal of detailed structure for classification. It is these types of photographs which led to the galaxy classification systems in use today.

In such photographs, we see many galaxies as a mix of structures. Inclined galaxies reveal the ubiquitous *disk* shape, the most highly flattened subcomponent of any galaxy. Studies of Doppler wavelength shifts in the spectra of disk objects (like HII regions and integrated star light) reveal that disks rotate differentially. If a galaxy is spiral, the disk is usually where the arms are found, and also where the bulk of interstellar matter is found. The radial luminosity profile of a disk is usually *exponential*, with departures from an exponential being due to the presence of other structures.

In the central area of a disk-shaped galaxy, there is also often a bright and sometimes less flattened mass concentration in the form of a *bulge*. The nature of bulges and how they form has been a topic of much recent research, and is discussed further in section 9. Disk galaxies range from virtually bulge-less to bulge-dominated. In the center there may also be

a conspicuous *nucleus*, a bright central concentration that was usually lost to overexposure in photographs. Nuclei may be dominated by ordinary star light, or may be *active*, meaning their spectra show evidence of violent gas motions.

Bars are the most important internal perturbations seen in disk-shaped galaxies. A bar is an elongated mass often made of old stars crossing the center. If spiral structure is present, the arms usually begin near the ends of the bar. Although most easily recognized in the face-on view, bars have generated great interest recently in the unique ways they can also be detected in the edge-on view. Not all bars are made exclusively of old stars. In some bulge-less galaxies, the bar has considerable gas and recent star formation.

Related to bars are elongated disk features known as *ovals*. Ovals usually differ from bars in lacking higher order Fourier components (i.e., have azimuthal intensity distributions that vary mainly as 2θ), but nevertheless can be major perturbations in a galactic disk. The entire disk of a galaxy may be oval, or a part of it may be oval. Oval disks are most easily detected if there is considerable light or structure at larger radii.

Rings are prominent features in some galaxies. Often defined by recent star formation, rings may be completely closed features or may be partial or open, the latter called "pseudorings." Rings can be narrow and sharp or broad and diffuse. It is particularly interesting that several kinds of rings are seen, and that some galaxies can have as many as four recognizeable ring features. *Nuclear rings* are the smallest rings and are typically seen in the centers of barred galaxies. *Inner rings* are intermediate-scale features that often envelop the bar in a barred galaxy. Outer rings are large, low surface brightness features that typically lie at about twice the radius of a bar. Other kinds of rings, called accretion rings, polar rings, and collisional rings, are also known but are much rarer than the inner, outer, and nuclear rings of barred galaxies. The latter kinds of rings are also not exclusive to barred galaxies, but may be found also in nonbarred galaxies.

Lenses are features, made usually of old stars, that have a shallow brightness gradient interior to a sharp edge. They are commonly seen in Hubble's disk-shaped S0 class (section 5.2). If a bar is present, the bar may fill a lens in one dimension. Lenses may be round or slightly elliptical in shape. If elliptical in shape they would also be considered ovals.

Nuclear bars are the small bars occasionally seen in the centers of barred galaxies, often lying within a nuclear ring. When present in a barred galaxy, the main bar is called the "primary bar" and the nuclear bar is called the "secondary bar." It is possible for a nuclear bar to exist in the absence of a primary bar.

Dust lanes are often seen in optical images of spiral galaxies, and may appear extremely regular and organized. They are most readily evident in edge-on or highly inclined disk galaxies, but are still detectable in the face-on view, often on the leading edges of bars or the concave sides of strong inner spiral arms.

Spiral arms may also show considerable morphological variation. Spirals may be regular 1, 2, 3, or 4-armed patterns, and may also be higher order multi-armed patterns. Spirals may be tightly wrapped (low pitch angle) or very open (high pitch angle.) A *grand-design* spiral is a well-defined global pattern, often detectable as smooth variations in the stellar density of old disk stars. A *flocculent* spiral is made of small pieces of spiral structure that appear sheared by differential rotation. Their appearance can be strongly affected by dust, such that at longer wavelengths a flocculent spiral may appear more grand-design. Pseudorings can be thought of as variable pitch angle spirals which close on themselves, as opposed to continuously opening, constant pitch angle, logarithmic spirals.

There are also numerous structures outside the scope of traditional galaxy classification, often connected with strong interactions between galaxies. Plus, the above described features are not necessarily applicable or relevant to what we see in very distant galaxies. Accounting for all of the observed features of nearby galaxies, and attempting to connect

what we see nearby to what is seen at high redshift, is a major goal of morphological studies.

3. Galaxy Classification

As noted by Sandage (1975), the first step in studying any class of objects is a classification of those objects. Classification built around small numbers of shared characteristics can be used for sorting galaxies into fundamental categories, which can then be the basis for further research. From such research, physical relationships between identified classes may emerge, and these relationships may foster a theoretical interpretation that places the whole class of objects into a global context. There is no doubt that such an approach greatly contributed to the development of the science of biology, and this is no less true for galaxies.

The genesis of galaxy classification is to take the complex combinations of structures described in the previous section and summarize them with a few type symbols. Sandage (1975) describes the earlier classification systems of Wolf, Reynolds, Lundmark, and Shapley that fell into dis-use more than 50 years ago. The Morgan (1958) spectral type/concentration classification system, which was based on a connection between morphology (specifically central concentration) and the stellar content of the central regions, was used recently by Bershady, Jangren, & Conselice (2000) in a mostly quantitative manner (see also Abraham et al. 2003). Thus, Morgan's system has in a way survived into the modern era but not in the purely visual form that he proposed. Only one Morgan galaxy type, the supergiant cD type, is still used extensively (section 10.6). Van den Bergh's luminosity/arm morphology classification system is described by van den Bergh (1998; see section 6.5).

The big survivor of the early visual classification systems was that of Hubble (1926,

1936), as later revised and expanded upon by Sandage (1961) and de Vaucouleurs (1959). Sandage (1975) has argued that one reason Hubble's view prevailed is that he did not try and account for every superficial detail, but kept his classes broad enough that the vast majority of galaxies could be sorted into one of his proposed bins. These bins were schematically illustrated in Hubble's famous "tuning fork"[2] (Hubble 1936; reproduced in Figure 2) recognizing a sequence of progressive flattenings from ellipticals to spirals. Ellipticals had only two classification details: the smoothly declining brightness distribution with no inflections, and no evidence for a disk; and the ellipticity of the isophotes, indicated by a number after the "E" symbol. (For example, E3 means the ellipticity is 0.3.) Spirals were systems more flattened than an E7 galaxy that could be subdivided according to the degree of central concentration, the degree of openness of the arms, the degree of resolution of the arms into complexes of star formation (all three criteria determining position along the fork), and on the presence or absence of a bar (determining the appropriate prong of the fork).

The S0 class at the juncture of the prongs of the fork was still hypothetical in 1936. As "armless disk galaxies," S0s were mysterious because all examples known in 1936 were barred. These were classified as SBa, but this was a troubling inconsistency because nonbarred Sa galaxies had full spiral patterns. Hubble predicted the existence of nonbarred S0s to fill the gap between type E7[3] and Sa and cure what he felt was a "cataclysmic"

---

[2]As recently noted by D. L. Block (Block et al. 2004a), this diagram may have been inspired by a similar schematic by Jeans (1929).

[3] van den Bergh (2009a) shows that E0-E4 galaxies are more luminous on average than are E5-E7 galaxies, suggesting that all E7 galaxies (and not many have been recognized) are actually S0 galaxies. Van den Bergh argues that genuine E galaxies may be no more flattened than E6.

transition.

It was not long before Hubble himself realized that the tuning fork could not adequately represent the full diversity of galaxy morphologies, and after 1936 he worked on a revision that included real examples of the sought group: nonbarred S0 galaxies. Based on fragmentary notes he left behind, Sandage (1961) prepared the *Hubble Atlas of Galaxies* to illustrate Hubble's revision, and also added a third dimension: the presence or absence of a ring. This was the first major galaxy atlas illustrating a classification system in a detailed, sophisticated way with beautifully produced photographs. Hubble's revision, with van den Bergh luminosity classes (Sandage & Tammann 1981), was updated and extended to types later than Sc by Sandage & Bedke (1994).

Because Sandage (1961) and Sandage & Bedke (1994) describe the Hubble-Sandage revision so thoroughly, the details will not be repeated here. Instead, the focus of the next section will be on the de Vaucouleurs revision as outlined in the dVA. The reasons for this are: (1) the de Vaucouleurs classification provides the most familar galaxy types to extragalactic researchers, mostly because of extensive continuing use of the Third Reference Catalogue of Bright Galaxies (RC3, de Vaucouleurs et al. 1991); and (2) the de Vaucouleurs classification is still evolving to cover more details of galaxy morphology considered significant at this time. It should be noted that both the de Vaucouleurs and Hubble-Sandage revisions are strictly applicable only to $z \approx 0$ galaxies and that it is often difficult to fit objects having $z > 0.5$ neatly into the categories defining these classification systems. High redshift galaxy morphology is described in section 13.

4. A Continuum of Galactic Forms

The Hubble tuning fork is useful because it provides a visual representation of information Hubble (1926) had only stated in words. The fork contains an implication of continuity. For example, it does not rule out that there might be galaxies intermediate in characteristics between an "Sa" or "Sb" spiral, or between a normal "S" spiral and a barred "SB" spiral. Continuity along the elliptical galaxy sequence was always implied as a smooth variation from round ellipticals (E0) to the most flattened ellipticals (E7). Sandage (1961) describes the modifications that made the Hubble system more three-dimensional: the introduction of the (r) (inner ring) and (s) (pure spiral) subtypes. Continuity even with this characteristic was possible, using the combined subtype (rs). Thus, already by 1961, the Hubble classification system had become much more complicated than it was in 1926 or 1936. The addition of the S0 class was one reason for this, but the (r) and (s) subtypes were another.

In the Hubble-Sandage classification, it became common to denote galaxies on the left part of the Hubble sequence as "early-type" galaxies and those on the right part as "late-type" galaxies. By the same token, Sa and SBa spirals became "early-type spirals" while Sc and SBc spirals became "late-type spirals." Sb and SBb types became known as "intermediate-type spirals." The reason for these terminologies was convenience and borrows terminology often used for stars. Young, massive stars of spectral classes O and B were known as "early-type stars" while older stars of cooler spectral types were known as "late-type stars." Hubble stated that his use of these temporal descriptions for galaxies had no evolutionary implications. An irony in this is that it eventually became clear that early-type galaxies are dominated by late-type stars, while late-type galaxies often have significant numbers of early-type stars.

De Vaucouleurs (1959) took the idea of continuity of galaxy morphology a step further

by developing what he referred to as the *classification volume* (Figure 3). In this revision of the Hubble-Sandage (1961) classification, galaxy morphology represents a continuous sequence of forms in a three-dimensional volume with a long axis and circular cross-sections of varying size. The long axis of the volume is the *stage*, or type, and it represents the long axis of the original Hubble tuning fork. The short axes are the family and the variety, which refer to apparent bar strength and the presence or absence of an inner ring, respectively. In addition to Hubble's original stages E, Sa, Sb, and Sc, the classification volume includes new stages: late ellipticals: E^+, "very late" spirals: Sd, "Magellanic spirals": Sm, and "Magellanic irregulars": Im. The S0 class is included in the same position along the sequence, between E's and spirals, but is subdivided into three stages. The characteristics defining individual stages are described further in section 5.2.

The stage is considered the most fundamental dimension of the classification volume because measured physical parameters, such as integrated color indices, mean surface brightnesses, and neutral hydrogen content correlate well with position along the sequence (e. g., Buta et al. 1994). Early-type galaxies tend to have redder colors, higher average surface brightnesses, and lower neutral hydrogen content than late-type galaxies. The family and variety axes of the classification volume indicate the considerable variations in morphology at a given stage. A famous sketch of families and varieties near stage Sb, drawn by de Vaucouleurs himself during a cloudy night at McDonald Observatory circa 1962, is shown in Sandage (1975) and in Figure 1.13 of the dVA. The classification volume is broader in the middle compared to the ends because the diversity of galaxy morphology is largest at stages like S0/a and Sa. Bars and rings are often most distinct and most recognizable at these stages. Such features are not characteristic of E galaxies, so the volume must be narrow at that end. Along the S0 sequence, bars and rings are barely developed among the earliest S0s ($S0^-$) and well-developed among the late S0s ($S0^+$), thus the volume begins to broaden. Among very late-type galaxies, Sd, Sdm, Sm, and Im, bars are actually very

frequent, but closed rings (r) are not. Thus, the volume narrows at that end as well.

For the purposes of illustrating morphology, blue light digital images converted to units of magnitudes per square arcsecond are used when available. This approach is described in the dVA, and requires calibration of the images, usually based on published photoelectric multi-aperture photometry. In addition, some of the illustrations used (especially in section 15) are from the Sloan Digital Sky Survey or from other sources. These are not in the same units but still provide excellent illustrations of morphology. SDSS color images differ from dVA images mainly in the central regions, where SDSS images sometimes lose detail.

Unlike the dVA, the scope of this article extends beyond the traditional $UBVRI$ wavebands. It is only during the past 20 years that significant morphological information has been obtained for galaxies outside these bands, mostly at mid- and far-ultraviolet and mid-IR wavelengths from space-based observatories capable of imaging in these wavelengths to unprecedented depths, providing a new view of galaxy morphology that is only beginning to be explored. A useful review of many issues in morphology is provided by van den Bergh (1998).

5. Galaxy Types: Stage, Family, and Variety

5.1. Elliptical and Spheroidal Galaxies

Elliptical galaxies are smooth, amorphous systems with a continuously declining brightness distribution and no breaks, inflections, zones, or structures, as well as no sign of a disk. Figure 4 shows some good examples. Because ellipticals are dominated by old stars and are relatively dust-free, they look much the same at different wavelengths. Hubble's subclassification of ellipticals according to apparent ellipticity (En, where n=10(1-b/a), b/a being the apparent flattening) was useful but virtually no physical characteristics of

ellipticals correlate with this parameter (Kormendy & Djorgovski 1989). The n value in the En classification is simply the projected ellipticity and not easily interpreted in terms of a true flattening without direct knowledge of the orientation of the symmetry planes. Luminous ellipticals are thought to be triaxial in structure with an anisotropic velocity dispersion tensor, while lower luminosity ellipticals are more isotropic oblate rotators (Davies et al. 1983). Studies of rotational to random kinetic energy (V/σ) versus apparent flattening (ϵ) show that massive ellipticals are slow anisotropic rotators. Ellipticals follow a fundamental plane relationship between the effective radius r_e of the light distribution, the central velocity dispersion σ_0, and mean effective surface brightness $< I_e >$ (see review by Kormendy & Djorgovski 1989). Dwarf elliptical galaxies may not follow the same relation as massive ellipticals; this is discussed by Ferguson & Binggeli (1994).

The lack of fundamental significance of Hubble's En classification led some authors to seek an alternative, more physically useful approach. Kormendy & Bender (1996; see also the review by Schweizer 1998) proposed a revision to Hubble's tuning fork handle that orders ellipticals according to their velocity anisotropy, since this is a significant determinant of E galaxy intrinsic shapes. Velocity anisotropy correlates with the *deviations* of E galaxy isophotes from pure elliptical shapes, measured by the parameter a_4/a, the relative amplitude of the $\cos 4\theta$ Fourier term of these deviations. If this relative amplitude is positive, then the isophotes are pointy, disky ovals, while if negative, the isophotes are boxy ovals. A boxy elliptical is classified as E(b), while a disky elliptical is classified as E(d). The correlation with anisotropy is such that E(b) galaxies have less rotation on average and more velocity anistropy than E(d) galaxies.

The Kormendy & Bender proposed classification is shown in Figure 5, together with two exceptional examples that show the characteristic isophote shapes. The leftmost of these two, NGC 7029, is an unusually obvious boxy elliptical at larger radii. This boxiness

is the basis for the classification E(b)5. However, NGC 7029 is not boxy throughout: it shows evidence of a small inner disk and hence is disky at small radii. This is not necessarily taken into account in the classification. The other image shown in Figure 5 is NGC 4697, a galaxy whose isophotes are visually disky. The idea with the Kormendy & Bender classification is that it is the disky ellipticals which connect to S0 galaxies, and not the boxy ellipticals. However, NGC 7029 demonstrates that diskiness and boxiness can be a function of radius, thus perhaps a smooth connection between E(b) and E(d) types [i.e., type E(b,d)] is possible and the order shown in the Kormendy & Bender revision to the Hubble tuning fork, with boxy Es blending into the disky Es, could be reasonable.

Note that while the classical En classifications of ellipticals were designed by Hubble to be estimated by eye, this is not easily done for the E(b) and E(d) classifications, which are most favored to be seen only when the disk is nearly edge-on. Face-on Es with imbedded disks will not show disky isophotes. For example, NGC 7029 and 4697 are extreme cases where the isophotal deviations are obvious by eye. But for most E galaxies, the E(b)n and E(d)n classifications can only be judged reliably with measurements of the a_4/a parameter.

The de Vaucouleurs classification of ellipticals includes a slightly more advanced type called E^+, or "late" ellipticals. It was originally intended to describe "the first stage of the transition to the S0 class" (de Vaucouleurs 1959). Five examples of E^+ galaxies are shown in the second row of Figure 4. Galaxies classified as E^+ can be the most subtle S0s, but many of the E^+ cases listed in RC3 are the brightest members of clusters that have shallow enough brightness profiles to appear to have an extended envelope (see section 10.6). Of the five E^+ galaxies shown, only NGC 4623 (rare type E^+7) seems consistent with de Vaucouleurs's original view. It is also a much lower luminosity system than the other four cases shown. While $S0^-$ is the type most often confused with ellipticals in visual classification, the bin has a wide spread from the most obvious to the least obvious cases.

Thus, a type like E^+ is still useful for distinguishing transitions from E to S0 galaxies.

The photometric properties of ellipticals depend on luminosity. In terms of Sersic $r^{\frac{1}{n}}$ profile fits, large, luminous ellipticals tend to have profiles described better by $n \gtrsim 4$, while smaller, lower luminosity ellipticals tend to have $n<4$, with values as low as 1 (e. g., Caon, Capaccioli, & D'Onofrio 1993). Graham & Guzmán (2003) discuss the implications of this correlation on proposed dichotomies of elliptical galaxies (e.g., Kormendy 1985; see also Ferrarese et al. 2006). These studies received a major impetus from the massive photometric analysis of Virgo Cluster elliptical galaxies by Kormendy et al. (2009). Two issues were considered by these authors (Figure 6). The first was whether galaxies classified as dwarf ellipticals ("dE"; see section 15.2) in the Virgo Cluster really are the low luminosity extension of more massive, conventional ellipticals, or something different altogether. Based on parameter correlations, such as $r_{10\%}$, the major axis radius of the isophote containing 10% of the total visual luminosity, versus $\mu_{10\%}$, the surface brightness of this isophote, Kormendy et al. show that even the most elliptical-like and luminous dE galaxies lie on a distinct sequence from normal elliptical galaxies, which tend to lie on a higher density sequence. In a graph of B-band central surface brightness versus absolute B-band magnitude, the dE galaxies lie in a region occupied by Magellanic irregular galaxies, suggesting a link between the groups and consistent with the earlier conclusions of Kormendy (1985). Kormendy et al. (2009) suggest reclassifying Binggeli, Sandage, & Tammann's (1985) "dE" galaxies and related objects (like dwarf S0, or dS0 galaxies) as "spheroidal" (Sph) galaxies, including the type "Sph,N", meaning "nucleated spheroidal" galaxy (section 15.2). Figure 6 shows several examples of Sph,N galaxies as compared with several genuine elliptical galaxies. The morphological appearance alone does not necessarily distinguish the two classes. The classification is physical, being based mainly on parameter correlations. Kormendy et al. suggest that Sph galaxies are formed from late-type systems by environmental effects and supernovae.

The second issue considered was the physical distinction between "core" elliptical galaxies, those where the surface brightness profile approaches either a constant level or a slightly sloped level with radius approaching zero, and "coreless" ellipticals (also known as "power law" Es) where the inner profile steepens with decreasing radius (Kormendy 1999). Kormendy et al. (2009) illustrated both types relative to a Sersic $r^{\frac{1}{n}}$ fit to the outer regions of the luminosity profiles. In this representation, core Es are "missing light" relative to the fit while coreless Es have "extra light." The top row of Figure 6 shows one core E (NGC 4472) and two coreless Es [NGC 4458 and IC 798 (VCC 1440), the latter a low-luminosity dwarf]. The subtle distinctions are evident in these images, with NGC 4472 showing a soft center and NGC 4458 showing a strong center. The terminology for both types is mostly historical (Kormendy 1999) and somewhat counter to the visual impression (i.e., NGC 4472 lacks a bright core while NGC 4458 has one, yet the latter is technically coreless). Kormendy et al. show that core and coreless E galaxies have different Sersic indices, velocity dispersion anisotropy, isophote shapes, and rotational character, with the core Es being of the boxy type and the coreless Es of the disky type in Figure 5. The distinction may be tied to the number of mergers that formed the system.

5.2. S0 and Spiral Galaxies

The full classification of spiral and S0 galaxies involves the recognition of the stage, family, and variety. In de Vaucouleurs's classification approach, the implication for bars, inner rings, and stages is a continuum of forms (de Vaucouleurs 1959), so that there are no sharp edges to any category or "cell" apart from the obvious ones (for example, there are no galaxies less "barred" than a nonbarred galaxy, nor are there galaxies more ringed than those with a perfectly closed ring).

The classification of S0 galaxies depends on recognizing the presence of a disk and a

bulge at minimum, and usually a lens as well, and no spiral arms. Examples are shown in Figure 7. The display of galaxy images in units of mag arcsec^{-2} makes lenses especially easy to detect, as noted in the dVA. Even if a lens isn't obvious, a galaxy could still be an S0 if it shows evidence of an exponential disk. (Lenses are also not exclusive to S0s.) The "no spiral arms" characteristic is much stricter in the Hubble-Sandage classification than in the de Vaucouleurs interpretation, because varieties (r, rs, and s) are carried into the de Vaucouleurs classifications of S0s. This allows the possibility of a classification like SA(s)0$^-$, which would be very difficult to recognize. Bars enter in the classification of S0s in a similar manner as for spirals. Figure 7 shows mainly stage differences among nonbarred and barred S0s. The stage for S0s ranges from early (S0$^-$), to intermediate (S0^o), and finally to late (S0$^+$), in a succession of increasing detail. The earliest nonbarred S0s may be mistaken for elliptical galaxies on photographic images, and indeed Sandage & Bedke (1994) note cases where they believe an S0 galaxy has been misclassified as an elliptical by de Vaucouleurs in his reference catalogues (see also *The Revised Shapley-Ames Catalogue*, RSA, Sandage & Tammann 1981). This kind of misinterpretation is less likely for types S0^o and S0$^+$, because these will tend to show more obvious structure.

The morphological distinction between E and S0 galaxies has been considered from a quantitative kinematic point of view by Emsellem et al. (2007). These authors argue that the division of early-type galaxies into E and S0 types is "contrived", and that it is more meaningful to divide them according to a quantitative kinematic parameter called λ_R, the specific angular momentum of the stellar component, which is derived from a two-dimensional velocity field obtained with the SAURON integral field spectrograph (Bacon et al. 2001). Based on this parameter, early-type galaxies are divided into slow and fast rotators, i. e., whether they are characterized by large-scale rotation or not. In a sample of 48 early-types, most were found to be fast rotators classified as a mix of E and S0 types, while the remainder were found to be slow rotators classified as Es. This kind of

approach, which provides a more physical distinction among early-types, does not negate completely the value of the E and S0 subdivisions, but highlights again the persistent difficulty of distinguishing the earliest S0s from Es by morphology alone.

The transition type S0/a shows the beginnings of spiral structure. Two examples are included in Figure 7, one nonbarred and the other barred. Type S0/a is a well-defined stage characterized in the de Vaucouleurs 3D classification volume as having a high diversity in family and variety characteristics. The type received a negative characterization as the "garbage bin" of the Hubble sequence at one time because troublesome dusty irregulars, those originally classified as "Irr II" by Holmberg (1950) and later as "I0" by de Vaucouleurs, seemed to fit better in that part of the sequence. [In fact, de Vaucouleurs, de Vaucouleurs, & Corwin (1976) assigned the numerical stage index T=0 to both S0/a and I0 galaxies.] However, this problem is only a problem at optical wavelengths. At longer wavelengths (e.g., 3.6 microns), types such as Irr II or I0 are less needed as they are defined mainly by dust (Buta et al. 2010a).

In general, the stage for spirals is based on the appearance of the spiral arms (degree of openness and resolution) and also on the relative prominence of the bulge or central concentration. These are the usual criteria originally applied by Hubble (1926, 1936). Figure 8 shows the stage sequence for spirals divided according to bar classification (SA, SAB, SB), and as modified and extended by de Vaucouleurs (1959) to include Sd and Sm types. Intermediate stages, such as Sab, Sbc, Scd, and Sdm, are shown in Figure 9. As noted by de Vaucouleurs (1963), these latter stages are almost as common as the basic ones.

The three Hubble criteria are basically seen in the illustrated galaxies. Sa galaxies tend to have significant bulges, and tightly-wrapped and relatively smooth spiral arms. Sab galaxies are similar to Sa galaxies, but show more obvious resolution of the arms. Sb galaxies have more resolution and more open arms, and generally smaller bulges than Sab

galaxies. Sbc galaxies have considerable resolution and openness of the arms, and also usually significant bulges. In Sc galaxies, the bulge tends to be very small and the arms patchy and open. Scd galaxies tend to be relatively bulgeless, patchy armed Sc galaxies. Stage Sd is distinctive mainly as almost completely bulgeless late-type spirals with often ill-defined spiral structure.

Stages Sdm and Sm are the most characteristically asymmetric stages, the latest spiral types along the de Vaucouleurs revised Hubble sequence. They are described in detail by de Vaucouleurs & Freeman (1972) and by Odewahn (1991). Sm is generally characterized by virtually no bulge and a single principle spiral arm. If a bar is present, it is usually not at the center of the disk isophotes, unlike what is normally seen in earlier type barred spirals. This leads to the concept of an *offset barred galaxy*. The single spiral arm emanates from one end of the bar. As noted by Freeman (1975), this is a basic and characteristic asymmetry of the mass distribution of Magellanic barred spirals. Sdm galaxies are similar, but may show a weaker or shorter second arm. In Figure 8, NGC 4618 is an especially good example of an SBm type (Odewahn 1991), while in Figure 9, NGC 4027 is illustrated as type SBdm.

An important issue regarding these galaxies is whether the optically offset bar is also offset from the dynamical rotation center of the disk. In a detailed HI study of the interacting galaxy pair NGC 4618 and 4625, Bush & Wilcots (2004) found very regular velocity fields and extended HI disks, but no strong offset of the rotation center from the center of the bar. This is similar to what Pence et al. (1988) found for the offset barred galaxy NGC 4027, based on optical Fabry-Perot interferometry. In contrast, both Magellanic Clouds, which are also offset barred galaxies, were found to have HI rotation centers significantly offset from the center of the bar (Kerr & de Vaucouleurs 1955).

In general, the application of Hubble's three spiral criteria allows consistent

classification of spiral types. Nevertheless, sometimes the criteria are inconsistent. For example, small bulge Sa galaxies are described by Sandage (1961) and Sandage & Bedke (1994). Barred galaxies with nuclear rings can have spiral arms like those of an earlier Hubble type and very small bulges. In such conflicting cases, the emphasis is usually placed on the appearance of the arms. Also, while late-type Sdm and Sm galaxies are characteristically asymmetric, other types may be asymmetric as well. On average, the bulge-to-total luminosity ratio is related to Hubble type, but the result is sensitive to how galaxies are decomposed (e. g., Laurikainen et al. 2005). Asymmetry has been quantified by Conselice (1997).

The family classifications SA, SAB, and SB are purely visual estimates of bar strength, for both spirals and S0s. They are highlighted already in Figures 7– 9, but the continuity of this characteristic is better illustrated in Figure 10, where de Vaucouleurs (1963) underline classifications (S$\underline{\text{A}}$B and SA$\underline{\text{B}}$) are also shown. An SA galaxy has no evident bar in general, although high inclination can cause a mistaken SA classification if a bar is highly foreshortened. Also, internal dust may obscure a bar (see, e. g., Eskridge et al. 2000). An SB galaxy should have a clear, well-defined bar. The intermediate bar classification SAB is one of the hallmarks of the de Vaucouleurs system, and is used to recognize galaxies having characteristics intermediate between barred and nonbarred galaxies. It is used for well-defined ovals or simply weaker-looking normal bars. The weakest primary bars are denoted S$\underline{\text{A}}$B while the classification SA$\underline{\text{B}}$ is usually assigned to more classical bars that appear only somewhat weaker than conventional bars. Most of the time, galaxies which should be classified as SA$\underline{\text{B}}$ are simply classified as SB.

Variety is also treated as a continuous classification parameter (Figure 10, second row). A spiral galaxy having a completely closed or very nearly completely closed inner ring is denoted (r). The spiral arms usually break from the ring. If the spiral arms break directly

from the central region or the ends of a bar, forming a continuously winding, open pattern, the variety is (s). The intermediate variety (rs) is also well-defined. Inner rings which appear broken or partial are in this category. The "dash-dot-dash in brackets" morphology: (-o-), where a bar with a bulge is bracketted by spiral arcs overshooting the bar axis, is very typical of variety (rs). The example of this shown in Figure 10 is NGC 4548. We use the notation $\underline{\text{r}}$s to denote an inner ring made up of tightly wrapped spiral arms that do not quite close, while the notation r$\underline{\text{s}}$ is used for very open, barely recognizable, inner pseudorings. A good example of the former is NGC 3450, while an example of the latter is NGC 5371.

A *spindle* is a highly inclined disk galaxy. For blue-light images, usually an "sp" after the classification automatically implies considerable uncertainty in the interpretation, because family and variety are not easily distinguished when the inclination is high. Figure 11 shows, however, that stages can be judged reasonably reliably for edge-on galaxies. One important development in the classification of edge-on galaxies has been the ability to recognize edge-on bars through boxy/peanut and "X"-shapes. Boxy/peanut bulges in edge-on galaxies were proven to be bars seen edge-on from kinematic considerations (e. g., Kuijken & Merrifield 1995). This shape is evident in NGC 4425 (Row 1, column 4 of Figure 11; see also section 9).

For spiral and S0 galaxies that are not too highly inclined (i.e., not spindles), once the stage, family, and variety are determined these are combined in the order family, variety, stage for a final full type. For example, NGC 1300 is of the family SB, variety (s), and stage b, thus its full type is SB(s)b. The $S0^+$ galaxy NGC 4340 has both a bar and inner ring and its full type is SB(r)0^+. The classification is flexible enough that if, for example, the family and variety of a galaxy cannot be reliably determined owing to high inclination, while the stage can still be assessed, then the symbols can be dropped and a type such as

"Sb" or "S0" can still be noted.

5.3. Irregular Galaxies

Magellanic irregular galaxies represent the last normal stage of the de Vaucouleurs revised Hubble sequence. Several examples are shown in Figure 12. The objects illustrated in the top row are all examples of (s)-variety irregulars with bars or some trace of a bar. Nevertheless, not all Magellanic irregulars have bars. Irregulars of the lowest luminosities are usually classified simply as Im since the sophistication of structure needed to distinguish something like "family" may not exist for such galaxies.

Irregular galaxies are important for their star formation characteristics. As noted by Hunter (1997), irregulars are similar to spirals in having both old and young stars, as well as dust, atomic, molecular, and ionized gas, but lack the spiral structure that might trigger star formation. Thus, they are useful laboratories for examining how star formation occurs in the absence of spiral arms.

Although irregulars are largely defined by a lack of well-organized structure like spiral arms, the two lower right galaxies in Figure 12 are not so disorganized looking and seem different from the other cases shown. NGC 5253 looks almost like a tilted S0 galaxy, yet it has no bulge at its center nor any obvious lenses. Instead, the central area is an irregular zone of active star formation. The central zone was interpreted by van den Bergh (1980a) as "fossil evidence" for a burst of star formation, possibly triggered by an interaction with neighboring M83. This is a case where the de Vaucouleurs classification of I0 seems reasonable: NGC 5253 is an early-type galaxy with a central starburst, probably the youngest and closest example known (Vanzi & Sauvage 2004). It is a Magellanic irregular galaxy imbedded in a smooth S0-like background known to have an early-type star

spectrum. NGC 1705, also shown in Figure 12, is similar but has a super star cluster near the center and obvious peculiar filaments. It is classified as a blue compact dwarf by Gil de Paz et al. (2003). Both galaxies are classified as Amorphous by Sandage & Bedke (1994).

6. Other Dimensions to Galaxy Morphology

The de Vaucouleurs classification volume recognizes three principal aspects of galaxy morphology, but clearly there are many more dimensions than three. Stage, family, and variety are the dimensions most clearly highlighted in blue light images and have a wide scope. Other dimensions may be considered and for some there is explicit notation in use.

6.1. Outer Rings and Pseudorings

Published de Vaucouleurs types include an extra dimension known as the outer ring/pseudoring classification. Several examples of outer rings and pseudorings are shown in Figure 13. An outer ring is a large, often diffuse structure, typically seen in barred early-type galaxies (stages $S0^+$ to Sa) at a radius approximately twice that of the bar. Closed outer rings are recognized with the type symbol (R) preceding the main part of the classification. For example, an $SB(r)0^+$ galaxy having an outer ring has a full classification of $(R)SB(r)0^+$. Interestingly, rare cases of double outer ring galaxies, type (RR), are known, where two detached outer rings are seen; an example is NGC 2273 shown in the upper left frame of Figure 13.

In later-type galaxies, a large outer ring-like feature is often seen made of outer spiral arms whose variable pitch angle causes them to close together. These features are classified as outer pseudorings, symbolized by (R′) preceding the main type symbols [e.g., as in (R′)SB(r)ab]. Outer pseudorings are mainly observed in Sa to Sbc galaxies, and are only

rarely seen in the very late stages Sc-Sm.

Among bright nearby galaxies, outer rings and pseudorings are found at about the 10% level (Buta & Combes 1996). Typically, outer rings are fainter than 24 mag arcsec^{-2} in blue light. With such low surface brightnesses, the rings can be easily lost to Galactic extinction. The division between outer rings and pseudorings is also not sharp. Some outer pseudorings are only barely distinguishable from outer rings. Continuity applies to these features as it does for inner rings although there is no symbol other than "S" for an outer spiral pattern which does not close into an outer pseudoring.

Although closed outer rings (R) are equally well-recognized in the RSA and the Carnegie and Hubble Atlases, outer pseudorings are a unique feature of the de Vaucouleurs revision. The value of recognizing these features is that many show morphologies consistent with the theoretical expectations of the outer Lindblad resonance (OLR, Schwarz 1981), one of the major low-order resonances that can play a role in disk evolution. Resonance rings are discussed further in section 10.1, but Figure 14 shows schematics of the morphologies generally linked to this resonance. The schematics are designed to highlight the subtle but well-defined aspects of these features, while Figure 15 shows images of several examples of each morphology, including the "models" used for the schematic. Outer rings of type R_1 are closed rings that are slightly dimpled towards the bar axis, a shape which connects directly to one of the main periodic orbit families near the OLR as shown in Schwarz (1981) and in the dVA. Outer pseudorings of type R'_1 are similar to type R_1 but are made of two spiral arms that wind approximately 180^o with respect to the ends of the bar. Even these will usually show a dimpled shape. Outer pseudorings of type R'_2 are different from this in that two spiral arms wind 270^o with respect to the ends of the bar, such that the arms are doubled in the quadrants immediately trailing the bar.

The shapes R_1, R'_1, and R'_2 were predicted by Schwarz (1981) based on "sticky-particle"

numerical simulations. Not predicted by those simulations (but later shown in extensions of those simulations by Byrd et al. 1994 and Rautiainen & Salo 2000) is an interesting combined ring morphology called $R_1R'_2$, which consists of a closed R_1 ring and an R'_2 pseudoring. This combination is especially important because it demonstrates not only a continuity of morphologies among outer rings and pseudorings different from the continuity between outer rings and pseudorings in general, but also it is a morphology that can be linked directly to the dynamics of barred galaxies.

Note that the classification shown in Figures 14 and 15 does not depend on whether the rings are in fact linked to the OLR. The illustrated morphologies are abundant and easily recognized regardless of how they are interpreted. (Section 10.1 discusses other interpretations that have been proposed.) Although the Schwarz models guided the search for these morphologies, Rautiainen, Salo, & Buta (2004) and Treuthardt et al. (2008) showed that some outer pseudorings classified as R'_1 are more likely related to the outer 4:1 resonance and not the OLR. These cases are generally recognizable by the presence of secondary spiral arcs in a four-armed pattern in the area of the bar (NGC 1433 in Figure 1 and ESO 566−24 in Figure 19 are examples).

The OLR subclassifications are used in the same manner as the plain outer ring and pseudoring classifications. For example, NGC 3081 has the full type $(R_1R'_2)$SAB(r)0/a.

6.2. Inner and Outer Lenses

The value of recognizing lenses as significant morphological components was first emphasized by Kormendy (1979), who suggested a dynamical link between inner lenses, which are often filled by a bar in one dimension, and dissolved or dissolving bars. Kormendy noted that lenses can be of the inner or outer type, in a manner analogous to inner and

outer rings. He suggested the notation (l) for inner lenses and (L) for outer lenses to be used in the same position of the classification as inner and outer rings. For example, the galaxy NGC 1543 is type (R)SB(l)0/a while galaxy NGC 2983 is type (L)SB(s)0^+. Figure 16 demonstrates the continuity between rings and lenses, which is evident not only among barred galaxies but among nonbarred ones as well. This continuity is recognized by the type symbol (rl), also used by Kormendy (1979). This type refers to a low contrast inner ring at the edge of a clear lens. Even underline classifications (<u>r</u>l) and (r<u>l</u>) may be recognized. A rare classification, (r′l), refers to an inner pseudoring/lens, a type of feature that is seen in NGC 4314 and recognized as such in the dVA.

Similarly, Figure 17 shows a continuity between outer rings and outer lenses through the type classification (RL), referring to an outer lens with a weak ring-like enhancement. Underline types <u>R</u>L and R<u>L</u> may also be recognized. The origin of outer lenses could be in highly evolved outer rings.

6.3. Nuclear Rings and Bars

The central regions of barred galaxies often include distinct morphological features in the form of small rings and secondary bars. The rings, known as nuclear rings because of their proximity to the nucleus well inside the ends of the primary bar, are sites of some of the most spectacular starbursts known in normal galaxies. The rings are typically ≈1.5 kpc in linear diameter and intrinsically circular in shape. Figure 18 (top row) shows three examples: NGC 1097, 3351, and 4314. These images highlight the small bulges that seem characteristic of nuclear-ringed barred galaxies. The three galaxies illustrated have types ranging from Sa to Sb, but based on the bulge size the types would be considerably later. For example, NGC 3351 has the bulge of an Sd galaxy.

Comerón et al. (2010) carried out an extensive statistical study of nuclear ring radii, and identified a subclass known as "ultra-compact" nuclear rings (UCNRs). Such rings were recognized mainly in Hubble Space Telescope images and are defined to be less than 200pc in diameter. (See Figure 26 for an example in NGC 3177.) Comerón et al. showed that UCNRs are the low size tail of the global nuclear ring population. This study also showed that bar strength impacts the sizes of nuclear rings, with stronger bars generally hosting smaller nuclear rings than weaker bars.

Comerón et al. (2010) were also able to derive a reliable estimate of the relative frequency of nuclear rings as 20%±2% over the type range $S0^-$ to Sd, confirming with smaller error bars the previous result of Knapen (2005). Assuming that nuclear rings are a normal part of galaxy evolution, these authors argue that the rings may survive for 2-3 Gyr. Interestingly, it was also found that 19%±4% of nuclear rings occur in nonbarred galaxies, implying either that the rings may have formed when a bar was stronger (evidence of bar evolution) or that ovals or other mechanisms can lead to their formation. Mazzuca et al. (2009; see also Knapen 2010) connect some of the properties of nuclear rings to the rate at which the rotation curve rises in the inner regions.

The most extreme nuclear ring known is found in the SBa galaxy ESO 565−11 (see also section 7). At 3.5kpc in diameter, not only is it one of the largest known nuclear rings, but also the ring has an extreme elongated shape compared to more typical nuclear rings.

Nuclear bars lie in the same radial zone as nuclear rings and sometimes lie inside a nuclear ring. Three examples are shown in the second row of Figure 18. These average about one-tenth the size of a primary bar. There is no preferred angle between the axis of the nuclear bar and the primary bar, suggesting that the two features have different pattern speeds (Buta & Combes 1996; dVA).

Neither nuclear rings nor nuclear bars were recognized in the original Hubble-Sandage-de

Vaucouleurs classifications, presumably in part because the use of small-scale photographic plates for extensive galaxy classification limited the detectability of the features in the (typically) overexposed centers. Modern multi-band digital imaging greatly facilitates the detection of the small rings and bars, allowing their inclusion in the classification. Buta & Combes (1996) and Buta et al. (2010a) suggested the notation nr for nuclear rings and nb[4] for nuclear bars, respectively, to be used as part of the variety classification as in, for example, SB(r,nr)b for NGC 3351, or SAB(l,nb)0/a for NGC 1291. Continuity may exist for these features like other rings and primary bars. [For example, nuclear lenses (nl) may also be recognized.] In blue light images, the appearance of the central region of a barred galaxy can be strongly affected by dust. For example, NGC 1365 shows a nuclear spiral in blue light, while in the infrared, the morphology is that of a nuclear ring (Buta et al. 2010a). The morphologies of some galaxies have a full complement of classifiable features. For example, accounting for all the rings and bars seen in NGC 3081, the classification is $(R_1R'_2)$SAB(r,nr,nb)0/a.

Lisker et al. (2006) use the terminology "S2B" for double-barred galaxies, a reasonable alternative approach to classifying these objects. Lisker et al. successfully identified nuclear bars in galaxies at redshifts z=0.10-0.15 (from HST ACS observations), the most distant ones recognized thus far.

6.4. Spiral Arm Morphologies

A classification such as "Sb" tells one that a galaxy is a spiral of moderate pitch angle and degree of resolution of the arms, and that a significant bulge may be present. The type

[4]In a study of galactic nuclei, van den Bergh (1995) proposed the notation "NB" for nuclear bars, although what he refers to are not the same as the features described here.

does not directly tell: (1) the multiplicity of the spiral pattern; (2) the character of the arms (massive, filamentary, grand design, or flocculent); or (3) the sense of winding of the arms (leading or trailing the direction of rotation). These are nevertheless additional dimensions to galaxy morphology.

The multiplicity of the spiral pattern refers to the actual number of spiral arms, usually denoted by the integer m. Examples of spirals having m=1 to 5 are illustrated in Figure 19. The multiplicity is not necessarily straightforward to determine and may be a function of radius. For example, a spiral may be two-armed in the inner regions and multi-armed in the outer regions. Spirals of low m are usually *grand design*, a term referring to a well-defined global (meaning galaxy-wide) pattern of strong arms. The typical grand design spiral has two main arms, as in NGC 5364 (lower left frame of Figure 19). In contrast, a flocculent spiral has piecewise continuous arms but no coherent global pattern (Elmegreen 1981). NGC 5055 is an example shown in the middle left frame of Figure 19. This category is relevant mainly to optical wavebands. In the infrared, an optically flocculent spiral like NGC 5055 reveals a more coherent global grand design spiral (Thornley 1996; see also Figure 44), indicating that dust is partly responsible for the flocculent appearance.

The terms "massive" and "filamentary" arms are due to Reynolds (1927) and are discussed by Sandage (1961, 1975). Massive arms are broad, diffuse, and of relatively low contrast, as in M33, while filamentary arms are relatively thin in comparison, and lined by knots or filaments, as in NGC 5457 (M101). De Vaucouleurs (1956) originally used these distinctions as part of his classification, but later dropped the references to spiral arm character probably because of the complexity it added to his types.

Elmegreen & Elmegreen (1987) used a different approach to spiral arm character by recognizing a series of spiral *arm classes* based on arm continuity and length (but not necessarily contrast). Ten classes ranging from flocculent (ACs 1-4) to grand design (5-12;

numbers 10 and 11 were later dropped). Examples of each are illustrated in Figure 20 (see Elmegreen & Elmegreen 1987 for a description of each class). Thus, spiral character is a well-developed additional dimension to galaxy classification. A simpler approach advocated by Elmegreen & Elmegreen is "G" for grand-design, "F" for flocculent, and "M" for multiple-armed. The arms of grand design spirals are in general thought to be density waves and may in fact represent quasi-steady wave modes (e.g., Bertin et al. 1989; Zhang 1996, 1998, 1999), although there is also some evidence that spirals may be transient (see review by Sellwood 2010). Flocculent spirals may be sheared self-propogating star formation regions (Seiden & Gerola 1982).

Figure 19 also shows two examples of a new class of spirals, called *counter-winding* spirals. In these cases, an inner spiral pattern winds outward in the opposite sense to an outer spiral pattern. In the case of NGC 4622 (row 2, middle), the inner pattern has only a single arm and the outer pattern has two arms, while in NGC 3124 (row 2, middle right), the inner pattern is two-armed while the outer pattern is at least four-armed. The two cases are very different because NGC 4622 is essentially nonbarred while in NGC 3124, the inner spiral is classified as a bar. The presence of oppositely winding spiral patterns in the same galaxy means that one set of arms is trailing (opening opposite the direction of rotation) while the other set is leading (opening into the direction of rotation). In general, studies of the dust distribution as well as the rotation of spirals has shown that trailing arms are the rule (de Vaucouleurs 1958). Surprisingly, straightforward analysis of a velocity field and the dust pattern in NGC 4622 led Buta, Byrd, & Freeman (2003) to conclude that the strong outer two-armed pattern in this galaxy is leading, while the inner single arm is trailing. This led to the characterization of NGC 4622 as a "backwards spiral galaxy," apparently rotating the wrong way. An additional nonbarred counter-winding spiral has been identified in ESO 297−27 by Grouchy et al. (2008). In this case, the same kind of analysis showed that an inner single arm leads while a 3-armed outer pattern trails. No comparable analysis

has yet been made for NGC 3124.

Vaisanen et al. (2008) have shown that a two-armed (but not counter-winding) spiral in the strongly interacting galaxy IRAS 18293-3413 is leading. Even with this, the number of known leading spirals is very small (dVA). Leading spirals are not expected to be as long-lived as trailing spirals since they do not transfer angular momentum outwards and this is needed for the long-term maintenance of a spiral wave (Lynden-Bell & Kalnajs 1972).

An interesting example of leading "armlets" was described by Knapen et al. (1995a), who used K-band imaging of the center of the grand design spiral M100 to reveal details of its nuclear bar and well-known nuclear ring/spiral. The nuclear bar has a leading twist that connects it to two bright K-band "knots" of star formation. This morphology was interpreted in terms of the expectations of gas orbits in the vicinity of an inner inner Lindblad resonance (IILR; Knapen et al. 1995b).

The final galaxy in Figure 19 is NGC 4921, an example of an *anemic* spiral. This is a type of spiral that is deficient in neutral atomic hydrogen gas, and as a consequence it has a lower amount of dust and star formation activity. The arms of NGC 4921 resemble those of an Sb or Sbc galaxy in pitch angle and extensiveness, but are as smooth as those typically seen in Sa galaxies. Anemic spirals were first recognized as galaxies with "fuzzy" arms (see van den Bergh 1998) where star formation has been suppressed due to ram-pressure stripping in the cluster environment. In the case of NGC 4921, the environment is the Coma Cluster. The idea is that such galaxies will eventually turn into S0 galaxies (van den Bergh 2009a). Anemic spiral galaxies are further discussed in section 10.2.

Seigar et al. (2008) have demonstrated the existence of a correlation between spiral arm pitch angles and supermassive central black hole masses. The sense of the correlation is such that black hole mass is highest for the most tightly wound spirals and lowest for the most open spirals. The correlation is expected because black hole mass is tightly correlated

to bulge mass and central mass concentration, and spiral arm pitch angle is tied to shear in galactic disks, which itself depends on mass concentration (Seigar et al. 2005).

6.5. Luminosity Effects

Luminosity effects are evident in the morphology of galaxies through surface brightness differences between giants and dwarfs, and through the sophistication of structure such as spiral arms. van den Bergh (1998) describes his classification system which takes luminosity effects into account using a set of luminosity classes that are analogous to those used for stars. The largest, most massive spirals have long and well-developed arms, while less massive spirals have less well-defined arms.

The nomenclature for the classes parallels that for stars: I (supergiant galaxies), II (bright giant galaxies), III (giant galaxies), IV (subgiant galaxies) and V (dwarf galaxies). Intermediate cases I-II, II-III, III-IV, and IV-V, are also recognized.

Figure 21 shows galaxies which van den Bergh (1998) considers primary luminosity standards of his classification system. The original van den Bergh standards for these classes were based on the small scale paper prints of the Palomar Sky Survey. Sandage and Tammann (1981) adopted the precepts of the van den Bergh classes but revised the standards based on large-scale plates. In general, luminosity class I galaxies have the longest, most well-developed arms, luminosity class III galaxies have short, patchy arms extending from the main body, while luminosity class V galaxies have very low surface brightness and only a hint of spiral structure. The classes are separated by type in Figure 21 because among Sb galaxies, few are of luminosity class III or fainter, while among Sc and later type galaxies, the full range of luminosity classes is found. van den Bergh does not use types like Sd or Sm for conventional de Vaucouleurs late-types, but instead uses S^- and

S^+ to denote "early" (smoother) and "late" (more patchy) subgiant spirals. Similarly, van den Bergh uses Sb^- and Sb^+ to denote "early" and "late" Sb spirals, respectively. (Some of these would be classified as Sab and Sbc by de Vaucouleurs.) According to the standards listed by van den Bergh (1998), an Sb I galaxy is 2-3 mag more luminous than an Sb III galaxy, while an Sc I galaxy is more than 4 mag more luminous than an S V galaxy.

7. The Morphology of Galactic Bars and Ovals

Bars are among the most common morphological features of disk-shaped galaxies. Unlike spiral arms, bars cross the "spiral-S0 divide" in the Hubble sequence and are abundant among spirals (at the 50-70% level) when both SAB and SB types are considered (de Vaucouleurs 1963; Sellwood & Wilkinson 1993). The bar fraction has cosmological significance (Sheth et al. 2008), and many estimates of the nearby galaxy bar fraction have been made from both optical and IR studies (see Buta et al. 2010a for a summary of recent work).

Bars are fairly well-understood features of galaxy morphology that have been tied to a natural instability in a rotationally supported stellar disk (see review by Sellwood & Wilkinson 1993). The long-term maintenance of a bar in a mostly isolated galaxy is thought to depend on how effectively it transfers angular momentum to other galaxy components, such as the halo (Athanassoula 2003). Bars are thought to be transient features that, in spiral galaxies, may dissolve and regenerate several times over a Hubble time (Bournaud & Combes 2002). Alternatively, bars may be long-lived density wave modes that drive secular evolution of both the stellar and gaseous distributions (Zhang & Buta 2007; Buta & Zhang 2009). The possible secular evolution of bars in S0 galaxies is discussed by Buta et al. (2010b). Bars are also thought to drive spiral density waves (Kormendy & Norman 1979; Buta et al. 2009; Salo et al. 2010).

The actual morphology of bars shows interesting variations that merit further study. The family classifications SAB and SB indicate some measure of bar strength, but do not allude to the varied appearances of bars even among those only classified as SB. Regular bars, such as those illustrated in Figure 8, are the conventional types that define the SB class. Figure 22 shows "ansae"-type bars, referring to bars which have "handles" or bright enhancements at the ends. Martinez-Valpuesta et al. (2007) carried out a statistical study and found that ansae are present in ≈40% of early-type barred galaxies and are very rare for types later than stage Sb. Ansae are usually detectable in direct images, but their visibility can be enhanced using unsharp-masking (all the right frames for each galaxy in Figure 22). Morphologically, ansae may be small round enhancements like those seen in NGC 5375 and 7020, but in some cases, ansae are approximately linear enhancements, giving the bar a parallelogram appearance as in NGC 7098, or curved arcs, giving the bar a partial ring appearance as in NGC 1079. Color index maps in the dVA show that ansae are generally as red as the rest of the bar, indicating the features are stellar dynamical in origin, rather than gas-dynamical. Nevertheless, ansae made of star-forming regions are known. Martinez-Valpuesta et al. (2007) illustrate the case of NGC 4151, a well-known Seyfert 1 galaxy with a strong bar-like inner oval. The appearance of this galaxy's ansae in the 1.65μm H-band is shown in the lower right frames of Figure 22, where the ansae are seen to have irregular shapes compared to the others shown.

Another subtlety about bars is their general boxy character. Athanassoula et al. (1990) showed that generalized ellipses fit the projected isophotes of bars better than do normal ellipses. For 11 or 12 SB0 galaxies examined in this study, a significant degree of boxiness was found near the bar semi-major axis radius.

The unsharp-masked image of NGC 7020 in Figure 22 shows an X-shaped pattern in the inner regions that is the likely signature of a significantly three-dimensional bar. NGC

1079 and 5375 shows hints of similar structure. The X-pattern is expected to be especially evident in edge-on galaxies which show the extended vertical structure of bars. Many examples have been analyzed (Bureau et al. 2006; see also the dVA). Buta et al. (2010a) have suggested that edge-on bars recognized from the X-pattern be denoted "SB$_x$."

The cause of bar ansae is uncertain. In simulations, Martinez-Valpuesta et al. (2006) found that ansae form late, after a second bar-buckling episode in a disk model with a live axisymmetric halo, and appear as density enhancements in both the face-on and edge-on views.

Figure 23 shows three examples of galaxies having oval inner disks. These features are described in detail by Kormendy and Kennicutt (2004=KK04), who present both photometric and kinematic criteria for recognizing them. The images in Figure 23 are optical and have been cleaned of foreground and background objects, and have also been deprojected based on the mean shape and major axis position angle of faint outer isophotes. In all three cases, the presence of an outer ring allows clear recognition of the oval shape, assuming that the inner and outer structures are in the same plane. The upper panels of Figure 23 show the full morpholopy with the outer rings, while the lower panels show the bright oval inner disks. The shapes of the oval disks are varied and range from axis ratio 0.84 for NGC 4736 to 0.55 for NGC 1808. The most striking example is NGC 4941, whose oval disk includes a bright, normal-looking spiral pattern with isophotal axis ratio 0.68. Many other examples are provided by KK04.

The ovals appear to play a bar-like role in these galaxies. The outer rings may be resonant responses to the nonaxisymmetric potential of the ovals, which clearly harbor a great deal of mass in spite of the mildness of their departures from axisymmetry. As noted by KK04, oval disk galaxies are expected to evolve secularly in much the same manner as typical barred galaxies. On the other hand, ovals themselves could be products of bar

secular evolution. Laurikainen et al. (2009) found that the near-IR bar fraction in S0 galaxies is significantly less than that in S0/a or early-type spiral galaxies (also found by Aguerri et al. 2009 in the optical), while the oval/lens fraction is higher, suggesting that some ovals/lenses might be dissolved bars. Further evidence that bars might be dissolving in some galaxies is the detection of extremely weak bars in residual images of visually nonbarred S0 galaxies where a two-dimensional decomposition model has been subtracted. Such a bar is detected in the SA0^o galaxy NGC 3998 (Laurikainen et al. 2009). Aguerri et al. (2009) suggest that central concentration is a key factor in bar evolution, and that a unimodal distribution of bar strengths argues against the idea that bars dissolve and reform (Bournaud & Combes 2002).

Regular barred galaxies also often include an oval bounded by an elongated inner ring. The deprojected blue light images of two examples are shown in Figure 24. NGC 1433 has a very strong normal bar and one of the most intrinsically elongated inner rings known. The inner ring lies at the edge of an oval which is more conspicuous at longer wavelengths. In NGC 1433, the inner ring, the oval, and the bar are all aligned parallel to each other. The situation is different in ESO 565−11, whose bright oval is strongly misaligned with a prominent bar, but similar to NGC 1433, the oval is bounded by an inner pseudoring. The suggestion in this case is that the bar and the oval are independent patterns.

8. Dust Morphologies

Dust lanes are often the most prominent part of the interstellar medium detectable in an optical image of a galaxy. Figure 25 shows different classes of dust lanes, using direct optical images on the left for each galaxy, and a color index map on the right. The color index maps are coded such that blue features are dark while red features (like dust lanes) are light.

The bars of intermediate (mainly Sab to Sbc) spirals often show *leading* dust lanes, that is, well-defined lanes that lie on the leading edges of the bars, assuming the spiral arms trail. The example shown in Figure 25, NGC 1530, has an exceptionally strong bar and the lanes are very straight, regular, and well-defined. These dust lanes are a dynamical effect associated with the bar. The lanes may be curved or straight. Athanassoula (1992) derived models of bar dust lanes and tied the curvature to the strength of the bar in the sense that models with stronger bars developed straighter dust lanes. Comerón et al. (2009) recently tested this idea by measuring the curvature of actual dust lanes as well as quantitative values of the bar strengths for 55 galaxies. They found that strong bars can only have straight dust lanes, while weaker bars can have straight or curved lanes.

In the same manner as bars, a strong spiral often has dust lanes on the concave sides of the inner arms. This is shown for NGC 1566 in the upper right panels of Figure 25. Both bar and spiral dust lanes are face-on patterns. Another type of face-on pattern is the *dust ring*. The inner dust ring of NGC 7217 is shown in the right, middle frames of Figure 25, and it appears as the dark, inner edge of a stellar ring having the same shape. Dust rings can also be detected in more inclined galaxies.

An inclined galaxy with a significant bulge also can show another dust effect: in such a case, the bulge is viewed through the dust layer on the near side of the disk, while the dust is viewed through the bulge on the far side of the disk. This leads to a reddening and extinction asymmetry across the minor axis such that the near side of the minor axis is more reddened and extinguished than the far side. In conjunction with rotation data, this near side/far side asymmetry was used by Hubble (1943) and de Vaucouleurs (1958) to show that most spirals trail the direction of rotation.

The lower frames of Figure 25 show the planar dust lanes seen in edge-on spiral galaxies. The lane in NGC 7814 (lower left frames) is red which indicates that the galaxy

is probably no later in type than Sa. This is consistent with the large bulge seen in the galaxy. However, the planar dust lane seen in NGC 891, type Sb, has a thin blue section in the middle of a wider red section. The blue color is likely due to outer star formation that suffers relatively low extinction. Some individual star forming regions can be seen along the dust lane. In spite of the blue color, we are only seeing the outer edge of the disk in the plane.

Also related to galactic dust distributions are observations of *occulting galaxy pairs*, where a foreground spiral galaxy partly occults a background galaxy, ideally an elliptical (White & Keel 1992). With such pairs, one can estimate the optical depth of the foreground dust, often in areas where it might not be seen easily in an isolated spiral. An excellent example is described by Holwerda et al. (2009), who are able to trace the dust distribution in an occulting galaxy to 1.5 times than the standard isophotal radius.

Another way of illustrating the dust distribution in galaxies is with *Spitzer Space Telescope* Infrared Array Camera (IRAC) images at 8.0μm wavelength. This is discussed further in section 12.

9. The Morphologies of Galactic Bulges

A bulge is a very important component of a disk galaxy. In the context of structure formation in a cold dark matter (CDM) cosmology, bulges may form by hierarchical merging of disk galaxies, a process thought to lead to elliptical galaxies if the disks have approximately equal mass. Bulges formed in this way should, then, resemble elliptical galaxies, especially for early-type spirals. The bulges of later-type spirals, however, can be very different from the expectations of a merger-built bulge (also known as a "classical" bulge). In many cases, the bulge appears to be made of material associated with the disk.

KK04 reviewed the concept of "pseudobulges," referring to galaxy bulges that may have formed by slow secular movement of disk gas to the central regions (also known as disk-like bulges; Athanassoula 2005). The main driving agent for movement of the gas is thought to be bars, which are widespread among spiral galaxies and which exert gravity torques that can move material by redistributing the angular momentum. Inside the corotation resonance, where the bar pattern speed equals the disk rotation rate, gas may be driven into the center to provide the raw material for building up a pseudobulge. KK04 review the evidence for such processes and argue that pseudobulges are a strong indication that secular evolution is an important process in disk-shaped galaxies.

Figure 26 shows the morphologies of both classical bulges and pseudobulges. The four classical bulge galaxies shown in the lower row, M31, NGC 2841, M81, and M104, have bright smooth centers and no evidence for spiral structure or star formation. Classical bulges also tend to have rounder shapes than disks, and can have significant bulge-to-total luminosity ratios as illustrated by M104. Classical bulges are also more supported by random motions than by rotation. Many references to classical bulge studies are given by KK04. Formation mechanisms of such bulges are discussed in detail by Athanassoula (2005).

The two upper rows of Figure 26 are all pseudobulges as recognized by KK04. The first row shows HST wide V-band (filter F606W) images of the inner 1-1.3 kpc of four galaxies, NGC 3177, 4030, 5377, and 1353, in the type range Sa-Sbc. The areas shown account for much of the rise in surface brightness above the inward extrapolation of the outer disk light in these galaxies, and would be considered bulges just on this basis. The HST images show, however, considerable spiral structure, dust, small rings, and likely star formation in these regions, characteristics not expected for a classical bulge. KK04 argue that instead these are pseudobulges that are highly flattened, have a projected shape similar to the outer disk

light, have approximately exponential brightness profiles (Sersic index n≈1-2), and have a high ratio of ordered rotation to random motions. KK04 argue that a low Sersic index compared to n=4 appears to be the hallmark of these pseudobulges, and a signature of secular evolution.

The second row in Figure 26 shows other kinds of pseudobulges discussed by KK04. NGC 6782 and 3081 (two left frames) have secondary bars, and KK04 considered that such features indicate the presence of a pseudobulge because bars are always disk features. In each case, the secondary bar lies inside a nuclear ring.

The other two galaxies in the second row of Figure 26, NGC 128 and 1381, are examples of boxy or box-peanut bulges. These features have been linked to the vertical heating of bars, and if this is what they actually are, then KK04 argue that boxy and box-peanut bulges are also examples of pseudobulges. However, boxy and box/peanut bulges would *not* necessarily be the result of slow movement of gas by bar torques, and subsequent star formation in the central regions, but instead would be related to the orbital structure of the bar itself (Athanassoula 2005).

Recent studies have shown that pseudobulges are the dominant type of central component in disk galaxies. Although originally thought to be important only for late-type galaxies, Laurikainen et al. (2007) showed that pseudobulges are found throughout the Hubble sequence, including among S0-S0/a galaxies, based on sophisticated two-dimensional photometric decompositions. Such galaxies frequently have nuclear bars, nuclear disks, or nuclear rings. Laurikainen et al. also found that bulge-to-total (B/T) flux ratios are much less than indicated by earlier studies, especially for early Hubble types, and that the Sersic index averages $\lesssim 2$ across all types. The lack of gas in S0 and S0/a galaxies complicates the interpretation of their pseudobulges in terms of bar-driven gas flow and subsequent star formation. Instead, Laurikainen et al. link the pseudobulges in early-type galaxies to the

evolution of bars. Laurikainen et al. (2010) also showed that S0s can have pseudobulges if they are stripped spirals, without invoking any bar-induced evolution.

10. Effects of Interactions and Mergers

Galaxy morphology is replete with evidence for gravitational interactions, ranging from minor, distant encounters, to violent collisions and major/minor mergers. Many of the most puzzling and exotic morphologies can be explained by interactions, and even sublimely normal galaxies, like ordinary ellipticals, have been connected to catastrophic encounters. Up to 4% of bright nearby galaxies are involved in a major interaction (Knapen & James 2009). In clusters, other types of interactions may occur, such as gas stripping and truncation of the star-forming disk. In this section, a variety of the types of morphologies that may be considered the results of external interactions are described and illustrated.

10.1. Normal versus Catastrophic Rings

The three types of rings described so far, nuclear, inner, and outer rings, are aspects of the morphology of relatively normal, undisturbed galaxies. Inner rings and pseudorings are found in more than 50% of normal disk galaxies (Buta & Combes 1996), while outer rings and pseudorings are found at the 10% level. The latter rings could be more frequent because their faintness may cause them to go undetected, which is less likely to occur for inner rings. As has been noted, nuclear rings are found at the 20% level (Comerón et al. 2010). The high abundance of these types of ring features suggests that they are mainly products of *internal* dynamics, and in fact all three ring types have been interpreted in terms of internal processes in barred galaxies. The main interpretation of these kinds of rings has been in terms of orbital resonances with the pattern speed of a bar, oval, or

spiral density wave. Resonances are special places where a bar can secularly gather gas owing to the properties of periodic orbits (Buta & Combes 1996). Buta (1995) showed that the intrinsic shapes and relative bar orientations of inner and outer rings and pseudorings supports the resonance interpretation of the features. Schwarz (1981) suggested the outer Lindblad resonance for outer rings and pseudorings, while Schwarz (1984) suggested the inner 4:1 ultraharmonic resonance for inner rings and pseudorings, and the inner Lindblad resonance for nuclear rings. Knapen et al. (1995b) and Buta & Combes (1996) provide further insight into these interpretations.

The resonance idea may only be valid in the case of weak perturbations. In the presence of a strong perturbation, the concept of a specific *resonance radius* can break down, although the idea of a broad *resonance region* could still hold (Contopoulos 1996). Regan and Teuben (2003, 2004) argue that nuclear rings and inner rings are better interpreted in terms of orbit transitions, that is, regions where periodic orbits transition from one major orbit family to another, as in the transition from the perpendicularly-aligned x_2 family to the bar-aligned x_1 family (Contopoulos & Grosbol 1989).

Normal rings have also been interpreted in terms of "invariant manifolds" which emanate from the unstable L_1 and L_2 Lagrangian points in the bar potential (Romero-Gómez et al. 2006, 2007; Athanassoula et al. 2009a,b). This approach has also had some success in predicting the shapes and orientations of inner and outer rings, such as the R_1, R_1', R_1R_2', and R_2' morphologies shown in Figure 14 and Figure 15. A morphology called "rR_1", which includes an oval inner ring and a figure eight-shaped R_1 ring (see NGC 1326 in Figure 15), is especially well-represented by this kind of model. The manifolds are tubes which guide orbits escaping the L_1 and L_2 regions. Note that in this interpretation, outer rings are not necessarily associated with the OLR (Romero-Gómez et al. 2006).

Although the vast majority of the ring-like patterns seen in galaxies are probably of

the resonance/orbit-transition/invariant-manifold type, other classes of rings are known that are likely the result of more catastrophic processes, such as galaxy collisions. Figure 27 shows resonance rings in comparison to three other types: accretion rings, polar rings, and collisional rings (the latter commonly referred to as "ring galaxies"). The three accretion rings shown, in Hoag's Object (Schweizer et al. 1987), IC 2006 (Schweizer et al. 1989), and NGC 7742 (de Zeeuw et al. 2002) are thought to be made of material from an accreted satellite galaxy. For IC 2006 and NGC 7742, the evidence for this is found in *counter-rotation*: the material in the rings counter-rotates with respect to the material in the rest of the galaxies. In Hoag's Object and IC 2006, the accreting galaxy is a normal E system.

Polar rings are also accreted features except that the accreting galaxy is usually a disk-shaped system, most often an S0 (Whitmore et al. 1990). In these cases, the accreted material comes in at a high angle to the plane of the disk. The configuration is most stable if the accretion angle is close to 90^o, or over the poles of the disk system. This limits the ability of differential precession to cause the ring material to quickly settle into the main disk. The polar feature can be a ring or simply an inclined and extended disk. Whitmore et al. (1990) presented an extensive catalogue of probable and possible polar ring galaxies.

The main example illustrated in Figure 27 is NGC 4650A, where the inner disk component is an S0. Galaxies like NGC 4650A have generated considerable research because polar rings probe the shape of the dark halo potential (e. g., Sackett et al. 1994). The galaxies are also special because the merging objects have retained their distinct identities, when most mergers lead to a single object. Brook et al. (2008) link the misaligned disks of polar ring galaxies to the process of hierarchical structure formation in a cold dark matter scenario.

While polar rings are most easily recognizable when both disks are nearly edge-on to us,

cases where one or the other disk is nearly face-on have also been recognized. One example, ESO 235−58 (Buta & Crocker 1993) is shown in the middle-right panel of Figure 27. In this case, the inner component is almost exactly edge-on and shows a planar dust lane, and is likely a spiral rather than an S0. The ring component is inclined significantly to the plane of this inner disk but may not be polar. The faint outer arms in this component caused ESO 235−58 to be misclassified as a late-type barred spiral in RC3. Spiral structure in polar disks has been shown to be excitable by the potential of the inner disk, which acts something like a bar (Theis, Sparke, & Gallagher 2006).

An example where the main disk is seen nearly face-on is NGC 2655 (Sparke et al. 2008). In this case, the polar ring material is seen as silhouetted dust lanes at an uncharacteristic angle to the inner isophotes. NGC 2655 also shows evidence of faint shells/ripples, indicative of a recent merger (section 10.3.3). Sil'chenko & Afanasiev (2004) have discussed NGC 2655 and other similar examples of inner polar rings in terms of the triaxiality of the potential.

Also illustrated in Figure 27 is NGC 660, which was listed as a possible polar ring galaxy by Whitmore et al. (1990). Like ESO 235−58, NGC 660 has an aligned dust lane in its inner disk component, which thus is likely to be a spiral, not an S0. The extraplanar disk is actually far from polar, being inclined only 55^o (van Driel et al. 1995). A recent study of massive stars in the ring is given by Karataeva et al. (2004).

Collisional ring galaxies (Arp 1966; Appleton & Struck-Marcell 1996) are thought to be cases where a larger galaxy suffers a head-on collision with a smaller galaxy down its polar axis. The collision causes an expanding density wave of massive star formation, and multiple rings are possible. Three examples are shown in Figure 27. Theys & Spiegel (1976) have discussed various classes of ring galaxies. Arp 147 (Arp 1966) is an example of type "RE", referring to a sharp elliptical ring with an empty interior. The Cartwheel (Higdon

1995) and the Lindsay-Shapley ring (Arp & Madore 1987) are examples of type "RN", meaning an elliptical ring with an off-center nucleus. Not shown in Figure 27 is a third category called "RK", where a single, large knot lies on one side of the ring, making the system very asymmetric.

Madore, Nelson, & Petrillo (2009) have published a comprehensive atlas of all known likely collisional ring galaxies, many taken from the catalogue of Arp & Madore (1987). Based on this study, only 1 in 1000 galaxies is a collisional ring galaxy. For entry, the Madore et al. atlas requires at least two objects in the immediate vicinity of the ring that might plausibly be the intruder galaxy. Most of the rings are not in cluster environments, however. The atlas also brings attention to several double-ring collisional systems, which have been predicted by numerical simulations (see Struck 2010 for a review). The unusual radial "spokes" in the Cartwheel, a feature not seen in any other collisional ring galaxy, could be related to interactive accretion streams (Struck et al. 1996).

Romano, Mayya, & Vorobyov (2008) present images of several ring galaxies that show the pre-collision stellar disk. They also show that rings are generally delineated by blue knots and that the off-centered nuclei are usually more yellow in color. In addition, some of the companion galaxies show diffuse asymmetric outer light suggesting that they are being stripped.

Figure 27 shows that accretion rings can account for some of the rings seen in nonbarred galaxies. Buta & Combes (1996) argue that a bar is an essential element in resonance ring formation. ESO 235−58 shows that a polar ring-related system can resemble a ringed, barred galaxy. The three collisional rings are all very distinctive from the others.

10.2. Environmental Effects on Star-Forming Disks

Galaxy clusters are excellent laboratories for detecting the effects of environment on galaxy morphology and structure. Frequent mergers and environmental conversion of spirals into S0s are thought to be at the heart of the morphology-density relation, where early-type galaxies dominate cluster cores, and spirals and irregulars are found mainly in the outer regions (Dressler 1980; van der Wel et al. 2010).

The issue of environmental effects has a direct bearing on how we might interpret the Hubble sequence. For example, the continuity of galaxy morphology certainly seems apparent from the discussions in previous sections of this review. The Hubble sequence E-S0-Sa-Sb-Sc-I appears physically significant when total colors, mean surface brightnesses, and HI mass-to-blue light ratios are considered, and the way features are recognized in the classification systems also favors the continuity. Morphological continuity does *not*, however, automatically imply that the galaxy types are in fact ordered correctly. For example, although Hubble placed S0s as a transition type between elliptical galaxies and spirals, this placement has been questioned by van den Bergh (1998, 2009a). Based on a statistical analysis of types given in the RSA, van den Bergh showed that S0 galaxies are typically 0.8-1.0 mag less luminous than E and Sa galaxies, implying that S0 galaxies, on the whole, cannot really be considered intermediate between E and Sa galaxies.[5] The preponderance of S0 galaxies in clusters led to the early suggestion (e.g., Spitzer & Baade 1951; Gunn & Gott 1972; Moore et al. 1996) that some type of external environmental interaction

[5] In contrast to van den Bergh's study of RSA S0 galaxies, Laurikainen et al. (2010) found that the absolute K_s-band magnitudes of a well-defined sample of S0s are similar to those of early-type spirals in the OSUBSGS sample. The sample was mostly drawn from RC3 and includes some galaxies classified as ellipticals in RC3 and as S0s in the RSA (see section 12).

was responsible for stripping a spiral galaxy of its interstellar medium. If this actually occurred, then, as suggested by van den Bergh (2009a), this could imply that S0 galaxies have lost a substantial fraction of their spiral mass due to interactions. Alternatively, van den Bergh (2009b) argues that stripping of a lower luminosity, late-type spiral should be easier than stripping of a higher luminosity, early-type spiral, which could also account for the luminosity difference. In an examination of the environment of S0 galaxies, van den Bergh (2009b) found no significant difference in the average luminosities, flattenings, or distribution of S0 subtypes in clusters, groups, or the field, indicating that some S0s develop as a result of internal effects, such as the influence of an active galactic nucleus.

Barway et al. (2011) noted that lower luminosity S0s have a higher bar fraction than higher luminosity S0s (83% versus 17%), suggesting that the two groups form in different ways (see also Barway et al. 2007). These authors suggest that faint S0s are stripped late-type spirals, which are known to have a high bar fraction (Barraza et al. 2008).

Environmental effects in clusters do not always have to involve drastic transformations in morphology. Sometimes the effects are more subtle. Figure 28 shows several spiral galaxies that are also members of the Virgo Cluster. These galaxies highlight processes that affect the star-forming disk while leaving the older stellar disk relatively unaffected. NGC 4580 and 4689 are galaxies having a patchy inner disk and a smooth outer disk, called "Virgo types" by van den Bergh et al. (1990). These objects suggest that the environment of such galaxies has somehow truncated the star-forming disk, with a greater concentration of truncated disks toward the cluster core. Similar results are obtained from observations of the HI gas disks of Virgo cluster galaxies (e.g., Giovanelli & Haynes 1985; Cayatte et al. 1994; Chung et al. 2009).

Koopmann & Kenney (2004) summarize the results of an extensive survey of Hα emission from Virgo Cluster galaxies, and identify different categories of environmentally-

influenced star formation characteristics based on Hα imaging. The blue light images of examples of each category are included in Figure 28, and show how the subtleties are manifested in regular morphology. Using a sample of isolated spiral galaxies to define "normal" star formation, Koopmann and Kenney defined several categories of Virgo spiral galaxy star-forming disks: Category "N" refers to disks whose star formation is within a factor of three of the normal levels. "E" cases have star formation enhanced by more than a factor of three compared to normal. "A" cases are "anemic" spirals (section 6.4) having star formation reduced by more than a factor of 3 compared to normal. "T/N" refers to galaxies where the star-forming disk is sharply cut off, but inside the cutoff, the star formation levels are normal (the [s] means truncation is severe). One of these, NGC 4580, is so unusual that Sandage & Bedke (1994) classify it as Sc(s)/Sa, where the Sc part is the inner disk and the Sa part is the outer disk. In "T/A galaxies", the inner star-formation is at a low level, as in anemic cases, while in "T/C" galaxies, most of the star formation is confined within the inner 1 kpc. Koopmann and Kenney found that the majority of Virgo Cluster spiral galaxies have truncated star-forming disks.

The idea is that the interstellar medium (ISM) of a cluster galaxy can interact with the intra-cluster medium (ICM), stripping the ISM (via ram pressure; Gunn and Gott 1972) but leaving the stellar disk intact. Truncated gas and star-forming disks result because ram-pressure stripping is more severe in the outer parts of galaxies (e. g., Book and Benson 2010 and references therein). In Virgo, most galaxies with truncated star-forming disks have relatively undisturbed stellar disks and normal to slightly enhanced inner disk star formation rates, suggesting that ICM-ISM stripping is the main mechanism in the reduction of their star formation rates. The cases found to have relatively normal or enhanced star formation rates are preferentially located in the outer parts of the cluster and likely have never visited the core region. Only galaxies which go near the center get significantly stripped. However, tidal effects also contribute to morphological changes. Several galaxies,

including many of the T/C class, display peculiarities consistent with tidal effects, such as nonaxisymmetric circumnuclear star formation, shell features (e.g., NGC 4424 in Figure 28), and enhanced inner star formation rates.

A recent study by Yagi et al. (2010) provides dramatic and clear evidence of disk gas stripping in galaxies thought to be relatively new arrivals to the core region of the Coma Cluster. Using deep Hα imaging, these authors detected ionized gas in clouds that are mostly outside the main disk of a dozen Coma galaxies. Three distinct morphologies of the distributions of these clouds were found: (1) connected clouds that blend with disk star formation; (2) long, connected lines of clouds that extend from a central gas knot but are not related to the disk light; and (3) clouds completely detached from the main disk. Examples of these categories are illustrated in Figure 29. Yagi et al. interpret them in terms of an evolutionary gas-stripping sequence where category (1) galaxies are in an earlier phase of stripping while the category (3) galaxies are in the most advanced phase. It is likely that large disk galaxies in Coma would be completely stripped eventually because of the cluster's high ICM density and broad velocity distribution. The same process seen in Coma likely occurs in Virgo but is only partial for the large spirals owing to the lower ICM density and velocities in Virgo (Koopmann & Kenney 2004).

10.3. Interacting and Peculiar Galaxies

10.3.1. Tidal Tails, Arms, and Bridges

It is perhaps fitting that the first major spiral galaxy discovered was in the interacting pair M51 (section 2). Numerical simulations (Salo & Laurikainen 2000a,b) have shown that both parabolic and bound passages of the companion, NGC 5195, can explain the observed morphology and other characteristics of the system. It turns out that M51 defines a class

of interacting systems known as M51-type pairs. Figure 30 shows an example in the pair NGC 2535-6. In each case, the larger component has a strong two-armed spiral, with one arm appearing "drawn" to the smaller companion. An extensive catalogue of M51-type pairs is provided by Jokimaki et al. (2008).

Other distant encounters can produce tidal tails or bridges of material between galaxies (top row, Figure 30). NGC 4676, also known as the "Mice," is a pair of strongly interacting galaxies where a very extended tidal tail has formed in one component. The strongly-interacting pair NGC 5216/18 has developed a bright connecting bridge of material, and each component shows tidal tails. The evolution of this system, and the role of encounters on bar formation, is described by Cullen et al. (2007).

10.3.2. Dust-Lane Ellipticals

Figure 30 also shows several examples of morphologies that may result from minor mergers of a small galaxy with a more massive, pre-existing elliptical galaxy. Bertola (1987) brought attention to the unusual class of *dust-lane ellipticals*, where an otherwise normal elliptical galaxy shows peculiar lanes of obscuring dust. It was de Vaucouleurs's personal view that "if an elliptical shows dust, then it's not an elliptical!" However, Bertola showed that an unusual case like the radio elliptical galaxy NGC 5128, where a strong dust lane lies along the *minor axis* of the outer light distribution, is simply the nearest example of a distinct class of objects. Further study showed that dust-lane ellipticals come in several varieties. The minor axis dust lane type appears most common, but cases of alignment along the major axis of the outer isophotes (major axis dust lanes) as well as cases of misalignment are also known (see the upper left panels of Figure 30). The origin of these very regular dust lanes is thought to be a merger of a gas-rich companion (e.g., Oosterloo et al. 2002). The regularity of the dust lanes suggests that the mergers are in advanced states.

10.3.3. Shell/Ripple Galaxies

The two lower left frames of Figure 30 show examples of galaxies having "shells,", or faint, arc-shaped brightness enhancements of varying morphology. They were first discovered on deep photographs by Malin (Malin & Carter 1980), and appeared to be associated mainly with elliptical galaxies. In fact, the first examples, NGC 1344 and 3923, are classified in catalogues as ordinary ellipticals because the shells are not detectable on photographs of average depth. Once the class was recognized, a detailed search led to other examples which were listed by Malin & Carter (1980, 1983). The term "shells" implies a particular three-dimensional geometry that Schweizer & Seitzer (1988) argued imposes a prejudice on the interpretation of the structures. They proposed instead the alternate term "ripples," which implies less of a restrictive geometry.

The explanation of shell/ripple galaxies is one of the great success stories in galactic dynamics (see review by Athanassoula & Bosma 1985). Shells are thought to be remnants of a minor merger between a massive elliptical and a lower mass disk-like galaxy. The main requirements are that the disk-shaped galaxy be "cold", or lack any random motions, and that the potential of the elliptical galaxy should be rigid, meaning the elliptical is much more massive than its companion. The smaller galaxy's stars fall into the center of the galaxy and phase wrap, or form alternating outward-moving density waves made of the disk galaxy's particles near the maximum excursions of their largely radial orbits in the rigid potential. Many, but not all, of the main properties of shell Es can be explained by this model. Other issues concerning shell galaxies are reviewed by Kormendy and Djorgovski (1989).

Taylor-Mager et al. (2007; see their Figure 2) have proposed a simple classification of interacting systems that highlights different interaction classes. A pre-merger (type pM) includes two interacting galaxies that are sufficiently far apart to suffer little apparent

distortion. A minor merger (mM) is two galaxies showing evidence of merging, but one component is much smaller than the other. A major merger (M) has two comparable brightness galaxies in the process of merging, while a merger remnant (MR) is a state sufficiently advanced that the merging components are no longer distinct.

10.3.4. Ultra-Luminous Infrared Galaxies

Related to interacting systems are the infrared-bright galaxies first identified by Rieke & Low (1972) based on 10μm photometry. From studies based on the Infrared Astronomical Satellite (IRAS), Sanders & Mirabel (1996) classified a galaxy as a "luminous infrared galaxy" (LIRG) if its luminosity in the 8-1000μm range is between 10^{11} and 10^{12} $L_\odot$. If the luminosity in the same wavelength range exceeds 10^{12} $L_\odot$, then the object is called an "ultra-luminous infrared galaxy" (ULIRG). Detailed studies have shown that at high redshifts, LIRGS and ULIRGS are a dominant population of objects (see discussion in Pereira-Santaella et al. 2010).

The morphologies of nine ULIRGS were studied using HST B and I-band images by Surace et al. (1998). Their montage of six of these objects is shown in Figure 31. In every case there are clear signs of interactions, and all are likely linked to mergers or mergers in progress. Several, like Mk 231, have bright Seyfert nuclei. Arribas et al. (2004) obtained extensive imaging of local LIRGS, and found a similar high proportion of strongly interacting and merging systems.

The merger rate is considered one of the most important parameters for understanding galaxy evolution. It has been difficult to estimate, and issues connected with it are discussed by Jogee et al. (2009; see also Conselice 2009). A merger is considered major if it involves a companion ranging from 1/4 to approximately equal mass to the main galaxy. A major

merger of two spiral galaxies can destroy both disks and lead to an $r^{\frac{1}{4}}$ law profile remnant through violent relaxation. Minor mergers involve companions having 1/10 to 1/4 the mass of the main galaxy. Both types of mergers, while in progress, can lead to many specific morphological features such as highly distorted shapes, tidal tails and bridges, shells and ripples, and warps. Even some bars and spiral patterns are thought to be connected to interactions, and especially galaxies with a double nucleus are thought to be mergers. As discussed in section 10.1, mergers or collisions may also be at the heart of rare morphologies such as ring and polar ring galaxies. Using visual classifications of merger types, Jogee et al. (2009) estimate that 16% of high mass galaxies have experienced a major merger, while 45% have experienced a minor merger, during the past 3-7Gyr (z=0.24-0.80).

10.4. Warps

A warp is an apparent bend or slight twist in the shape of the disk of a spiral galaxy (see Sellwood 2010 and references therein). In a warp, stars and gas clouds move in roughly circular orbits, but the orientation of these orbits relative to the inner disk plane changes with increasing radius. Warps are most easily detected in edge-on galaxies because the bending of the outer orbits makes the galaxy look like an integral sign. Although often most pronounced in an HI map, warps can be seen in ordinary optical images of edge-on galaxies. Figure 32 shows three galaxies having strong optical warping of the disk plane. In two of the galaxies, the bright inner disk is unwarped, while a fainter and thicker outer disk zone is twisted relative to the inner disk. In UGC 3697, the warping is exceptionally visible. In general, optical warping is less severe than HI warping.

Warping is a very common aspect of spiral galaxies (e.g., Binney 1992) and has been interpreted in terms of perturbations (gaseous infall or interactions) that trigger bending instabilities (e.g., Revaz & Pfenniger 2007). Garcia-Ruiz, Sancisi, & Kuijken (2002)

estimated HI warp angles, the angle between the inner disk plane and the assumed linear warping zone, to range from nearly 0^o to more than 30^o. A useful summary of previous warp studies is provided by Saha et al. (2009), who examine warp onset radii in mid-IR images. The theory of warps is reviewed by Sellwood (2010).

10.5. The Morphology of Active Galaxies

The morphology of active galaxies (also called "excited" galaxies by van den Bergh 1998) is important to consider because of a possible link between morphological features and the fueling of the active nucleus. Early studies showed a preponderance of ring, pseudoring, and bar features in Seyfert galaxies that suggested the link was bar-driven gas flow (Simkin, Su, & Schwarz 1980). Several examples of the morphology of Seyfert and other active galaxies are shown in Figure 33. The activity classifications are based mainly on spectroscopy, not on morphology, and are described by Veron-Cetty & Veron (2006).

A detailed study of active galaxy morphologies by Hunt & Malkan (1999) provided similar results to the early studies. These authors examined the morphologies of a large sample of galaxies selected on the basis of their 12μm emission, and found that outer rings and inner/outer ring combinations are 3-4 times higher in Seyfert galaxies than in normal spirals. In contrast, bars were found to occur with the same frequency ($\approx$69%) in Seyferts as in normal spirals, while for HII/starburst galaxies, the frequency was much higher (>80%). Although outer rings are found mostly in barred galaxies, bars do not promote the nuclear activity of Seyfert galaxies. Hunt & Malkan (1999) interpret this inconsistency in terms of timescales: it takes roughly 3×10^9 yr for a closed outer ring to form, a timescale during which a bar may weaken or dissolve. Because of this, a high ring frequency in Seyferts would indicate an advanced evolutionary state. Related to the same issue, Comerón et al. (2010) found that nuclear rings do not correlate with the presence of nuclear activity.

The study of Hunt & Malkan (1999) used mostly RC3 classifications to deduce the bar fraction in active galaxies. These visual classifications are based on blue light images and hence dust could effectively obscure some bars. Knapen et al. (2000) used high resolution near-IR images of well-defined samples and quantitative bar detection methods to deduce that bars are more frequent in Seyfert galaxies than in a control sample of non-active galaxies: 79% ± 7.5% versus 59% ± 9% (see also Laine et al. 2002). Laurikainen, Salo, & Buta (2004) came to a similar conclusion for 180 galaxies in the OSUBSGS, based on near-IR H-band images. The former studies used ellipse fits to identify bars, while Laurikainen et al. used Fourier analysis.

McKernan, Ford, & Reynolds (2010) also consider outer rings and pseudorings as probes of models of AGN fueling from interactions and mergers. The idea is that a closed outer ring takes a long time to form and is very fragile, being sensitive to interactions and changes in the bar pattern speed (e.g., Bagley et al. 2009). An interaction can change a closed outer ring into a pseudoring and could possibly destroy the ring. Thus, rings are probes of the interaction history of active galaxies. McKernan et al. found no difference between the AGN found in ringed galaxies and those found in galaxies without rings. But in those with rings, recent interactions can be ruled out and activity may be tied to short-term internal secular evolutionary processes.

Bahcall et al. (1997) presented HST images of 20 luminous, low redshift quasars observed with a wide V-band filter. Figure 34 is reproduced from their paper and shows images of the host galaxies after removal of most of the quasar light. The images show a variety of morphologies, including ellipticals, interacting pairs, systems with obvious tidal disturbances, and normal-looking spirals. An example of the latter is PG1402+261 (z=0.164), which is type (R'_1)SB(rs)a based partly also on the image shown in Figure 7 of Bahcall et al. Based on the number of hosts showing signs of interactions, as well as the

number of companions, Bahcall et al. conclude that interactions may trigger the quasar phenomenon.

10.6. The Morphology of Brightest Cluster Members

Matthews, Morgan, & Schmidt (1964) observed the optical morphologies of the radio sources identified with the brightest members of rich galaxy clusters. They found that the most common form was what Morgan (1958) called a "D" galaxy, meaning a galaxy having an elliptical-like inner region surrounded by an extensive envelope (see discussion in van den Bergh 1998). Although these superficially resembled Hubble's S0s, none were found having a highly-elongated shape, implying that the galaxies are not as highly flattened as typical S0s. Another characteristic of the cluster D galaxies was their very large linear size and exceptional luminosity, much larger than a typical cluster member. To denote these extreme objects in the Morgan system, the prefix c was added as in the old classification of supergiant stars. Even today, Morgan's notation "cD" is used to describe these supergiant galaxies which are generally considered outside the scope of the Hubble system.

The most detailed study of the photometric properties of brightest cluster members (BCMs) was made by Schombert (1986, 1987, 1988; see also various references therein). The main BCM types Schombert considered were gE (giant ellipticals), D, and cD, distinguished mainly from the appearance of profile shape. D galaxies are larger and more diffuse with shallower profiles than gE galaxies, while a cD galaxy is the same as a D galaxy but with a large extended envelope (Schombert 1987). cD envelopes can extend to 500 kpc or more. Kormendy & Djorgovski (1989) argue that only cD galaxies are sufficiently physically distinct from ellipticals to merit being a separate class, and recommended that the "D" class not be used.

Two cD galaxies and two gE galaxies are shown in Figure 35. To give an idea of the scale of these objects, the vertical dimension of the frames corresponds to 201, 232, and 132 kpc for (left to right) UGC 10143 (A2152), NGC 4874/89 (A1656), and NGC 6041 (A2151), respectively. The cD classification of NGC 4874 is due to Schombert (1988), and one can see in Figure 35 that it is much larger and has a shallower brightness profile than nearby NGC 4889. The cD envelope is detected as an excess of light in the outer regions relative to a generalized brightness profile, and may not even be the light that leads to the visual classification of cD.

Based on structural deviations such as the large radii, shallow profile slopes, and bright inner regions, Schombert (1987) concluded that BCMs fit well with the predictions of merger simulations, including accretion and "cannibalism" of smaller cluster members. Properties of cD envelopes (as separated photometrically from the parent galaxy) may suggest a stripping process for their formation (Schombert 1988).

As noted in section 5.1, many BCMs in RC3 received the classification E^+, suggesting that the characteristic brightness profiles give a hint of an envelope interpreted as an incipient disk. The distribution of axial ratios of cDs actually is flatter on average than normal ellipticals (Schombert 1986), but it is not clear that the perceived envelopes in BCM E^+ galaxies are actually as flattened as a typical disk. A local example of a gE galaxy is M87, classified as type E^+0-1 by de Vaucouleurs.

11. Star Formation Morphologies

11.1. Hα Imaging

The standard waveband for galaxy classification, the B-band, is sensitive enough to the extreme population I component that the degree of resolution of spiral arms into

star-forming complexes is part of the classification. The B-band, however, also includes a substantial contribution from the older stellar background. One way to isolate only the star-forming regions in a galaxy is imaging in Hα, which traces HII regions. Apart from showing the distribution of star formation (modified by extinction), Hα imaging also traces the rate of global photoionization, which in turn directly traces the rate of formation of stars more massive than about $10M_{\odot}$ (Kennicutt, Tamblyn, & Congdon 1994). The initial mass function (IMF), either assumed or constrained in some way (using, for example, broadband colors), allows Hα fluxes to be converted to the total star formation rate over all stellar masses.

Hα imaging often shows well-organized patterns of HII regions that follow structures like spiral arms and especially rings. Images of six early-to-intermediate-type ringed galaxies are shown in Figure 36 (Crocker, Baugus, & Buta 1996). The way Hα imaging usually works is a galaxy is imaged in or near its redshifted Hα wavelength, and then in a nearby red continuum wavelength. The net Hα image is the difference between the Hα image and the scaled red continuum image. Often, the Hα filter used is broad enough to include emission from [NII] 6548 and 6584. For each of the galaxies shown in Figure 36, the left image is the red continuum image, while the right image is the net Hα image. Of the four barred spirals shown (NGC 1433, 7329, 6782, and 7267), three show no HII regions associated with the bar. These three (NGC 1433, 7329, and 6782) all have conspicuous inner rings which are lined with HII regions. As shown by Crocker, Baugus, & Buta (1996), the distribution of HII regions around inner rings is sensitive to the intrinsic shape of the ring. When the ring is highly elongated, the HII regions concentrate around the ends of the major axis (which coincide with the bar axis; NGC 6782), while when the ring is circular, the HII regions are more uniformly spread around the ring (NGC 7329). Inner ring shapes do not correlate well with maximum relative bar torques in a galaxy (dVA), but Grouchy et al. (2010) have shown that when local forcing is considered instead, ring shapes and bar

strengths are well-correlated.

The case of NGC 7267 is different in that most of its Hα emission is concentrated in the bar. Martin & Friedli (1997) have argued that star formation along galactic bars could provide clues to gas flow in the inner regions of galaxies and the fueling of starbursts and AGN. These authors present models which suggest an evolution from a pure Hα bar, to an Hα bar with ionized gas in the center, to a gas-poor bar with strong nuclear or circumnuclear star formation. This suggests that the bar of NGC 7267 is younger than those in NGC 1433, 7329, and 6782.

The two other galaxies shown in Figure 36 are nonbarred or only weakly-barred. NGC 6935 is an interesting case where a nonbarred galaxy has a strong ring of star formation. Grouchy et al. (2010) found that the star formation properties of inner rings, but not the distribution of HII regions, are independent of the ring shapes and bar strengths in a small sample. The case of NGC 7702 is different from the others. This is a late S0 (type S0$^+$) showing a very strong and largely stellar inner ring. The ring shows little ionized gas and appears to be in a quiescent phase of evolution.

11.2. Ultraviolet Imaging

The best global imaging of nearby galaxies at ultraviolet wavelengths has been obtained with the *Galaxy Evolution Explorer* (GALEX, Martin et al. 2005), which provided detailed images of galaxies of all types at wavelengths of 0.225 and 0.152μm. These images reveal young stars generally less than ≈100 Myr old but are affected by dust extinction. There is a strong correlation between the UV morphology and the Hα morphology (Figure 37). Like Hα, UV fluxes from galaxies can be used to estimate star formation rates once extinction is estimated, and are particularly sensitive to the ratio of the present to the average past

star formation rate. UV imaging is an effective way of decoupling the recent star formation history of a galaxy from its overall, long-term star formation history.

Figure 38 shows near-UV (0.225μm) images of eight galaxies over a range of Hubble types. The two earliest types, NGC 1317 and 4314 (both Sa) show a near-UV morphology dominated by a bright circumnuclear ring of star formation. The SB(r)b galaxy NGC 3351 shows a conspicuous inner ring of star formation and little emission from its bar region. In contrast, the SBc galaxy NGC 7479 shows strong near-UV emission from its bar. The late-type galaxies NGC 628 [type SA(s)c] and NGC 5474 [type SA(s)m] are typical of their types, but most interesting is NGC 4625. A key finding of GALEX was extended UV emission well beyond the optical extent of some galaxies. NGC 4625 is an example where the main optical part [type SABm] is only a small fraction of the extent of the UV disk (Gil de Paz et al. 2005).

The final object shown in Figure 38 is NGC 5253, a basic example of what de Vaucouleurs classified as I0 (section 5.3). The inner region is a bright boxy zone of star formation, and even the extended disk is prominent.

11.3. Atomic and Molecular Gas Morphology

Related to star formation morphologies are the distributions of atomic and molecular gas. Far from being randomly-distributed clouds of interstellar material, atomic and molecular gas morphologies can be highly organized, well-defined patterns. Recent high quality surveys have provided some of the best maps of these distributions in normal galaxies. Atomic hydrogen is mapped with the 21cm fine structure emission line, which has the advantage of not being affected by extinction and for being sufficiently optically thin in general to allow total HI masses to be derived directly from HI surface brightness maps.

In addition, HI maps provide information on the kinematics and dynamics of the ISM, as well on the existence and distribution of dark matter in galaxies. Molecular hydrogen is generally mapped using the ^{12}CO J=1-0 rotational transition at a wavelength of 2.6mm, under the assumption that CO and hydrogen mix in a roughly fixed proportion.

Although numerous maps have been made of the HI distribution in nearby galaxies, the most sophisticated and detailed survey made to date is the "The HI Nearby Galaxies Survey" (THINGS, Walter et al. 2008). The earliest surveys had shown that HI is a tracer of spiral structure in galaxies, and the THINGS provides some of the highest quality maps revealing this correlation as well as other characteristics. From a morphological point of view, HI maps tend to reveal: (1) enhanced surface brightness in star-forming features such as spiral arms, rings, and pseudorings; (2) extended gaseous disks, such that the HI extent can exceed the optical extent by several times; and (3) supernova-driven and star-formation driven, wind-blown holes.

Figure 39 shows the HI morphologies of eight THINGS galaxies ranging from the Sab galaxy NGC 4736 to the Sm galaxy DDO 50 (Holmberg II). Bright Sc galaxies like NGC 628 (M74) and NGC 5236 (M83) show HI distributions that extend well beyond the optical disks. These extended patterns can include large spirals as in NGC 628. In M81 and M83, the HI traces the optical spiral structure well. Large rings or pseudorings are seen in NGC 2841 and NGC 4258, while M81 shows an intermediate-scale ring of gas that is much less evident optically. The bright star-forming inner ring in NGC 4736 is well-defined and easily distinguished in HI, but the galaxy's diffuse stellar outer ring is more of an asymmetric spiral zone.

Most interesting in HI maps are the obvious holes where there appears to be a deficiency of neutral gas compared to surrounding regions. Especially large holes are seen in the HI morphology of the late-type dwarf DDO 50. These holes are thought to be regions

cleared by the stellar winds and explosions of massive stars contained or once contained within them. The holes are 100pc to 2kpc in size, and have different systematic properties in early and late-type galaxies in the sense that holes may last longer in late-type dwarfs owing to the lack of serious shear due to strong differential rotation (Bagetakos et al. 2009). Holes may also be found outside the standard isophotal optical angular diameter.

The dwarf galaxy DDO 154 shown in Figure 39 has one of the largest ratios of HI to optical diameter, a factor of 6 at least according to Carignan & Purton (1998), who also estimated that 90% of the mass of the galaxy is in the form of dark matter. The HI and optical morphologies bear little resemblance to one another. Another example of strongly uncorrelated HI and optical morphologies is NGC 2915, a very gas-rich galaxy whose optical morphology is a blue compact dwarf while its at least 5 times larger HI morphology includes a prominent outer spiral with no optical counterpart (Meurer et al. 1996), leading to the concept of a purely "dark spiral." Bertin & Amorisco (2010) consider a general intepretation of such large outer HI spirals, especially those seen in galaxies like NGC 628 and NGC 6946: the spirals represent short trailing waves that carry angular momentum outwards from corotation and, at least in the gaseous component, penetrate a normal barrier at the OLR of the stellar disk pattern and go far out into the HI disk. The short trailing waves are thought to excite the global spiral arms seen in the main optical body of the galaxy (where the prominent optical spirals of NGC 628 and NGC 6946 are found). How NGC 2915 fits into this picture is unclear since the main stellar body of this galaxy is not a grand-design spiral.

Galaxies whose HI disks do not extend much beyond the optical light distribution are also of interest. NGC 4736 in Figure 39 is an example. The large, nearby ringed barred spiral NGC 1433 was found by Ryder et al. (1996) to have neutral hydrogen gas concentrated in its central area, its inner ring, and in its outer pseudoring, with no gas

outside the visible disk light and a lower amount of gas in the bar region compared to the ring regions. Higdon et al. (1998) showed that in the ringed, barred spiral NGC 5850, neutral gas is concentrated in the inner ring and in the asymmetric outer arm pattern, with little or no emission detected outside this pattern. The asymmetry led Higdon et al. to propose that NGC 5850 has possibly experienced a high speed collision with nearby NGC 5846.

In galaxy clusters, it is well-known that environmental effects can truncate an HI disk so that it is *smaller* than the optical disk light. This is dramatically illustrated in the high resolution VLA HI maps of Virgo Cluster galaxies by Chung et al. (2009), who found that galaxies within 0.5 Mpc of the cluster core have severely truncated HI disks typically less than half the size of the optical standard isohotal diameter, D_{25}. A variety of earlier studies had already shown these galaxies to be HI-deficient compared to field galaxies of similar types. As noted in section 10.2, an interaction between a cluster galaxy's ISM and the intra-cluster medium can account for these unsual modifications of HI morphology. Chung et al. also provide evidence for this interaction in some morphologies that appear to be gas stripping in progress.

The Berkeley-Illinois-Maryland Survey of Nearby Galaxies (BIMA SONG; Regan et al. 2001; Helfer et al. 2003) provided some of the highest quality CO maps of normal galaxies. CO emission is often seen in intermediate (Sab-Sd) galaxies, which have a high enough gas content and metallicity to allow the ^{12}CO J=1-0 2.6mm emission line to be detectable. The CO distributions of eight such galaxies from this survey are shown in Figure 40. These display some of the range of molecular gas morphologies seen. CO traces the inner spiral arms of NGC 628, 1068, and 4535, and is seen along the bar of NGC 2903. A common CO morphology is a large-diameter ring of giant molecular clouds (GMCs), without a central CO concentration, as seen in NGC 2841 and 7331. The rings are the

peaks of exponentially-declining distributions. The coherent inner molecular gas ring in NGC 7331 appears more like a typical resonance ring, and has an estimated molecular gas mass of 3.4×10^9 $M_\odot$ (Regan et al. 2004). The CO distribution in NGC 2403 appears to be concentrated in individual GMCs, with little diffuse emission, while that in NGC 3351 is characterized by a small central bar aligned nearly perpendicular to the galaxy's primary bar. Helfer et al. (2003) show that the Milky Way, M31, and M33 have CO morphologies that are consistent with the range of morphologies found by BIMA SONG.

12. Infrared Observations: Galactic Stellar Mass Morphology

Infrared observations have considerable advantages over optical observations of galaxies. While traditional B-band images are sensitive to dust and extinction (both internal and external), the effects of extinction in the near- and mid-IR are much less, and become virtually negligible at 3.6μm. Spiral galaxies imaged at wavelengths successively longer than B-band become progressively smoother-looking, not only due to the reduced effect of extinction, but also to the de-emphasis of the young blue stellar component. The combination of these effects has led to the popular idea that IR imaging reveals the "stellar backbone" of galaxies, i. e., the distribution of actual stellar mass (e. g., Rix & Rieke 1993; Block et al. 1994). Thus, infrared imaging has become a staple for studies of the gravitational potential and stellar mass distribution in galaxies (e. g., Quillen, Frogel, & González 1994), and for the quantification of bar strength from maximum relative gravitational torques (e.g., Buta & Block 2001; Laurikainen & Salo 2002).

Infrared imaging has also revealed interesting outer structures such as the large outer red arcs seen in M33, which have been interpreted by Block et al. (2004b) to be swaths of extremely luminous carbon stars formed from external accretion of low metallicity gas. Power spectrum analysis of the IR structures in classical spirals has been used to detect

azimuthal "star streams" and to evaluate the role of turbulence on star formation and spiral structure (Block et al. 2009 and references therein).

Near-infrared imaging from 0.8-2.2μm can be successfully obtained from groundbased observatories but with the serious drawback that the brightness of the sky background increases substantially over this range. As a result, it has not been possible to achieve a depth of exposure at, for example, 2.2μm comparable to the kinds of depths achievable at optical wavelengths without excessive amounts of observing time. The first major near-IR survey designed for large-scale morphological studies was the Ohio State University Bright Spiral Galaxy Survey (OSUBSGS, Eskridge et al. 2002), which included optical $BVRI$ and near-IR JHK images of 205 bright galaxies of types S0/a to Sm in a statistically well-defined sample selected to have total blue magnitude $B_T \leq 12.0$ and isophotal diameter $D_{25} \leq 6'.5$. This survey allowed a direct demonstration of how galaxy morphology actually changes from optical to near-IR wavelengths, not merely for a small, selected sample of galaxies, but for a large sample covering all spiral subtypes. The main near-IR filter used in this survey was the H-band at 1.65μm.

The OSUBSGS was later complemented by the *Near-Infrared S0 Survey* (NIRS0S, Laurikainen et al. 2005, 2006, 2007, 2009, 2010; Buta et al. 2006), a K_s-band imaging survey of 174 early-type galaxies in the type range S0$^-$ to Sa, but mostly including S0s, some of which were misclassified as ellipticals in RC3. NIRS0S images are deeper than OSUBSGS near-IR images owing to the use of larger telescopes and longer on-source times. Although S0 galaxies are dominated by old stars and are usually smooth even in blue light images, the K_s band was chosen to complement the OSUBSGS sample of spirals in order to make a fair comparison between bar strengths and bulge properties of S0s and spirals. Also, S0 galaxies are not necessarily dust-free, and near-IR imaging is still necessary to penetrate what dust they have. NIRS0S has led to several important findings about S0

galaxies: (1) a class of S0s, not previously recognized, having prominent lenses but very small bulges that are more typical of Sc galaxies than of earlier type spirals (example: NGC 1411, Laurikainen et al. 2006); (2) considerable evidence that S0 galaxies have pseudobulges just as in many spirals (Laurikainen et al. 2007). While the bulges of the latter are likely to be made of rearranged disk material in many cases (section 9), those in S0s are likely to be related to the evolution of bars. S0 bulges tend to be nearly exponential (Sersic index $n \leq 2$), are supported against gravity by rotation rather than random motions, and often include clear inner disks; (3) good correlations between bulge effective radii, r_e, and disk radial scalelength, h_R, as well as between the K_s-band absolute magnitudes of the bulge and disk, suggest that S0 bulges are not formed from hierarchical mergers, implying that S0s could be stripped spirals, although the lower bar fraction in S0s suggest that this is in conjunction with evolution due to bars and ovals; (4) 70% of S0-S0/a galaxies have ovals or lenses, suggesting that bars have been weakened in such galaxies over time; and (5) not only bulges, but also disks of S0s are similar to those in S0/a-Scd spirals.

The *Two-Micron All-Sky Survey* (2MASS, Skrutskie et al. 2006) provided near-IR JHK_s images of a much larger galaxy sample than either the OSUBSGS or NIRS0S, although these images lack the depth of the OSUBSGS and NIRS0S images in general. 2MASS provided considerable information on near-infrared galaxy morphology, which led to the extensive *2MASS Large Galaxy Atlas* (Jarrett et al. 2003).

The best imaging of galaxies at mid-IR wavelengths has been obtained with the *Spitzer Space Telescope* using the Infrared Array Camera (IRAC, Fazio et al. 2004) and 3.6, 4.5, 5.8, and 8.0μm filters. The 3.6 and 4.5μm filters provide the most extinction-free views of the stellar mass distribution in galaxies, while the 5.8 and 8.0μm filters reveal the interstellar medium (ISM) (Pahre et al. 2004). The loss of coolant in 2008 prevented further observations with the 5.8 and 8.0μm filters, but the 3.6 and 4.5μm filters could still

be used. This led to the *Spitzer Survey of Stellar Structure in Galaxies* (S^{4}G, Sheth et al. 2010), a 3.6 and 4.5μm survey of 2,331 galaxies of all types closer than 40Mpc. These wavelengths sample the Rayleigh-Jeans decline of the stellar spectral energy distribution of all stars hotter than 2000K. S^{4}G images shown here are from Buta et al. (2010a) and are based on pre-survey archival images processed in the same manner as survey images. *Spitzer* observations have a very low background compared to groundbased near-IR observations, and thus IRAC images are the deepest galaxy images ever obtained in the IR.

Figure 41 compares images of M51 at four wavelengths: the GALEX 0.15μm band, the B-band (0.44μm), the near-infrared K_s band (2.2μm), and the IRAC 3.6μm band. Only the B and K_s-band images are from groundbased observations. The GALEX image reveals the extensive star formation in the spiral arms, and the complete absence of star formation in the companion NGC 5195 as well as in the complex tidal material north of the companion. The star formation in the arms is more subdued in the B-band, and almost completely subdued in the K_s-band. The arms are so smooth in the K_s band that the galaxy resembles an Sa or Sab system. (The B-band type is Sbc.) Surprisingly, this is not the case in the 3.6μm image whose considerably greater depth compared to the K_s-band image is evident. The spiral arms in the 3.6μm band are lined by numerous resolved objects, many of which are correlated with the star-forming regions seen in the B-band. This is dramatically seen also in the SB(s)cd galaxy NGC 1559 (Figure 42), where an IRAC 3.6μm image is compared with a B-band image. These show that resolved features in the deep 3.6μm image are well-correlated with B-band star-forming complexes. Thus, mid-IR 3.6μm images are *not* completely free of the effects of the extreme population I stellar component (see discussions in Block et al. 2009 and Buta et al. 2010a).

A sampling of S^{4}G images as compared to B-band images for the same galaxies from the dVA is shown in Figure 43. The four galaxies shown, NGC 584, 1097, 628, and 428,

have dVA types of S0$^-$, SBb, Sc, and Sm, respectively, thus covering almost the entire Hubble-de Vaucouleurs sequence. Although the very dusty interacting system NGC 1097 looks slightly "earlier" at 3.6μm, these images show again that on the whole the morphology in the two wavebands is very similar. The same is seen for other galaxies described by Buta et al. (2010a), who found that 3.6μm types, judged using the same precepts described in the dVA for blue light images, are well-correlated with blue-light types. On average mid-IR classifications for RC3 S0/a-Sc galaxies are about 1 stage interval earlier than B-band classifications, with little difference for types outside this range. The correlation is much better than what was expected from previous near-IR studies (Eskridge et al. 2002). 3.6μm galaxy morphology is sufficiently contaminated by recent star formation to allow the same criteria defined for blue light images to be used for galaxy classification, a surprising result.

Drastic differences between 3.6μm and B-band morphology are seen only for the most dusty galaxies. One example is NGC 5195, shown also in Figure 41. This galaxy, classified as Irr II in the Hubble Atlas and as I0 by de Vaucouleurs, appears as a regular early-type galaxy of type SAB(r)0/a (see also Block et al. 1994). Other galaxies that can look very different are flocculent spirals such as NGC 5055 (Figure 44). The flocculence largely disappears at 3.6μm, and a more global pattern is seen (see also Thornley 1996). The type of NGC 5055, Sbc, remains largely unchanged from B to 3.6 μm.

As noted by Helou et al. (2004), the mid-IR wavelength domain marks the transition from emission dominated by starlight to emission dominated by interstellar dust. While images at 3.6μm show the stellar bulge and disk almost completely free of dust extinction, an image at 8μm shows very little starlight but considerable emission from the ISM in the form of glowing dust.

Figure 45 shows an 8μm image of the nearby spiral galaxy M81 as compared to a $B-I$ color index map coded such that blue star-forming features are dark while red dust lanes

are light. The 8μm image of M81 shows that its ISM is closely associated with its spiral arms. Comparison with the $B-I$ color index shows that both the star-forming arms as well as near-side dust lanes can be seen at 8μm. Even the far-side lanes in the bulge region are clear at 8μm, where no tilt asymmetry is manifested. Willner et al. (2004) argue that the dust emission from M81's ISM is likely dominated by polycyclic aromatic hydrocarbons (PAHs; Gillett et al. 1973) which have a prominent emission feature at 7.7μm. Willner et al. also showed good correspondence between the nonstellar dust emission in M81 and the distribution of near-ultraviolet (NUV) emission. Some regions with bright dust emission and little NUV emission were attributed to excessive UV extinction, while areas with bright NUV and little dust emission were attributed to the effects of supernovae.

The $B-I$ color index map of M81 shows an additional set of dust lanes that have no counterpart in the 8μm map. These lanes are oriented roughly perpendicularly to the major axis about halfway between the center and the northern arm. Sandage & Bedke (1994) interpret these as foreground dust associated with high galactic latitude nebulosities in the halo of our Galaxy.

13. Intermediate and High Redshift Galaxy Morphology

The key to detecting observable evidence for galaxy evolution, that is, to actually see morphological differences that are likely attributable to evolution, is to observe galaxies at high redshift with sufficient resolution to reveal significant details of morphology. Butcher & Oemler (1978) had already found strong evidence for morphological evolution in the excess number of blue galaxies in very distant (z=0.4-0.5) rich galaxy clusters. These authors suggested that the blue galaxies are spiral galaxies, and that by the present epoch, these are the galaxies that become the S0s that dominate nearby rich, relaxed clusters (like the Coma Cluster, Abell 1656). An excellent summary of the issues connected with high

redshift morphological studies is provided by van den Bergh (1998).

Progress on galaxy morphology at high redshift could only be achieved with the resolution and depth of the Hubble Space Telescope. The Hubble Deep Field North (HDF-N, Williams et al. 1996), South (HDFS, Volonteri et al. 2000), and Ultra-Deep Field (HUDF, Beckwith et al. 2006), and the GOODS (Great Observatories Origins Deep Survey; Giavalisco et al. 2004), GEMS (Galaxy Evolution from Morphology and SEDS; Rix et al. 2004), COSMOS (Cosmic Evolution Survey; Scoville et al. 2007), and other surveys (e.g., Cowie et al. 1995), have provided a large body of information to work with. For example, studies of galaxies in the redshift range $0.3 \leq z \leq 0.9$ show that the proportion of irregular-shaped galaxies dramatically increases (e.g., Abraham et al. 1996). This means that the Hubble sequence as we know it did not always exist but was built up over time via mergers or secular evolution or both. Observations of submillimeter sources (Chapman et al. 2003) suggest some of these irregulars are extended major mergers.

Interpretation of evolution in the various deep surveys depends on knowledge of redshifts, which can be difficult to measure spectroscopically. A very useful technique for isolating galaxies in high redshift ranges is the UV-drop out method (Steidel & Hamilton 1992). Galaxies are compared in different filters, such as B_{435}, V_{606}, i_{775}, and z_{850}. If the redshift is high enough to move the Lyman limit at 0.0912μm out of any of the first three filters, there will be a significant drop in flux owing to absorption by hydrogen, and the galaxy is said to "drop out." Galaxies found in this way are called "Lyman break" galaxies because the effect is partly caused by the spectral characteristics of hot stars, which show such a break. (Another cause is UV self-absorption.)

Steidel et al. (1996) used the UV drop-out approach to identify high z galaxies in the HDF-N, and also used direct spectroscopy to confirm that the method works. Beckwith et al. (2006) utilized the method to identify galaxies in the HUDF having z from 3.5 to 7. If

a galaxy is seen to drop out of a U-band filter such as F300W and seen in a B-band filter such as F450W (both used for the HDF-N; Williams et al. 1996), then the redshift range selected is z=2.4 to 3.4. van den Bergh (1998) argues that most Lyman break galaxies are young ellipticals or bulges.

Van den Bergh et al. (2000) describe the issues connected with morphological classifications of galaxies to redshifts of $z\approx1$. Resolution, band-shifting, and selection effects due to the magnitude-limited nature of surveys all enter into the interpretation of intermediate to high redshift galaxy morphology. Resolution is important because, typically, a nearby galaxy will have 100 times or more pixels in the image than a high z galaxy will have for classification. This is fewer pixels than sky survey images of nearby galaxies would have. The bandpass effect is important because the B-band, the standard wavelength for historical galaxy classification, is not sampling the same part of the spectrum as it would for nearby galaxies. For example, at z=1, a B-band filter samples mid-ultraviolet light ($\approx0.22\mu$m) and would be much more sensitive to young star-forming regions than it would be for nearby galaxies. Ideally, then, for comparison with nearby galaxies we would like to choose a redshifted band as close as possible to the *rest-frame* B-band. Even accounting for all these effects, significant differences between nearby and distant morphologies do exist. For example, van den Bergh et al. (2000) discuss the paucity of grand-design spirals and barred galaxies in the HDF-N, and use artifically redshifted images of nearby galaxies to demonstrate that the deficiencies are likely to be real.

Figure 46 shows several of the different categories of intermediate and high redshift galaxy morphologies, based on V and i-band images from the GEMS and Hubble UDF. The redshifts range from 0.42 to 3.35 and provide a wide range of look-back times. First, in such a range, some galaxies look relatively normal, as shown by the spiral and elliptical galaxies in the two upper left frames of Figure 46. The z=0.59 spiral is classifiable as type

SA(s)bc and the elliptical as type E3. The z=0.99 spiral shown in the middle right frame of Figure 46 has larger clumps, no clear central object, and more asymmetry than the z=0.59 spiral, but is still recognizable as a spiral. However, other less familiar categories are found. In general, high redshift galaxies are smaller than nearby galaxies on average (e.g., Elmegreen et al. 2007a=EEFM07).

"Chain galaxies" were first identified by Cowie et al. (1995) and are linear structures with superposed bright knots that have sizes and blue colors similar to normal late-type galaxies and relatively flat major axis luminosity profiles. They have the shapes of edge-on disk galaxies but lack clear bulges or nuclei. A recent study by Elmegreen, Elmegreen, & Sheets (2004=EES04) of faint galaxy morphologies (redshifts 0.5-2) in the Advanced Camera for Surveys (ACS)"Tadpole" galaxy (UGC10214) field showed that chain galaxies are the most common linear morphology at magnitudes fainter than I=22, accounting for more than 40% of the sample. Their dominance (also found by Cowie et al. 1995) is interpreted by EES04 as a selection effect because relatively optically thin edge-on galaxies are more favored to be seen near the limit owing to a higher projected surface brightness than for face-on versions of the same galaxies. EES04 suggest that chain galaxies are edge-on irregular galaxies that will evolve to late-type disk galaxies. Chains are the most flattened linear morphology at faint magnitudes.

"Clump clusters" (EES04) are somewhat irregular collections of blue knots or clumps with very faint emission between clumps. The clumps have sizes of ≈500pc and masses of ≈10^8–10^9 $M_\odot$. Both of the examples shown in Figure 46 have z>1. Elmegreen, Elmegreen, & Hirst (2004=EEH04) identified clump clusters as the face-on counterparts of the linear chain galaxies, based on the similarities of the properties of the clumps with those seen in chain galaxies, and on the distribution of axis ratios of the systems as compared with normal disk galaxies. The lack of a bulge clump is also consistent with this conclusion.

Nevertheless, analysis of NICMOS IR images in the HUDF led Elmegreen et al. (2009a) to conclude that 30% of clump clusters and 50% of chain galaxies show evidence of young bulges, implying that at least half of these galaxies might be genuinely bulgeless. In a related study, Elmegreen et al. (2009b) show that the best local analogues of clump clusters are dwarf irregular galaxies like Ho II, scaled up by a factor of 10-100 in mass. This study also brought attention to clump clusters with faint red background disks, as opposed to blue clump clusters which lack such a feature. Elmegreen et al. argue that the red background clump clusters are part of an evolutionary sequence leading from the blue clump clusters to spirals with a "classical" bulge (e.g., KK04). The clumps, formed by gravitational instabilities in a turbulent disk, are large and few in number, and thus will eventually coalesce near the galaxy center if they survive the effects of supernova explosions (e. g., Elmegreen, Bournaud, & Elmegreen 2008).

"Tadpoles" (van den Bergh et al. 1996) are asymmetrically-shaped "head-tail" morphologies with a bright off-centered nucleus and a tail, like a tadpole. A rare local example is NGC 3991. Tadpoles were recognized in 3% of the galaxies in HDF-N and were found to be very blue in color. Usually both the head and the tail are blue, but van den Bergh et al. (1996) show one example where the head is red and the tail is blue. EEH04 showed that tadpoles have neither exponential major axis profiles nor clear bulges, and in their sample of linear objects, tadpoles are the least frequently seen.

The bottom frames of Figure 46 show bent chains and rings or partial rings (Elmegreen & Elmegreen 2006=EE06). The rings and partial rings are thought to be mostly collisional in nature (i.e., like the conventional ring galaxies shown in Figure 27) and show the different morphologies expected when small companions plunge through a larger disk galaxy in different ways (Appleton & Struck-Marcell 1996). Although bent chains resemble the partial rings, they lack offset nuclei and any evidence of a background, more face-on disk. EE06

suggest that bent chains are simply warped versions of the more common linear chains that have suffered an interaction. The ages of the bent chain clumps are younger than those found in rings and partial rings, and EE06 argue that relative separations and sizes of the clumps indicate they form by gravitational instabilities.

Elmegreen et al. (2005) show that approximately 1/3 of the ellipticals catalogued in the HUDF have prominent blue clumps in their centers (see also Menanteau et al. 2001, 2004). They argued that these clumps probably imply accretion events based on comparison of their magnitudes and colors with local field objects. Menanteau et al. (2001) were able to reproduce the color distributions with a model having a starburst superposed on a pre-existing older stellar population.

Galaxy morphology at intermediate and high redshifts also includes obvious interacting cases as well as possible merger morphologies. Bridges, tidal tails, plumes, and even M51 analogues are seen as in nearby galaxies, but are smaller in scale than for nearby objects (EEFM07). The middle frame of the bottom row shows a possible merger in progress of two bent chains (or, alternatively, two interacting spirals), called an "assembly galaxy" by EEFM07 because they appear to be assembling from smaller objects. EEH04 and EEFM07 also discuss the double systems, considered another category of the linear systems. The double systems like the z=3.35 one shown in Figure 46 are probably merging ellipticals. EEFM07 also describe "shrimp galaxies", which appear to be interacting galaxies with a single curved arm or tail, curling at one end into a "body."

Other studies of high redshift galaxy morphology have focussed on the specific redshift ranges that are selected by the UV drop-out technique. Conselice & Arnold (2009) examined the morphologies of galaxies in the z=4-6 range from the HUDF, and measured quantitatve parameters such as the concentration-asymmetry-clumpiness (star formation) parameters (CAS; Conselice 2003) and other related parameters that are useful for distinguishing

mergers from normal galaxies. The CAS system is based on simple global parameters that are easily derived automatically for large numbers of galaxies. Conselice (2003) tied the C parameter to the past evolutionary history of galaxies while parameters A and S measure more active evolution from mergers and star formation. Conselice & Arnold found that half of the HUDF drop-out galaxies they studied have significant asymmetries and may be undergoing merging, while the other half is mainly smooth symmetric systems that may have collapsed quickly into a temporary, quiescent state.

Other quantitative approaches to these issues include the Sersic n index that characterizes radial luminosity profiles (Ravindranath et al. 2006; Elmegreen et al. 2007b) and the Gini coefficient (Abraham et al. 2003; Lotz et al. 2006). The Gini coefficient provides a way of quantifying high redshift morphology that does not depend on galaxy shape or the existence of a well-defined center, and is well-suited to the kinds of objects shown in Figure 46. Lotz et al. (2006) found in a sample of 82 Lyman break galaxies that 10-25% are likely mergers, 30% are relatively undisturbed spheroids, and the remainder are disks, minor mergers, or post-mergers.

Given the rise in peculiar and irregular-shaped galaxies with increasing redshift, the question naturally arises: when did the Hubble sequence and all its accompanying details fall into place? This question is considered by Conselice et al. (2004), who quantitatively analyzed a well-defined high redshift sample using the CAS system. Conselice et al. identify "luminous diffuse objects" (LDOs) as galaxies having C less than 1σ below the average, and "luminous asymmetric objects" (LAOs) as galaxies having $A > S$. Some of both classes of objects are covered by the Elmegreen et al. categories described above. All of the LDOs and LAOs have $M_B < -19$, and Conselice et al. suggest such objects might be the precursors of modern disk and elliptical galaxies. These are found in the redshift range $0.2 < z < 2$, suggesting the present day Hubble sequence began taking shape in this interval.

Conselice et al. (2008) consider the morphologies of galaxies more massive than 10^{10} $M_{\odot}$ and in the range $1.2< z < 3$. To a z_{850} magnitude of 27, the majority of these galaxies are peculiar. They conclude that such galaxies undergo 4.3±0.8 mergers to z=3.

14. Giant Low Surface Brightness Galaxies

The van den Bergh luminosity classes highlight how luminosity and surface brightness generally go together. Low surface brightness usually means low luminosity and small size, hence a dwarf classification. However, the discovery of rare giant low surface brighness (GLSB) galaxies by Bothun et al. (1987) shows that morphology can sometimes be misleading for judging absolute luminosity. The hallmarks of these objects are a relatively normal bulge and an extremely low surface brightness, very large disk. Disk radial scalelengths and luminosities are unusually large, and extrapolated disk central surface brightnesses are unusually faint, compared to more normal spirals. The disks tend to be relatively smooth with a few large, isolated HII regions. Bothun et al. (1987) point to a model whereby the disks of these galaxies have such a low gas surface density that they are largely unevolved, due to the inefficiency of star formation.

GLSB galaxies can be classified within the Hubble-Sandage and de Vaucouleurs classification systems although, as noted by McGaugh, Schombert, and Bothun (1995), the majority are classified later than stage Sc. Bulges, bars, rings, and spiral patterns are evident in some examples, in spite of the low disk surface brightness. Figure 47 shows three of the originally recognized GLSB examples (McGaugh, Schombert, & Bothun 1995): Malin 2 (also known as F568−6), UGC 1230, and UGC 6614. In the images, the length of a side is 131, 38, and 77 kpc, respectively. These can compared to the giant normal spiral NGC 7531 in the far right frame, where the length of a side is also 38 kpc. Malin 2 and UGC 6614 are especially enormous physical objects. UGC 1230 is also very large for

such a late-type morphology. van den Bergh (1998) likens the size of Malin 2 to the core of a cluster of galaxies. He considers "monsters" like Malin 1 and Malin 2 to be only one of three types of LSB galaxies. Some LSB galaxies are as big as normal galaxies, like UGC 1230. Most LSB galaxies, however, are dwarfs: ellipticals, irregulars and, less frequently, spirals. These are described further in section 15.2.

An example of another object that could be considered a large LSB galaxy, but which lacks a bulge or any evident recent star formation, is SGC 2311.8−4353, the mysterious ghost-like companion close to the right of NGC 7531 in Figure 47. This peculiar object is 2/3 the size of NGC 7531 (Buta 1987) but has unknown redshift. If it is associated with NGC 7531, it would be as much as 30 kpc in diameter at the faintest detectable isophote level and would clearly not be a dwarf.

A recent study of three GLSBs (Malin 1, UGC 6614, and UGC 9024) by Rahman et al. (2007) showed that IR emission from such objects is consistent with their optically-determined low star formation rates, with the diffuse optical disks being undetected from two of the three. A dynamical study of two GLSBs (Malin 1 and NGC 7589) by Lelli, Fraternali, & Sancisi (2010) led the authors to conclude that at least in these cases, the GLSB galaxy can be thought of as an inner high surface brightness galaxy having a very extended LSB disk. This is based on the steeply rising rotation curves found for these galaxies, which is very much like what is seen in early-type high surface brightness galaxies.

Impey & Bothun (1997) argue that LSB galaxies brighter than M_B=−14 contribute significantly to the luminosity density of the local universe, are dark-matter-dominated at almost all radii, and have an evolutionary history involving late collapse of a low amplitude perturbation, a low star formation rate, and very slow changes. Large LSBs are greatly underrepresented in galaxy catalogues but are clearly an important class of objects.

15. Galaxy Morphology in Color

15.1. Normal Galaxies

The Sloan Digital Sky Survey (York et al. 2000; Gunn et al. 1998) provides the largest body of information on the colors of galaxies. The multi-wavelength imaging in *ugriz* filters has allowed the production of high quality color images for thousands of galaxies. Although the Hubble-Sandage-de Vaucouleurs classification systems were based on blue light images alone, it is still possible to reliably classify galaxies with SDSS color images, which are based on combined *gri* images (Lupton et al. 2004). In such images one can directly see the stellar population differences that characterize different galaxy types.

Figure 48 shows the color Hubble sequence from E to Sm. Once galaxy colors were systematically measured using photoelectric photometry (de Vaucouleurs, de Vaucouleurs, & Corwin 1976), it was noted that integrated colors vary smoothly with advancing stage along the Hubble sequence. The latest stages have corrected total color index $(B-V)^o_T \approx$0.3-0.4 while E and S0 galaxies have $(B-V)^o_T \approx$0.9-1.0 (e.g., Buta et al. 1994). The latter colors correspond to yellow-orange while the former are bluish-white. The colors begin to change at S0/a and Sa and become progressively bluer. Figure 48 shows the reason for the change. Galaxies earlier than Sa are dominated by old stars having the colors of K giants. As stage advances from Sa to Sm, the spiral structure becomes progressively more important compared to the bulge. Since the arms are dominated by complexes of massive young stars, this makes the integrated colors of the galaxies become progressively bluer until by the end of the sequence, the bluer colors of these stars have overcome the yellowish light of the background old disk stars. Figure 48 also shows that the intermediate colors of intermediate types such as Sb and Sc are due to the yellowish-orange colors of bulges and bars as combined with the bluer colors of spiral arms.

The analysis of integrated SDSS galaxy colors for more than 100,000 galaxies led to one of the most dramatic findings of the survey: a clear bimodality in the distribution of color that correlates with morphology: a red peak that includes mainly E, S0, and Sa galaxies, and a blue peak that includes mainly Sb, Sc, and Irr galaxies (Strateva et al. 2001). Although the correlation of galaxy color with types had been known for a long time from photoelectric measurements (e. g., de Vaucouleurs 1961; Buta et al. 1994), the large sample provided by SDSS allowed the bimodality to be demonstrated to a high degree of significance. In plots of $u - r$ color index versus absolute M_r magnitude, the galactic equivalent of a stellar H-R diagram, nearby early-type galaxies follow a narrow band called the red sequence, while nearby later-type, mostly star-forming galaxies appear as a broad blue sequence (also sometimes called the "blue cloud"). Baldry et al. (2004) showed that the bimodality (in the form of a double Gaussian number distribution over all types) is detectable from $M_r \approx -15.5$ to $M_r \approx -23$, being undetectable only for the most luminous galaxies. Wyder et al. (2007) showed that use of GALEX near-ultraviolet magnitudes and optical r-band magnitudes provides even greater discrimination between the Gaussian components. Bell et al. (2004) showed that the bimodality is detectable in faint galaxies to $z \approx 1$, indicating that this characteristic of the galaxy population extends to a lookback time of at least 9Gyr. It is thought that galaxies evolve from the blue sequence to the red sequence as their star formation is quenched, perhaps through mergers, gas depletion, or AGN feedback (e.g., Martin et al. 2007). The possibility of evolution has engendered great interest in the galaxies lying near the minimum of the bimodal distribution (the so-called "green valley"; Thilker et al. 2010 and references therein).

15.2. Dwarf Galaxies

Virtually all the galaxies shown in Figure 48 are of relatively high luminosity, with absolute blue magnitudes M_B^o averaging about -20. When physical parameters such as M_B^o are considered, it becomes clear that the peculiar shape of the de Vaucouleurs classification volume shown in Figure 3 only highlights the morphological diversity of families and varieties at each stage, but does not tell us about the *physical parameter space* at each stage, which expands considerably at each end of the volume (McGaugh, Schombert, and Bothun 1995). Most known dwarf galaxies are either early or late-type, but not intermediate.

15.2.1. dE, dS0, BCD, and cE Galaxies

The most extensive study of dwarf galaxy morphologies was made by Binggeli, Sandage, & Tammann (1985=BST), who used deep photographs to probe the low luminosity population of the Virgo Cluster, using mostly morphology to deduce cluster membership. Examples of several categories of Virgo Cluster dwarf galaxies are shown in Figure 49 using SDSS color images and the classifications of BST. The most common type is the dwarf elliptical, or dE type, which accounts for 80% of the galaxies in the BST catalogue. dE galaxies range from $M_B = -18$ to -8 (Ferguson & Binggeli 1994). Many dEs have an unresolved, star-like nucleus whose presence is indicated by an N attached to the type, as in dE0,N. The top right panels of Figure 49 show three fairly typical examples. Possibly related to these normal dE systems are the larger, lower surface brightness ellipticals ("large dE") shown in the two lower right frames of Figure 49.

The second row of Figure 49 shows examples of the interesting class of dwarf S0 galaxies. All of the examples shown are distinct from dEs in showing a smooth structure but with additional features such as a lens or a weak bar. dS0 galaxies can also be nucleated

and are called dS0,N. In addition to the low surface brightness dEs and dS0s, the Virgo Cluster includes two high surface brightness classes of dwarfs. The cE category refers to compact ellipticals that resemble M32.

The blue compact dwarf (BCD) galaxies are a special class of star-forming dwarf irregulars characterized by a few bright knots imbedded in a stellar background of low surface brightness (Sandage and Binggeli 1984). The most extreme cases are nearly stellar (Thuan & Martin 1981). The knots are often super star clusters associated with 30-Doradus-like HII regions, and the faint background can be very blue (Thuan et al. 1997). Spectroscopically, BCDs have narrow emission lines superposed on a blue continuum, and the lines indicate a low metallicity. Figure 49 shows three examples from the BST Virgo Cluster catalogue. Gil de Paz et al. (2003) present an atlas of more than 100 BCDs that highlight their structure.

As described in section 5.1, the dE galaxies shown in Figure 49 are *not* the low luminosity extension of more luminous ellipticals. These together with the dS0 class are labeled "spheroidal" galaxies by Kormendy et al. (2009; see Figure 6), who confirmed the finding by Kormendy (1985) that these galaxies are more related to evolved low luminosity spirals and irregulars than to genuine ellipticals. Based on correlations of well-defined photometric parameters (e.g., central surface brightness or velocity dispersion versus core radius or absolute magnitude), these authors link ellipticals like M32 to the actual low luminosity end of the E galaxy sequence (see also Wirth & Gallagher 1984). Thus, the cE galaxies shown in Figure 49 are in a sense truer "dwarf ellipticals" than the dE galaxies shown. This does not negate the value of the BST classifications, since these are purely morphological interpretations.

15.2.2. Local Group Dwarf Spheroidals and Irregulars

The lowest luminosity galaxies that we can study in detail are in the Local Group. Fortunately, a few are in the area covered by the SDSS so that they can be illustrated in color. These objects, all fainter than M_V=−12, are shown in Figure 50. Leo I and Leo II are usually called dwarf spheroidal, or dSph, galaxies (e.g., Ferguson & Binggeli 1994). dSph galaxies tend to have to have absolute visual magnitudes $M_V > -15$ and a low degree of flattening; they are believed to be the most abundant type of galaxy in the Universe. Leo I (M_V=−11.9) and Leo II (M_V=−9.6) look different in part because of their different star formation histories. dSph and dwarf irregular (dI) galaxies are now known to have complex and varied star formation histories that may involve multiple episodes of star formation and effects of interactions (Mateo 1998 and references therein). The other two galaxies in Figure 50, Leo A and DDO 155, are dwarf irregulars having $M_V \approx -11.5$. A detailed HST study of the stellar content of Leo A (Cole et al. 2007) showed that 90% of the star formation in the galaxy occurred less than 8 Gyr ago, with a peak at 1.5-3 Gyr ago. A useful summary of the properties of dSph galaxies is provided by van den Bergh (1998) and, most recently, by Tolstoy, Hill, & Tosi (2009), who also discuss the star formation histories of Local Group dI galaxies.

The SDSS has facilitated the discovery of many new Local Group dwarf galaxies (Belokurov et al. 2007). For example, the SDSS led to the discovery of one of the faintest known dSph galaxies, a new dwarf in Ursa Major (called the UMa dSph) having $M_V \approx -7$ (Willman et al. 2007). Most interesting is Leo T, which is an $M_V = -7.1$ dSph galaxy with some recent star formation, providing one of the most dramatic illustrations of the link between dSph and dI galaxies, and the least luminous galaxy known to have recent star formation (Irwin et al. 2007).

15.2.3. Dwarf Spirals

Sandage & Binggeli (1984) described the classification of dwarf galaxies based on the Virgo Cluster, and concluded that there are "no real dwarf spirals." This refers mainly to dwarf spirals that might be classified as types Sa, Sb, or Sc, i.e., having both a bulge and a disk. Dwarf late-type spirals are already built into de Vaucouleurs's modified Hubble sequence as Sd-Sm types and connect directly to Magellanic irregulars, as shown in Figure 1 of Sandage & Binggeli (1984). Thus, any genuine examples of dwarf Sa, Sb, or Sc spirals would be of great interest as they would challenge the idea that for a galaxy to be able to make well-defined spiral arms, it would have to be more massive than some lower limit (estimated as $5{\times}10^9$ $M_\odot$ by Sandage & Binggeli).

Four of the best cases of genuine dwarf spirals are illustrated in Figure 51. The two rightmost frames show IC 783 (BST type dS0,N) and IC 3328 (BST type dE1,N), both Virgo Cluster members having absolute magnitudes $M_B^o \approx -16$ to -17, and found to have subtle spiral structure by Barazza, Binggeli, & Jerjen (2002) and Jerjen, Kalnajs, & Binggeli (2000), respectively. The patterns are hard to see in the direct SDSS color images shown in Figure 51, but these authors use photometric models, Fourier decomposition, and unsharp-masking to verify the reality of the patterns. Barraza et al. conclude that many of the bright early-type dwarfs in the Virgo Cluster have disks. An example with a bar *and* spiral arms is NGC 4431 (shown as dS0 in Figure 49).

The leftmost panel of Figure 51 shows an HST wide V-band image (Carollo et al. 1997) of NGC 3928, an absolute magnitude $M_B^o = -18$ galaxy which on small-scale, overexposed images looks like an E0, but which harbors a miniature (2kpc diameter), low-luminosity Sb spiral (van den Bergh 1980b). Based on spectroscopic analysis, Taniguchi & Watanabe (1987) have suggested that NGC 3928 is a spheroidal galaxy which experienced an accretion event that supplied the gas for star formation in the miniature disk.

Schombert et al. (1995) brought attention to possible dwarf field spirals. One of their examples, D563−4, is shown in the second frame from the left in Figure 51. This galaxy has $M_B^o \approx -17$. A few other examples are given in the paper, and Schombert et al. find that they are not in general grand design spirals, are physically small, and have low HI masses. However, van den Bergh (1998) considers all of Schombert et al.'s examples as subgiant spirals rather then true dwarf spirals. A possible true dwarf spiral given by van den Bergh is DDO 122 (type S V).

15.3. Galaxy Zoo Project

The Galaxy Zoo project (Lintott et al. 2008) has made extensive use of SDSS color images. The project uses a website to enlist the help of citizen scientists worldwide to classify a million galaxies as well as note interesting and unusual cases in various forum threads. With such a large database to work from, and the potential for discovery being real, the project has attracted many competent amateur galaxy morphologists. One such discovery was a new class of galaxies called "green peas," which are star-like objects that appear green in the SDSS composite color images (Figure 52, left). Cardemone et al. (2009) used auxiliary SDSS data to show that peas are galaxies that are green because of a high equivalent width of [OIII] 5007 emission. They are sufficiently distinct from normal galaxies and quasars in a two-color $g - r$ vs. $r - i$ plot that such a plot can be used to identify more examples. Other characteristics noted are that peas are rare, no bigger than 5 kpc in radius, lie in lower density environments than normal galaxies, but may still have morphological characteristics driven by mergers, are relatively low in mass and metallicity, and have a high star formation rate. Cardemone et al. conclude that peas are a distinct class of galaxies that share some properties with luminous blue compact galaxies and UV-luminous high redshift galaxies.

Another prominent colorful galactic-sized object identified by Galaxy Zoo is "Hanny's Voorwerp" (Figure 52), a peculiar collection of blue clumps just south of IC 2497. Lintott et al. (2009) found that the Voorwerp is mostly ionized gas, and after ruling out some possible sources of ionizing radiation, concluded that the object could be the first identified case of a quasar light echo. The implication is that the companion galaxy underwent a temporary quasar phase.

Masters et al. (2010) examine the properties of face-on late-type spiral galaxies whose colors are much redder than is typical (Figure 52, right panels), suggesting that they are passive objects where star formation has largely ceased or is lower than normal. These authors showed that red spirals are not excessively dusty and tend to be near the high end of the mass spectrum. A range of environmental densities was found, implying that environment alone is not sufficient to make a spiral red. A significantly higher bar fraction was found for red spirals as compared to blue spirals, which Masters et al. suggest could mean the bars themselves may have acted to shut down the star formation in these galaxies.

A major philosophical aspect of Galaxy Zoo is the value of human visual interpretation of galaxy morphology. That is, the human eye can integrate the detail in an image more reliably than a computer program can, in spite of the latter's ability to classify numbers of galaxies well beyond the capability of a single individual. This philosophy was used to compile a major catalogue of galaxy merger pairs described by Darg et al. (2010). In the initial set-up of Galaxy Zoo, a single button allowed a classifier to select whether an object was a "merger" based simply on the appearance of peculiarities. For each galaxy, a weighted average number, f_m, was derived that characterized the fraction of classifiers who interpreted a pair of galaxies as a merger, essentially "morphology by vote" and in a way reminiscent of RC3 where morphological types were in many cases based on a weighted average from a small number of classifiers (Buta et al. 1994). Taking $f_m > 0.4$, Darg et al.

(2004) identified 3003 pairs and groups of merging galaxies, and also showed that the spiral to elliptical galaxy ratio in merger pairs is a factor of two higher than for the global galaxy population, suggesting that mergers involving spirals are detectable for a longer period than those that do not involve spirals.

A similar philosophy to Galaxy Zoo was used by Buta (1995) to compile the Catalogue of Southern Ringed Galaxies, and also by Schawinski et al. (2007), who visually classified 48,023 SDSS galaxies to identify a significant-sized sample of early-type galaxies for a study of the connection between nuclear activity and star formation. In the latter study, visual interpretation was argued to be needed to avoid bias against star-forming early-type galaxies which would be excluded from color-selected samples. A major result of this study was the identification of a time sequence whereby an early-type galaxy has its star formation suppressed by nuclear activity, a manifestation of AGN feedback.

15.4. Isolated Galaxies

If interactions and mergers can have profound effects on galaxy morphology, then the morphology of *isolated* galaxies clearly is of great interest. Such galaxies allow us to see how internal evolution alone affects morphology, i. e., what pure "nature" morphologies look like. Karachentseva (1973) compiled a large catalogue (the Catalogue of Isolated Galaxies, or CIG) of 1050 isolated galaxies that has proven very useful for examining this issue. A galaxy of diameter D is sugggested to be isolated if it has no comparable-sized companions of diameter d between $D/4$ and $4D$ within a distance of $20d$. Verdes-Montenegro et al. (2005) show that this means that an isolated galaxy 25 kpc in diameter, in the presence of a typical field galaxy velocity of 150 km s^{-1}, has not been visited by a comparable mass companion during the past 3Gyr. These authors discuss the limitations of the CIG (e. g., the isolation criteria do not always work), but in general it is the best source of isolated

galaxies available.

Sulentic et al. (2006) examined all 1050 CIG galaxies on Palomar II sky suvey charts in order to refine the sample and found that isolated galaxies cover all Hubble types. Of these, 14% were found to be E/S0 types, while 63% were Sb-Sc types, with the spiral population more luminous than the E/S0 population. Over the type range Sa-Sd, the proportion rises to 82%. Thus, an isolated galaxy sample is very spiral-rich. Nevertheless, the presence of early-type galaxies in the sample implies that these are not likely to be "nurture" formed, as such galaxies might be in denser environments. The refinement of the CIG sample forms the basis of the Analysis of the Interstellar Medium of Isolated Galaxies (AMIGA) project (Verdes-Montenegro et al. 2005).

Figure 53 shows six examples of isolated Sb-Sc galaxies from the AMIGA sample, based on SDSS color images. All of these look relatively normal, but it is interesting how nonbarred galaxies like NGC 2649 and 5622 (upper left frames in Figure 53) show such conspicuous global spirals, which argues that the spirals in these galaxies have not been excited by an interaction.

Durbala et al. (2008) analyzed the photometric properties of 100 isolated Sb-Sc AMIGA galaxies, and found that a majority have pseudobulges rather than classical bulges. In comparing the properties of isolated galaxies with a sample of Sb-Sc galaxies selected without an isolation criterion, Durbala et al. found that isolated spirals have longer bars and, using CAS parameters, also less asymmetry, central concentration, and clumpiness,

Durbala et al. (2009) analyzed the Fourier properties of the same set of 100 isolated spirals, and estimated bar lengths and strengths. Earlier types in the sample were found to have longer and higher contrast bars than later types. Spiral arm multiplicities were investigated also, and it was shown that cases having an inner m=2 pattern and an outer m=3 pattern occurred in 28% of the sample. Elmegreen, Elmegreen, & Montenegro (1992)

argued that in such morphologies, the m=3 pattern is driven internally by the m=2 pattern, and that three-armed patterns measure the time elapsed since an interaction.

15.5. Deep Field Color Imaging

Particularly interesting in the domain of color galaxy morphology are the various deep field surveys that have been at the heart of high redshift studies. The most recent is the HST Wide Field Camera 3 Early Release Science (ERS) data (Windhorst et al. 2010), which provides very deep panchromatic images based on 10 filters ranging from 0.2μm to 2μm in wavlength. Figure 54 shows three subsections of the main ERS field, which coincides with the GOODS south field (Giavalisco et al. 2004). The galaxies seen range in redshift from z=0.08 to at least z=3. Windhorst et al. (2010) argue that images like the ERS field are deep enough to allow probing of galaxy evolution in the crucial redshift range $z\approx$1-3 where the galaxies assembled into their massive shapes. By $z\approx$1, the Hubble sequence was largely in place. Figure 54 shows a variety of interesting nearby as well as high z morphologies, including some of those illustrated in Figure 46. Images like the ERS field allow us to connect the local and distant galaxy populations in unprecedented detail.

16. Large-Scale Automated Galaxy Classification

The process of galaxy classification thus far described is a manual exercise where an observer attempts to sort a galaxy into its appropriate stage, family, variety, outer ring classification, etc., by visual inspection alone. For a small number of observers, this has been done for as many as 14,000 galaxies by Nair & Abraham (2010) and 48,000 galaxies by Schawinski et al. (2007), while for a large number of observers working in concert (e.g., the Galaxy Zoo project) it has been done for a million galaxies. But critical to such ventures

is the preparation of images for classification, and a need for a homogeneous, objective approach to very large numbers of galaxies. This has led to extensive application of automated methods for classifying galaxies. For example, Nair & Abraham (2010) visually classified galaxies into coded bins for the purpose of training an automatic classification algorithm.

(The remainder of this part will be found in the printed publication.)

17. The Status and Future of Morphological Studies

The large number of illustrations in this article attests to the richness of the diversity of galaxy morphology. It is, of course, not possible to illustrate all aspects of morphology that might be worth discussing, but most interesting is how far *physical galaxy morphology* has come in the 35 years since Allan Sandage wrote his review of galaxy morphology in Volume IX of *Stars and Stellar Systems*. Galaxy morphology is no longer the purely descriptive subject it once used to be.

Internal perturbations such as bars are apparently capable of generating a great deal of the interesting structure we see in disk galaxies, and more theoretical and observational studies should elucidate this further. The impact of bars on morphology seems well understood, as summarized in detail by KK04 in their monumental review article on pseudobulges. Bars redistribute angular momentum and reorganize gas clouds to flow into resonance regions and fuel star formation. The gathering of gas into resonance regions can drive the formation of rings, and indeed can also build up the central mass concentration to the point of bar destruction. Even failing this, the pile-up of gas into the nuclear region can lead to the formation of a pseudobulge. The richness of barred galaxy morphology attests to the strong role secular evolution plays in structuring galaxies.

Progress in understanding the role of mergers and interactions on galaxy morphology has also proceeded at a rapid pace. Great success in numerical simulations and the theory of interacting galaxies has made it possible to link a specific type of interaction to a specific morphology (e. g., collisional ring galaxies). The complex structure of early-type galaxies, with boxy and disky isophote shapes, shells and ripples, and other features, shows that interactions and mergers play an important role in molding galaxies (see the excellent review by Schweizer 1998). With the advent of the Hubble Space Telescope, this role has been elucidated even more clearly because the merger rate was higher in the past.

In spite of the theoretical progress, it is interesting that classical morphology has not lost its relevance or usefulness even after more than 80 years since Hubble published his famous 1926 paper. No matter how much progress in understanding the physical basis for morphology is made, there is still a need for the ordering and insights provided by classical Hubble-Sandage-de Vaucouleurs galaxy classifications. Morphology went through a low phase in the 1980s and 90s when it was perceived that galaxy classification placed too much emphasis on unimportant details and was too descriptive to be useful. It was thought that the Hubble classification had gone as far as it can go, and that another approach needed to be tried to build a more physical picture of galaxies. At that time, there was a sense that the focus should be more on the component "building blocks" of galaxies, or what might be called galactic subsystems (e.g., Djorgovski 1992). Quantification of morphology became more possible as advanced instrumentation allowed more detailed physical measurements to be made. In the end, as morphology became better understood, it also became clear what a type such as "(R)SB(r)ab" might really mean, which enhanced the value of classification (KK04). In addition, numerical simulations became sophisticated enough to make predictions about morphology (e.g., the R_1 and R_2 subclasses of outer rings and pseudorings). These types of things, as well as the movement of morphology from the photographic domain to the digital imaging domain, the broadening of the

wavelength coverage available to morphological studies from the optical to the ultraviolet and infrared domains, the Sloan Digital Sky Survey, and the accessiblity of high redshift galaxies to unprecedentedly detailed morphological study, all played a role in bringing galaxy morphology to the forefront of extragalactic research.

Even so, the writing of this article has shown that many important galaxies and classes of galaxies have not been studied well enough to have much modern data available. For example, in spite of the considerable interest in collisional ring galaxies the past 20 years or so, Struck (2010) was forced to lament that ring galaxies "are underobserved." The same can be said for resonance ring galaxies, giant low surface brightness galaxies, dwarf spirals, Magellanic barred spirals, counter-winding spirals, and other classes of interacting galaxies. The most that can be said about this is that further studies will likely be made, especially if instrumentation facilitates the objects in question. Rotation and dynamics are far short of photometry for most classes of galaxies, but would add a great deal of insight if obtainable.

At the other extreme, early-type (E and S0 galaxies) continue to be the focus of major photometric, kinematic, and theoretical research projects. Important clues to the formation and evolution of such galaxies are contained in their intrinsic shapes (oblate, prolate, triaxial), in the ages, metallicities, and radial mass-to-light ratios of their stellar populations, in their three-dimensional orbital structure, and in the kinematic peculiarities often found in such systems (de Zeeuw et al. 2002). Among the most recent studies are the massive photometric analysis of early-types in the Virgo Cluster by Kormendy et al. (2009), and the ATLAS^{3D} project described by Cappellari et al. (2011). ATLAS^{3D} is the largest kinematic database of high-quality two-dimensional velocity field information ever obtained for early-type galaxies, including 260 such galaxies in a well-defined and complete sample. This survey is simply the latest part of the long-term effort by many researchers, beginning in the 1980s, to understand early-type galaxies in terms of quantitative parameters that can

be tied to theoretical models. Early-types have been a persistent enigma in morphological studies, and considerable evidence suggests that the E, S0 sequence as defined by Hubble, Sandage, and de Vaucouleurs hides a great deal of important physics associated with these objects. The ATLAS^{3D} project was designed to exploit the λ_R parameter described by Emsellem et al. (2007; see section 5.1), which separates early-types into fast and slow rotators and discriminates galaxies along the red color sequence (section 15.1).

These advances for early-type galaxies do not mean that quantitative analyses of later-type galaxies are lacking. As codes for two-dimensional photometric decomposition become ever more sophisticated (e. g., Peng et al. 2010; Laurikainen et al. 2010 and references therein), parameters that characterize the bulges, disks, bars, lenses, rings, and spiral patterns are being derived for large numbers of galaxies (especially barred galaxies) that were not reliably decomposable with earlier one-dimensional approaches.

For the future, it is to be hoped that the Sloan Digital Sky Survey will be extended to cover the whole sky, and provide access to high quality morphological studies of several million more galaxies, some of which might have new and exotic structures. The *James Webb Space Telescope* should be able to carry the HST's torch to greater depths and resolutions of high redshift galaxies, to further enhance our understanding of galaxy evolution.

This article is dedicated to Allan Sandage (1926-2010), one of the 20th century's greatest astronomers, who helped set the stage for galaxy morphology to be one of the most active fields of modern extragalactic research. It was Dr. Sandage's efforts that firmly cemented Hubble's ideas on morphology into astronomy. The author is grateful to Dr. Sandage for the inspiration he provided for this article and for his standard of excellence in astronomy.

The author also gratefully acknowledges the helpful comments and suggestions from the

following people that considerably improved this article: Martin Bureau, Adriana Durbala, Debra Elmegreen, William Keel, Jeffrey Kenney, Johan H. Knapen, Rebecca Koopmann, John Kormendy, Eija Laurikainen, Barry Madore, Karen L. Masters, Patrick M. Treuthardt, Sidney van den Bergh, and Xiaolei Zhang. The author also thanks Debra Elmegreen for providing the images of high redshift galaxies shown in Figure 46, Masfumi Yagi for the illustrations in Figure 29, and John Kormendy, Jason Surace, Donald P. Schneider, and Rogier Windhorst for the use of published illustrations from specific papers. This article uses images from many sources too numerous to acknowledge here, but mainly drawn from the dVA, the NASA/IPAC Extragalactic Database, the Ohio State University Bright Spiral Galaxy Survey (OSUBSGS), the Sloan Digital Sky Survey, and several published papers by other authors. The NASA/IPAC Extragalactic Database (NED) is operated by the Jet Propulsion Laboratory, California Institute of Technology, under contract with the National Aeronautics and Space Administration. Funding for the OSUBSGS was provided by grants from the NSF (grants AST 92-17716 and AST 96-17006), with additional funding from the Ohio State University. Funding for the creation and distribution of the SDSS Archive has been provided by the Alfred P. Sloan Foundation, the Participating Institutions, NASA, NSF, the U.S. Department of Energy, the Japanese Monbukagakusho, and Max Planck Society. Observations with the NASA/ESA *Hubble Space Telescope* were obtained at the Space Telescope Science Institute, which is operated by the Association of Universities for Research in Astronomy, Inc., under contract NAS 5-26555. The *Spitzer Space Telescope* is operated by the Jet Propulsion Laboratory, California Institute of Technology, under NASA contract 1407. The *Two Micron All-Sky Survey* is a joint project of the University of Massachusetts and the Infrared Processing and Analysis Center/California Institute of Technology, funded by the National Aeronautics and Space Administration and the National Science Foundation. GALEX is a NASA mission operated by the Jet Propulsion Laboratory. GALEX data is from the Multimission Archive at the Space Telescope Science

Institute (MAST). Support for MAST for non-HST data is provided by the NASA Office of Space Science via grant NNX09AF08G and by other grants and contracts. This article has also made use of THINGS, "The HI Nearby Galaxy Survey" (Walter et al. 2008), and BIMA-SONG, the Berkeley-Illinois-Maryland Survey of Nearby Galaxies (Helfer et al. 2003).

REFERENCES

Abraham, R. G., van den Bergh, S., Glazebrook, K., Ellis, R. S., Santiago, B. X., Surma, P., & Griffiths, R. E. 1996, ApJS, 107, 1

Abraham, R. G., van den Bergh, S., & Nair, P. 2003, ApJ, 588, 218

Aguerri, J. A. L., Méndez-Abreu, J., & Corsini, E. M. 2009, A&A, 495, 491

Appleton, P. & Struck-Marcell, C. 1996, Fundamentals of Cosmic Physics, 16, 111

Arp, H. 1966, ApJS, 14, 1

Arp, H. C. & Madore, B. F. 1987, Catalogue of Southern Peculiar Galaxies and Associations, Cambridge, Cambridge Univ. Press

Arribas, S., Bushouse, H., Lucas, R. A., Colina, L., & Borne, K. D. 2004, AJ, 127, 2522

Athanassoula, E. 1992, MNRAS, 259, 328

Athanassoula, E. 2003, MNRAS, 341, 1179

Athanassoula, E. 2005, MNRAS, 358, 1477

Athanassoula, E. & Bosma, A. 1985, ARA&A, 23, 147

Athanassoula, E. et al. 1990, MNRAS, 245, 130

Athanassoula, E., Romero-Gómez, M., & Masdemont, J. J. 2009a, MNRAS, 394, 67

Athanassoula, E., Romero-Gómez, M., Bosma, A., & Masdemont, J. J. 2009b, MNRAS, 400, 1706

Bacon, R. et al. 2001, MNRAS, 326, 23

Bagetakos, I. Brinks, E., Walter, F., de Blok, W. J. G., Rich, J, W., Usero, A., & Kennicutt, R. C. 2009, in The Evolving ISM in the Milky Way and Other Galaxies, K. Sheth, A. Noriega-Crespo, J. Ingalls, and R. Paladini, eds., http://ssc.spitzer.caltech.edu/mtgs/ismevol, E17

Bagley, M., Minchev, I., & Quillen, A. C. 2009, MNRAS, 395, 537

Bahcall, J. N., Kirhakos, S., Saxe, D. H., & Schneider, D. P. 1997, ApJ, 479, 642

Baldry, I. K., Glazebrook, K., Brinkmann, J., Ivezić, Z., Lupton, R. H., Nichol, R. C., & Szalay, A. S. 2004, ApJ, 600, 681

Banerji, M. et al. 2010, MNRAS, 406, 342

Barazza, F. D., Binggeli, B., & Jerjen, H. 2002, AJ, 124, 1954

Barazza, F. D., Jogee, S., & Marinova, I. 2008, ApJ, 675, 1194

Barway, S., Khembavi, A., Wadadekar, Y., Ravikumar, C. D., & Mayya, Y. D. 2007, ApJ, 661, L37

Barway, S., Wadadekar, Y., & Khembavi, A. K. 2011, MNRAS, 410, L18

Beckwith, S. V. W. et al. 2006, AJ, 132, 1729

Bell, E. et al. 2004, ApJ, 608, 752

Belokurov, V. et al. 2007, ApJ, 654, 897

Bershady, M., Jangren, A., & Conselice, C. J. 2000, AJ, 119, 2645

Bertin, G., Lin, C. C., Lowe, S. A., & Thurstans, R. P. 1989, ApJ, 338, 78

Bertola, F. 1987, in IAU Symp. 127, p. 135

Bertin, G. & Amorisco, N. C. 2010, A&A, 512, 17

Binggeli, B., Sandage, A., & Tammann, G. A. 1985, AJ, 90, 1681

Binney, J. 1992, ARA& A, 30, 51

Blakeslee, J. P. 1999, AJ, 118, 1506

Block, D. L., Bertin, G., Stockton, A., Grosbol, P., Moorwood, A. F. M., Peletier, R. F. 1994, A&A, 288, 365

Block, D., Freeman, K. C., Puerari, I., Combes, F., Buta, R., Jarrett, T., & Worthey, G. 2004a, in Penetrating Bars Through Masks of Cosmic Dust, eds. D. L. Block, I. Puerari, K. C. Freeman, R. Groess, & E. Block, Springer, Kluwer, p. 15

Block, D. L., Freeman, K. C., Jarrett, T. H., Puerari, I., Worthy, G., Combes, F., & Groess, R. 2004b, A&A, 425, L37

Block, D. L., Puerari, I., Elmegreen, B. G., Elmegreen, D. M., Fazio, G. G., & Gehrz, R. D. 2009, ApJ, 694, 115

Book, L. G. & Benson, A. J. 2010, ApJ, 716, 810

Bothun, G., Impey, C. D., Malin, D. F., & Mould, J. R. 1987, AJ, 94, 23

Bournaud, F. & Combes, F. 2002, A&A, 392, 83

Brook, C., Governato, F., Quinn, T., Wadsley, J., Brooks, A. M., Willman, B., Stilp, A., & Jonsson, P. 2008, ApJ, 689, 678

Bureau, M., Aronica, G., Athanassoula, E., Dettmar, R.-J., Bosma, A., Freeman, K. C.

2006, MNRAS, 370, 753

Bush, S. J. & Wilcots, E. M. 2004, AJ, 128, 2789

Buta, R. 1987, ApJS, 64, 1

Buta, R. 1995, ApJS, 96, 39

Buta, R. & Block, D. L. 2001, ApJ, 550, 243

Buta, R. & Combes, F. 1996, Fund. Cosmic Phys. 17, 95

Buta R. & Crocker D. A. 1993, AJ, 106, 939

Buta, R., Byrd, G., & Freeman, T. 2003, AJ, 125, 634

Buta, R. J., Corwin, H. G., & Odewahn, S. C. 2007, The de Vaucouleurs Atlas of Galaxies, Cambridge: Cambridge U. Press (dVA)

Buta, R. J., Knapen, J. K., Elmegreen, B. G., Salo, H., Laurikainen, E., Elmegreen, D. M., Puerari, I., & Block, D. L. 2009, AJ, 137, 4487

Buta, R. et al. 2010a, ApJS, 190, 147

Buta, R., Laurikainen, E., Salo, H., & Knapen, J. H. 2010b, ApJ, 721, 259

Buta, R., Mitra, S., de Vaucouleurs, G., & Corwin, H. G. 1994, AJ, 107, 118

Buta, R., Laurikainen, E., Salo, H., Block, D. L., & Knapen, J. H. 2006, AJ, 132, 1859

Buta, R. & Zhang, X, 2009, ApJS, 182, 559

Butcher, H. & Oemler, A. 1978, ApJ, 219, 18

Byrd, G. G., Rautiainen, P. Salo, H., Buta, R., & Crocker, D. A. 1994, AJ, 108, 476

Caon, N., Capaccioli, M., & D'Onofrio, M. 1993, MNRAS, 265, 1013

Cappellari, M. et al. 2011, astro-ph 1012.1551

Cardemone, C. et al. 2009, MNRAS, 399, 1191

Carignan, C. & Purton, C. 1998, ApJ, 506, 125

Carollo, C. M., Stiavelli, M., de Zeeuw, P. T., & Mack, J. 1997, AJ, 114, 2366

Cayatte, V., Kotanyi, C., Balkowski, C., & van Gorkom, J. H. 1994, AJ, 107, 1003

Chapman, S. C., Windhorst, R., Odewahn, S., et al. 2003, ApJ, 599, 92

Chung, A., van Gorkom, J. H., Kenney, J. D. P., Crowl, Hugh, & Vollmer, B. 2009, AJ, 138, 1741

Cole, A. A. et al. 2007, ApJ, 659, L17

Comerón, S., Knapen, J. H., Beckman, J. E., Laurikainen, E., Salo, H., Martinez-Valpuesta, I., & Buta, R. J. 2010, MNRAS, 402, 2462

Comerón, S., Martinez-Valpuesta, I., Knapen, J. H., & Beckman, J. 2009, ApJ, 706, L25

Conselice, C. J. 1997, PASP, 109, 1251

Conselice, C. J. 2003, ApJS, 147, 1

Conselice, C. J. et al. 2004, ApJ, 600, L139

Conselice, C. J., Rajgor, S., & Myers, R. 2008, MNRAS, 386, 909

Conselice, C. J. 2009, MNRAS, 399, L16

Conselice, C. J. & Arnold, J. 2009, MNRAS, 397, 208

Contopoulos, G. 1996, ASP Conf. Ser. 91, p. 454

Contopoulos, G. & Grosbol, P. 1989, Astr. Astrophys. Rev. 1, 261

Cowie, L., Hu, E., & Songaila, A. 1995, AJ, 110, 1576

Crocker, D. A., Baugus, P. D., & Buta, R. 1996, ApJS, 105, 353

Cullen, H., Alexander, P., Green, D. A., & Sheth, K. 2007, MNRAS, 376, 98

Darg, D. W. et al. 2010, MNRAS, 401, 1043

Davies, R. L., Efstathiou, G., Fall, S. M., Illingworth, G., & Schechter, P. L. 1983, ApJ, 266, 41

de Vaucouleurs, G. 1956, Mem. Comm. Obs., 3, No. 13

de Vaucouleurs, G. 1958, ApJ, 127, 487

de Vaucouleurs, G. 1959, Handbuch der Physik, 53, 275

de Vaucouleurs, G. 1961, ApJS, 5, 233

de Vaucouleurs, G. 1963, ApJS, 8, 31

de Vaucouleurs, G. & Freeman, K. C. 1972, Vistas in Astronomy 14, 163

de Vaucouleurs, G. de Vaucouleurs, A., & Corwin, H. G. (1976), *Second Reference Catalogue of Bright Galaxies*, Univ. Texas Mono. Astr. No. 2 (RC2)

de Vaucouleurs, G., de Vaucouleurs, A., Corwin, H. G., Buta, R., Paturel, G., & Fouque, P. 1991, Third Reference Catalogue of Bright Galaxies, New York, Springer (RC3)

de Zeeuw, P. T. et al. 2002, MNRAS, 329, 513

Djorgovski, S. 1992, in Morphological and Physical Classification of Galaxies, G. Longo, M. Capaccioli, & G. Busarello, eds., Dordrecht, Kluwer, p. 337

Dressler, A. 1980, ApJ, 236, 351

Durbala, A., Buta, R., Sulentic, J. W., & Verdes-Montenegro, L. 2009, MNRAS, 397, 1756

Durbala, A., Sulentic, J. W., Buta, R., & Verdes=Montenegro, L. 2008, MNRAS, 390, 881

Elmegreen, D. M. 1981, ApJS, 47, 229

Elmegreen, D. M. & Elmegreen, B. G. 1987, ApJ, 314, 3

Elmegreen, D. & Elmegreen, B. G. 2006, ApJ, 651, 676 (EE06)

Elmegreen, D., Elmegreen, B. G., & Sheets, C. 2004, ApJ, 603, 74 (EES04)

Elmegreen, D., Elmegreen, B. G., & Ferguson, T. E. 2005, ApJ, 623, L71

Elmegreen, D., Elmegreen, B. G., Ferguson, T. E., & Mullan, B. 2007a, ApJ, 663, 734 (EEFM07)

Elmegreen, D. M., Elmegreen, B. G., Ravindranath, S., & Coe, D. A. 2007b, ApJ, 658, 763

Elmegreen, D., Elmegreen, B. G., & Hirst, A. 2004, ApJ, 604, L21 (EEH04)

Elmegreen, D. M., Elmegreen, B. G., Marcus, M. T., Shainyan, K., Yau, A., & Petersen, M. 2009b, ApJ, 701, 306

Elmegreen, B.. G., Bournaud, F., & Elmegreen, D. M. 2008, ApJ, 688, 67

Elmegreen, B. G., Elmegreen, D. M., & Leitner, S. N. 2003, ApJ, 590, 271 (EEL03)

Elmegreen, B. G., Elmegreen, D. M., & Montenegro, L. 1992, ApJS, 79, 37

Elmegreen, B. G., Elmegreen, D. M., Fernandez, M. X., & Lemonias, J. J. 2009a, ApJ, 692, 12

Emsellem, E. et al. 2007, MNRAS, 379, 401

Eskridge, P. B. et al. 2000, AJ, 119, 536

Eskridge, P. B. et al. 2002, ApJS, 143, 73

Fazio, G. G. et al. 2004, ApJS, 154, 10

Ferguson, H. C. & Binggeli, B. 1994, Astr. Ap. Rev. 6, 67

Ferrarese, L. et al. 2006, ApJS, 164, 334

Freeman, K. C. 1975, in Galaxies and the Universe, A. Sandage, M. Sandage, & J. Kristian, eds., Chicao, University of Chicago Press, p. 409

Garcia-Ruiz, I., Sancisi, R., & Kuijken, K. 2002, A&A, 394, 769

Giavalisco, M. et al. 2004, ApJ, 600, L93

Gil de Paz, A., Madore, B. F., & Pevunova, O. 2003, ApJS, 147, 29

Gil de Paz, A. et al. 2005, ApJ, 627, L29

Gillett, F. C., Forrest, W. J., & Merrill, K. M. 1973, ApJ, 183, 87

Giovanelli, R. & Haynes, M. P. 1985, AJ, 292, 404

Graham, A. W. & Guzmán, R. 2003, AJ, 125, 2936

Grouchy, R. D., Buta, R., Salo, H., Laurikainen, E., & Speltincx, T. 2008, AJ, 136, 980

Grouchy, R. D., Buta, R. J., Salo, H., & Laurikainen, E. 2010, AJ, 139, 2465

Gunn, J. E. & Gott, J. R. 1972, ApJ, 176, 1

Gunn, J. E. et al. 1998, AJ, 116, 3040

Helfer, T. T., Thornley, M. D., Regan, M. W., Wong, T., Sheth, K., Vogel, S. N., Blitz, L., & Bock, D. C.-J. 2003, ApJS, 145, 259

Helou, G. et al. 2004, ApJS, 154, 253

Higdon, J. L. 1995, ApJ, 455, 524

Higdon, J. L., Buta, R. J., & Purcell, G. B. 1998, AJ, 115, 80

Holmberg, E. 1950, Medd. Lunds. Astron. Obs., Ser. II, No. 128

Holwerda, B. W., Keel, W. C., Williams, B., Dalcanton, J. J., & de Jong, R. S. 2009, AJ, 137, 3000

Hubble, E. 1926, ApJ, 64, 321

Hubble, E. 1936, *The Realm of the Nebulae*, Yale Univ. Press, Yale.

Hubble, E. 1943, ApJ, 97, 112

Hunt, L. K. & Malkan, M. A. 1999, ApJ, 516, 660

Hunter, D. A. 1997, PASP, 109, 937

Impey, C. & Bothun, G. D. 1997, ARA&A, 35, 267

Irwin, M. J. et al. 2007, ApJ, 656, L13

Jarrett, T. H. et al. 2003, AJ, 125, 525

Jeans, J. 1929, Astronomy and Cosmogony, Cambridge, Cambridge University press

Jerjen, H., Kalnajs, A., & Binggeli, B. 2000, A&A, 358, 845

Jogee, S. et al. 2009, ApJ, 697, 1971

Jokimaki, A., Orr, H., & Russell, D. G. 2008, AP&SS, 315, 249

Karachentseva, V. E. 1973, Astrofiz. Issled-Izv. Spets. Astrofiz. Obs. 8, 3

Karataeva, G. M., Tikhonov, N. A., Galazutdinova, O. A., Hagen-Thorn, V. A., & Yakovleva, V. A. 2004, A&A, 421, 833

Kennicutt, R. C., Tambln, P., & Congdon, C. W. 1994, ApJ, 435, 22

Kerr, F. & de Vaucouleurs, G. 1955, Australian Journal of Physics, 8, 508

Knapen, J. H. 2005, A&A, 429, 141

Knapen, J., Beckman, J. E., Shlosman, I., Peletier, R. F., Heller, C. H., & de Jong, R. S. 1995a, ApJ, 443, L73

Knapen, J., Beckman, J. E., Heller, C. H., Shlosman, I., & de Jong, R. S. 1995b, ApJ, 454, 623

Knapen, J. H., Shlosman, I., & Peletier, R. F. 2000, ApJ, 529, 93

Knapen, J. H. 2010, in Galaxies and Their Masks, D. L. Block, K. C. Freeman, & I. Puerari, eds., New York, Spinger, in press

Knapen, J. H. & James, P. A. 2009, ApJ, 698, 1437

Koopmann, R. & Kenney, J. D. P. 2004, ApJ, 613, 866

Kormendy, J. 1979, ApJ, 227, 714

Kormendy, J. 1985, ApJ, 295, 73

Kormendy, J. 1999, ASPC, 182, 124

Kormendy, J. & Bender, R. 1996, ApJ, 464, L119

Kormendy, J. & Djorgovski, S. 1989, ARA&A, 27, 235

Kormendy, J. & Kennicutt, R. C. 2004, ARA&A, 42, 603 (KK04)

Kormendy, J. & Norman, C. A. 1979, ApJ, 233, 539

Kormendy, J., Fisher, D. B., Cornell, M. E., & Bender, R. 2009, ApJS, 182, 216

Kuijken, K. & Merrifield, M. R. 1995, ApJ, 443, L13

Laine, S., Shlosman, I., Knapen, J., & Peletier, R. F. 2002, ApJ, 567, 97

Laurikainen, E. & Salo, H. 2002, MNRAS, 337, 1118

Laurikainen, E., Salo, H., & Buta, R. 2004, ApJ, 607, 103

Laurikainen, E., Salo, H., & Buta, R. 2005, MNRAS, 362, 1319

Laurikainen, E., Salo, H., Buta, R., Knapen, J., Speltincx, T., & Block, D. L. 2006, MNRAS, 132, 2634

Laurikainen, E., Salo, H., Buta, R., & Knapen, J. 2007, MNRAS, 381, 401

Laurikainen, E., Salo, H., Buta, R., & Knapen, J. 2009, ApJ, 692, L34

Laurikainen, E., Salo, H., Buta, R., Knapen, J. H., & Comerón, S. 2010, MNRAS, 405, 1089

Lelli, F., Fraternali, F., & Sancisi, R. 2010, A&A, 516, 11

Lintott, C. et al. 2008, MNRAS, 389, 1179

Lintott, C. et al. 2009, MNRAS, 399, 129

Lisker, T., Debattista, V. P., Ferreras, I., & Erwin, P. 2006, MNRAS, 370, 477

Lotz, J. M., Madau, P., Giavalisco, M., Primack, J., & Ferguson, H. C. 2006, ApJ, 636, 592

Lupton, R., Blanton, M. R., Fekete, G., Hogg, D. W., O'Mullane, W., Szalay, A., & Wherry, N. 2004, PASP, 116, 133

Lynden-Bell, D. & Kalnajs, A. J. 1972, MNRAS, 157, 1

Madore, B. F., Nelson, E., & Petrillo, K. 2009, ApJS, 181, 572

Malin, D. F. & Carter, D. 1980, Nature, 285, 643

Malin, D. F. & Carter, D. 1983, ApJ, 274, 534

Martin, D. C. et al. 2005, ApJ, 619, L1

Martin, D. C. et al. 2007, ApJS, 173, 342

Martin, P. & Friedli, D. 1997, A&A, 326, 449

Martinez-Valpuesta, I., Shlosman, I., & Heller, C. 2006, ApJ, 637, 214

Martinez-Valpuesta, I., Knapen, J. H., & Buta, R. 2007, AJ, 134, 1863

Masters, K. L. et al. 2010, MNRAS, 405, 783

Mateo, M. 1998, ARA&A, 36, 435

Matthews, T. A., Morgan, W. W., & Schmidt, M. 1964, ApJ, 140, 35

Mazzuca, L. M., Swaters, R. A., Veilleux, S., & Knapen, J. H. 2009, BAAS, 41, 693

McGaugh, S., Schombert, J. M., & Bothun, G. D. 1995, AJ, 109, 2019

McKernan, B., Ford, K. E. S., & Reynolds, C. S. 2010, astro-ph 1005.4907

Menanteau, F., Abraham, R. G., & Ellis, R. S. 2001, MNRAS, 322, 1

Menanteau, F. et al. 2004, ApJ, 612, 202

Meurer, G. R., Carignan, C., Beaulieu, S. F., & Freeman, K. C. 1996, AJ, 111, 1551

Moore, B., Katz, N., Lake, G., Dressler, A., & Oemler, A. 1996, Nature, 379, 613

Morgan, W. W. 1958, PASP, 70, 364

Nair, P. B. & Abraham, R. G. 2010, ApJS, 186, 427

Odewahn, S. C. 1991, AJ, 101, 829

Odewahn, S. C., Stockwell, E. B., Pennington, R. L., Humphreys, R. M., & Zumach, W. A. 1992, AJ, 103, 318

Oosterloo, T. A., Morganti, R., Sadler, E. M., Vergani, D., & Caldwell, N. 2002, AJ, 123, 729

Pahre, M., Ashby, M. L. N., Fazio, G. G., & Willner, S. P. 2004, ApJS, 154, 235

Pence, W. D., Taylor, K., Freeman, K. C., de Vaucouleurs, G., & Atherton, P. 1988, ApJ, 326, 564

Peng, C. Y., Ho, L. C., Impey, C. D., & Rix, H-W. 2010, AJ, 139, 2097

Pereira-Santaella, M., Alonso-Herrero, A., Rieke, G. H., Colina, L. Díaz-Santos, T., Smith, J.-D. T., Pérez-González, P. G., & Engelbracht, C. W. 2010, ApJS, 188, 447

Quillen, A. C., Frogel, J. A., & González, R. A. 1994, ApJ, 437, 162

Rahman, N., Howell, J. H., Helou, G., Mazzarella, J. M., & Buckalew, B. 2007, ApJ, 663, 908

Rautiainen, P. & Salo, H. 2000, A&A, 362, 465

Rautiainen, P., Salo, H., & Buta, R. 2004, MNRAS, 349, 933

Ravindranath, S. et al. 2006, ApJ, 652, 963

Regan, M. & Teuben, P. 2003, ApJ, 582, 723

Regan, M. & Teuben, P. 2004, ApJ, 600, 595

Regan, M. W., Thornley, M. D., Helfer, T. T.; Sheth, K., Wong, T., Vogel, S. N., Blitz, L., & Bock, D. C.-J. 2001, ApJ, 561, 218

Regan, M. et al. 2004, ApJS, 154, 204

Reynolds, J. H. 1927, Observatory, 50, 185

Revaz, Y. & Pfenniger, D. 2007, in Island Universes, Astrophysics & Space Science

Proceedings, p. 149

Rieke, G. H. & Low, F. J. 1972, ApJ, 176, L95

Rix, H.-W. & Rieke, M. J. 1993, ApJ, 418, 123

Rix, H.-W. et al. 2004, ApJS, 152, 163

Romano, R., Mayya, Y. D., & Vorobyov, E. I. 2008, AJ, 136, 1259

Romero-Gómez, M., Masdemont, J. J., Athanassoula, E., & García-Gómez, C. 2006, A&A, 453, 39

Romero-Gómez, M., Athanassoual, E., Masdemont, J. J., & García-Gómez, C. 2007, A&A, 472, 63

Ryder, S. D., Buta, R. J., Toledo, H., Shukla, H. Staveley-Smith, L., & Walsh, W. 1996, ApJ, 460, 665

Sackett, P. D., Rix, H.-W., Jarvis, B. J., & Freeman, K. C. 1994, ApJ, 436, 629

Saha, K., de Jong, R., & Holwerda, B. 2009, MNRAS, 396, 409

Salo, H. & Laurikainen, E. 2000a, MNRAS, 319, 377

Salo, H. & Laurikainen, E. 2000b, MNRAS, 319, 393

Salo, H., Laurikainen, E., Buta, R., & Knapen, J. H. 2010, ApJ, 715, L56

Sandage, A. 1961, The Hubble Atlas of Galaxies, Carnegie Inst. of Wash. Publ. No. 618

Sandage, A. 1975, in *Galaxies and the Universe, Stars and Stellar Systems, Vol. IX*, A. Sandage, M. Sandage, & J. Kristian, eds., p. 1.

Sandage, A. & Bedke, J. 1994, The Carnegie Atlas of Galaxies, Carnegie Inst. of Wash. Pub. No. 638

Sandage, A. & Binggeli, B. 1984, AJ, 89, 919

Sandage, A. & Tammann, G. A. 1981, *A Revised Shapley-Ames Catalog of Bright Galaxies*, Carnegie Institute of Washington Publ. No. 635 (first edition) (RSA)

Sanders, D. B. & Mirabel, I. F. 1996, ARA&A, 34, 749

Schawinski, K., Thomas, D., Sarzi, M., Maraston, C., Kavaraj, S., Joo, S., Yi, S. K., & Silk, J. 2007, MNRAS, 382, 1415

Schombert, J. 1986, ApJS, 60, 603

Schombert, J. 1987, ApJS, 64, 643

Schombert, J. 1988, ApJ, 328, 475

Schombert, J., Pildis, R. A., Eder, J. A., & Oemler, A. 1995, AJ, 110, 2067

Schwarz, M. P. 1981, ApJ, 247, 77

Schwarz, M. P. 1984, MNRAS, 209, 93

Schweizer, F. 1998, in Galaxies: Interactions and Induced Star Formation, R. C. Kennicutt, et al., eds., Berlin, Springer, p. 105

Schweizer, F. & Seitzer, P. 1988, ApJ, 328, 88

Schweizer, F., Ford, W. K., Jedrzejewski, R., & Giovanelli, R. 1987, ApJ, 320, 454

Schweizer, F., van Gorkom, J., & Seitzer, P. 1989, ApJ, 338, 770

Scoville, N. et a. 2007, ApJS, 172, 38

Seiden, P. E. & Gerola, H. 1982, Fund. Cosmic Phys. 7, 241

Seigar, M. S., Block, D. L., Puerari, I., Chorney, N. E., & James, P. A. 2005, MNRAS, 359, 1065

Seigar, M. S., Kennefick, D., Kennefick, J., & Lacy, C. H. 2008, ApJ, 678, L93

Sellwood, J. A. 2010, in Planets, Stars, and Stellar Systems, Vol. 5, in production

Sellwood, J. A. & Wilkinson, A. 1993, Reports on Progress in Physics, 56, 173

Shamir, L. 2009, MNRAS, 399, 1367

Sheth, K. et al. 2008, ApJ, 675, 1141

Sheth, K. et al. 2010, PASP, 122, 1397

Sil'chenko, O. K. & Afanasiev, V. L. 2004, AJ, 127, 2641

Simkin, S. M., Su, H. J., & Schwarz, M. P. 1980, ApJ, 237, 404

Skrutskie, M. F. et al. 2006, AJ, 131, 1163

Sparke, L. S., van Moorsel, G., Erwin, P., & Wehner, E. M. H. 2008, AJ, 135, 99

Spitzer, L. & Baade, W. 1951, ApJ, 113, 413

Steidel, C. & Hamilton, D. 1992, AJ, 104, 941

Steidel, C., Giavalisco, M., Dickinson, M., & Adelberger, K. 1996, AJ, 112, 352

Strateva, I. et al. 2001, AJ, 122, 1861

Struck, C. 2010, MNRAS, 403, 1516

Struck, C., Appleton, P. N., Borne, K. D., & Lucas, R. A. 1996, AJ, 112, 1868

Sulentic, J. et al. 2006, A&A, 449, 937

Surace, J. A., Sanders, D. B., Vacca, W. D., Veilleux, S., & Mazzarella, J. M. 1998, ApJ, 492, 116

Taniguchi, Y. & Watanabe, M. 1987, ApJ, 313, 89

Taylor-Mager, V. A., Conselice, C. J., Windhorst, R. A., & Jansen, R. A. 2007, ApJ, 659, 162

Theis, C., Sparke, L., & Gallagher, J. 2006, A&A, 446, 905

Theys, J. C. & Spiegel, J. C. 1976, ApJ, 208, 650

Thilker, D. A. et al. 2010, ApJ, 714, L171

Thornley, M. 1996, ApJ, 469, 45

Thuan, T. X. & Martin, G. E. 1981, ApJ, 247, 823

Thuan, T. X., Izotov, Y. I., Lipovetsky, V. A. 1997, ApJ, 477, 661

Tolstoy, E., Hill, V., & Tosi, M. 2009,ARA&A, 47, 371

Treuthardt, P., Salo, H., Rautinainen, P., & Buta, R. 2008, AJ, 136, 300

Vaisanen, P., Ryder, S., Mattila, S., & Kotilainen, J. 2008, ApJ, 689, L37

van den Bergh, S. 1980a, PASP, 92, 122

van den Bergh, S. 1980b, PASP, 92, 409

van den Bergh, S. 1995, AJ, 110, 613

van den Bergh, S. 1998, Galaxy Morphology and Classification, Cambridge, Cambridge University Press

van den Bergh, S. 2009a, ApJ, 694, L120

van den Bergh, S. 2009b, ApJ, 702, 1502

van den Bergh, S., Abraham, R. G., Ellis, R. S., Tanvir, N. R., Santiago, B. X., & Glazebrook, K. G 1996, AJ, 112, 359

van den Bergh, S., Cohen, J. G., Hogg, D. W., & Blandford, R. 2000, AJ, 120, 2190

van den Bergh, S., Pierce, M., & Tully, R. B. 1990, ApJ, 359, 4

van der Wel, A., Bell, E. F., Holden, B. P., Skibba, R. A., & Rix, H.-W. 2010, ApJ, 714, 1779

van Driel, W. et al. 1995, AJ, 109, 942

Vanzi, L. & Sauvage, M. 2004, A&A, 415, 509

Verdes-Montenegro, L., Sulentic, J., Lisenfeld, U., Leon, S., Espada, D., Garcia, E., Sabater, J., & Verley, S. 2005, A&A, 436, 443

Veron-Cetty, M. & Veron, P. 2006, A&A, 455, 773

Volonteri, M., Saracco, P., Chincarini, G., & Bolzonella, M. 2000, A&A, 362, 487

Walter, F., Brinks, E., de Blok, W. J. G., Bigiel, F., Kennicutt, R. C., Thornley. M. D., & Leroy, A. 2008, AJ,136, 2563

White, R. E. & Keel, W. C. 1992, Nature, 359, 129

Whitmore, B. C., Lucas, R. A., McElroy, D. B., Steiman-Cameron, T. Y., Sackett, P. D., & Olling, R. P. 1990, AJ, 100, 1489

Williams, R. E. et al. 1996, ApJ, 112, 1335

Willman, B. et al. 2005, ApJ, 626, L85

Willner, S. et al. 2004, ApJS, 154, 222

Windhorst, R. et al. 2010, ApJS, May, 2010, in press

Wirth, A. & Gallagher, J. S. 1984, ApJ, 282, 85

Wyder, T. K. et al. 2007, ApJS, 173, 293

Yagi, M., Yoshida, M., Komiyama, Y., Kashikawa, N.; Furusawa, H., Okamura, S., Graham, A. W.; Miller, N. A.; Carter, D., Mobasher, B., & Jogee, S. 2010, AJ, 140, 1814

York, D. G. et al. 2000, AJ, 120, 1579

Zhang, X. 1996, ApJ, 457, 125

Zhang, X. 1998, ApJ, 499, 93

Zhang, X. 1999, ApJ, 518, 613

Zhang, X. & Buta, R. 2007, AJ, 133, 2584

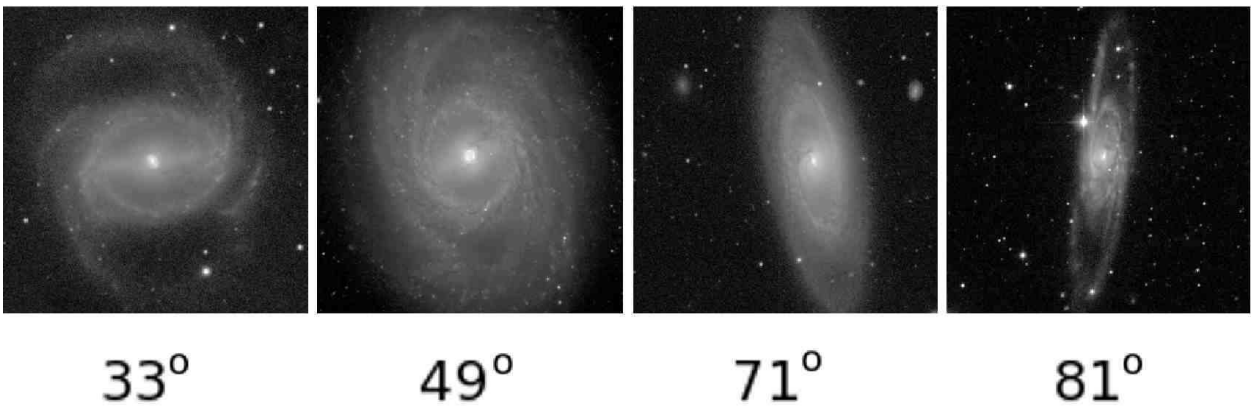

Fig. 1.— Four galaxies of likely similar face-on morphology viewed at different inclinations (number below each image). The galaxies are (left to right): NGC 1433, NGC 3351, NGC 4274, and NGC 5792. Images are from the dVA (filters B and g).

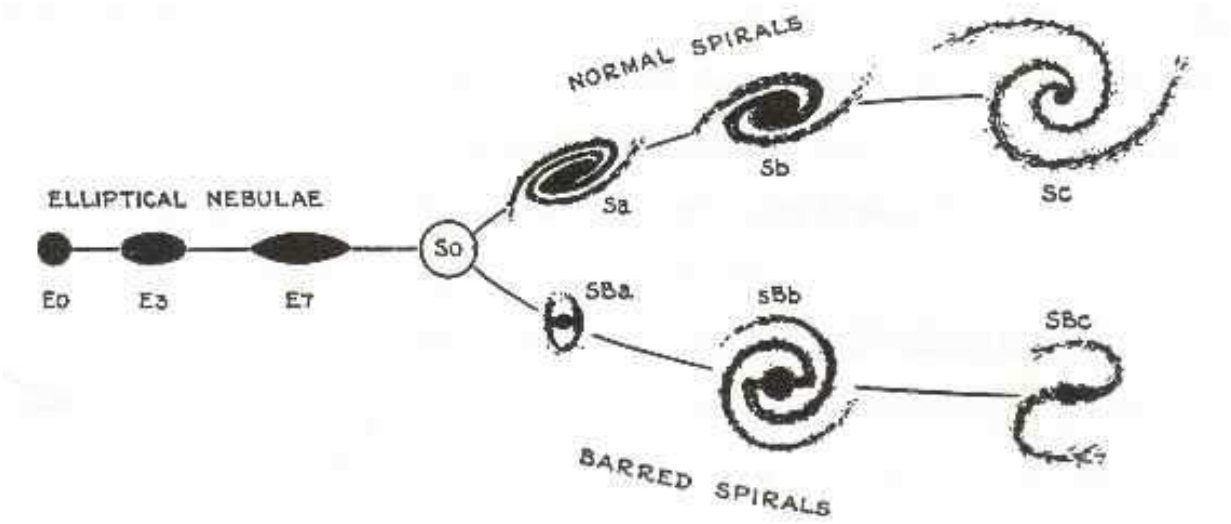

Fig. 2.— Hubble's (1936) "tuning fork" of galaxy morphologies is the basis for modern galaxy classification.

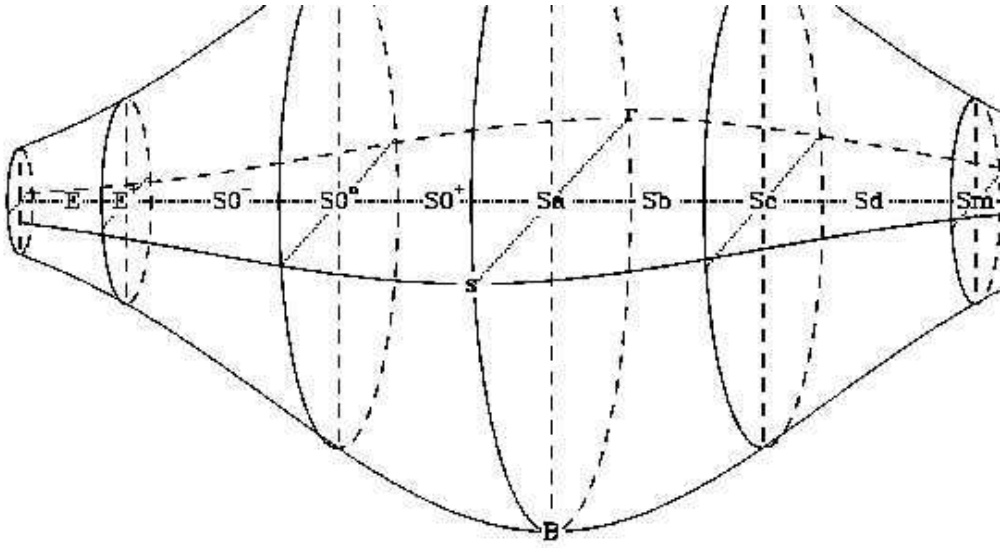

Fig. 3.— de Vaucouleurs's (1959) classification volume, a revision and extension of the Hubble tuning fork. The three dimensions are the stage (Hubble type), the family (apparent bar strength), and the variety (presence or absence of an inner ring).

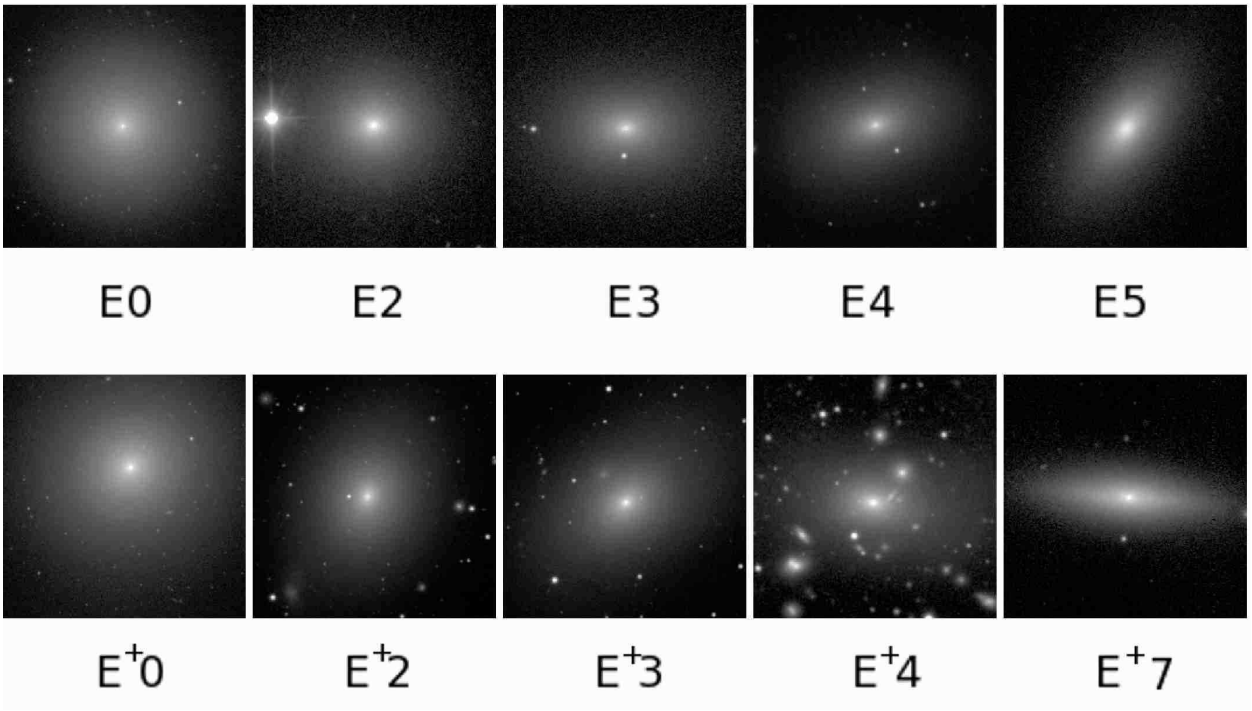

Fig. 4.— Examples of elliptical galaxies of different projected shapes. Type E galaxies are normal ellipticals with no structural details. From left to right the galaxies shown are NGC 1379, 3193, 5322, 1426, and 720. Type E^+ galaxies are "late" ellipticals, which may include faint extended envelopes typical of large cluster ellipticals, or simple transition types to $S0^-$. The examples shown are (left to right): NGC 1374, 4472, 4406, 4889, and 4623. All of these images are from the dVA (filters B, V, and g).

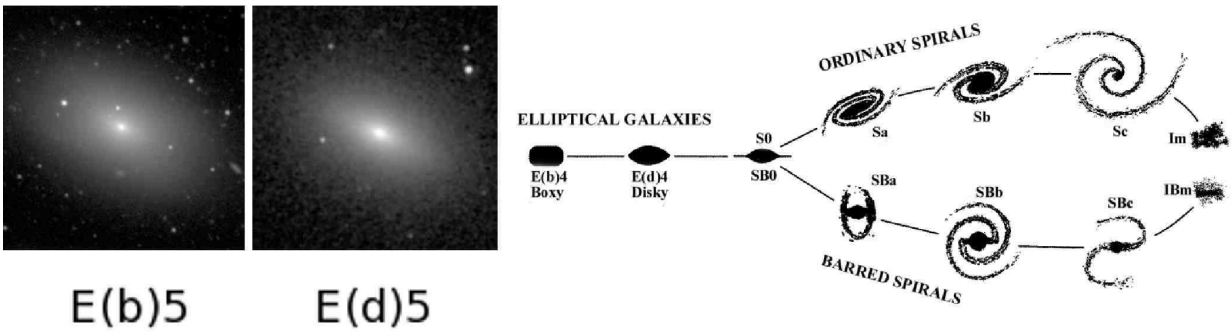

Fig. 5.— Revised classification of elliptical galaxies from Kormendy & Bender (1996), as schematically incorporated into Hubble's (1936) "tuning fork." At left are two examples of boxy and disky ellipticals: NGC 7029 (left, B-band) and NGC 4697 (JHK_s composite, 2MASS image from NED).

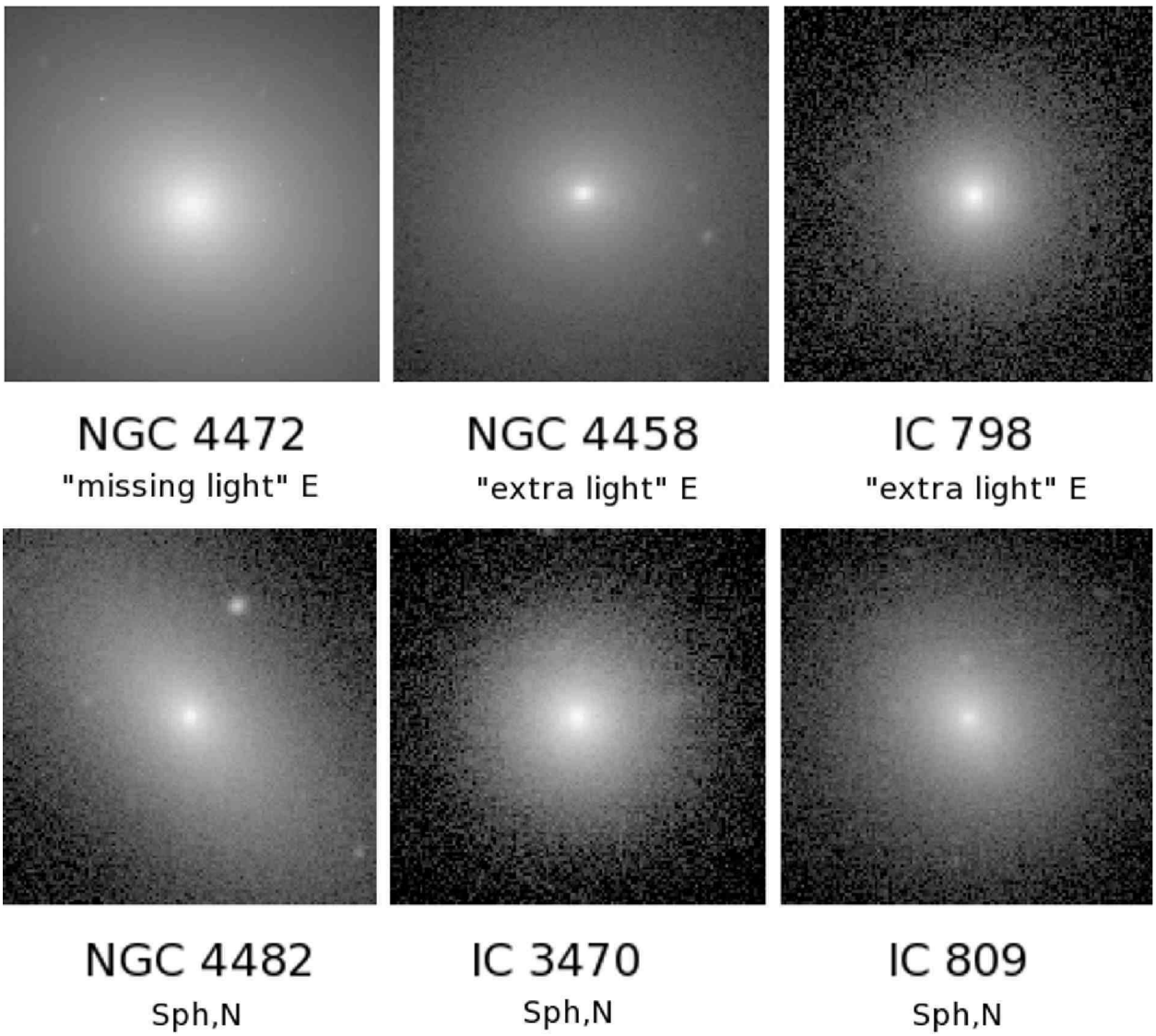

Fig. 6.— Illustrations of 6 early-type galaxies in the Virgo Cluster with photometric classifications from Kormendy et al. (2009): NGC 4472 (core E, $M_V = -23.2$); NGC 4458 (coreless E, $M_V = -19.0$); IC 798 (VCC 1440; 'coreless E, $M_V = -16.9$); NGC 4482 (nucleated spheroidal, $M_V = -18.4$); IC 3470 (VCC 1431; nucleated spheroidal, $M_V = -17.4$); IC 809 (VCC 1910; nucleated spheroidal, $M_V = -17.4$). The images shown are all based on SDSS g-band single or mosaic images, and are in units of mag arcsec^{-2}.

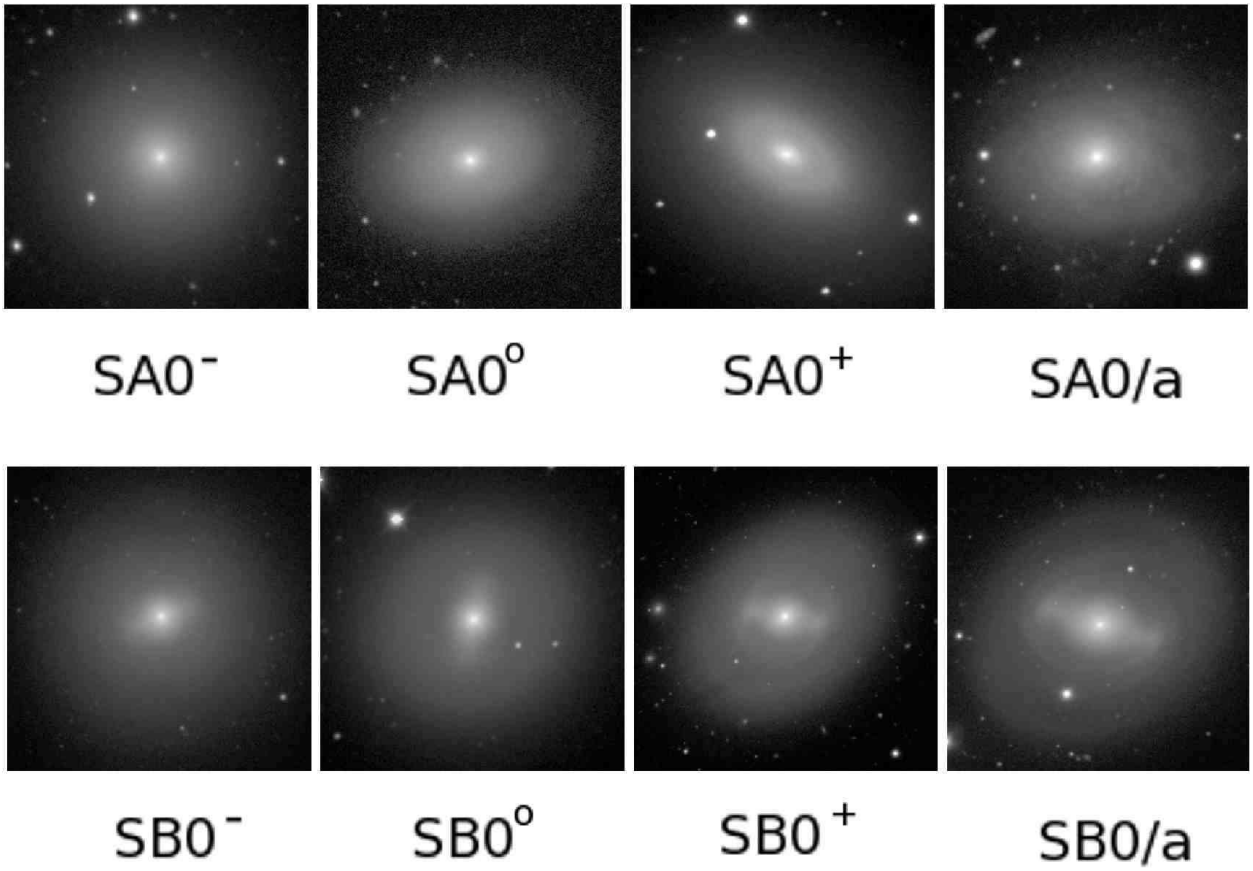

Fig. 7.— Examples of barred and nonbarred S0 galaxies of different stages from "early" ($S0^-$), to "intermediate" ($S0^o$), to "late" ($S0^+$), including the transition stage to spirals, S0/a. The galaxies shown are (left to right): Row 1 - NGC 7192, 1411, 1553, and 7377; Row 2 - NGC 1387, 1533, 936, and 4596. All images are from the dVA (filters B and V).

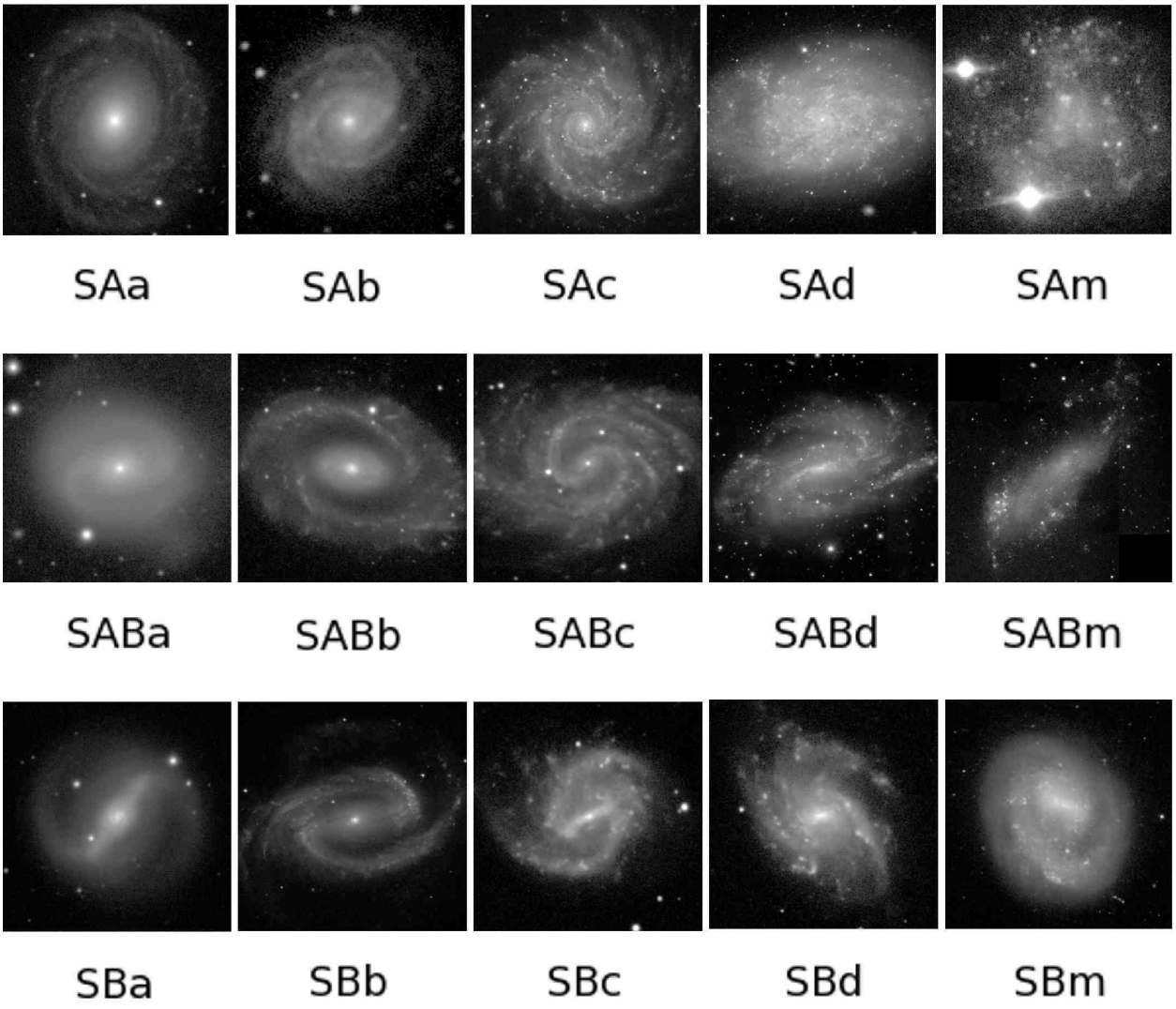

Fig. 8.— Stage classifications for spirals, divided according to bar classifications into parallel sequences. The galaxies illustrated are (left to right): Row 1 - NGC 4378, 7042, 628, 7793, and IC 4182; Row 2 - NGC 7743, 210, 4535, 925, and IC 2574; Row 3 - NGC 4314, 1300, 3513, 4519, and 4618. All images are B-band from the dVA.

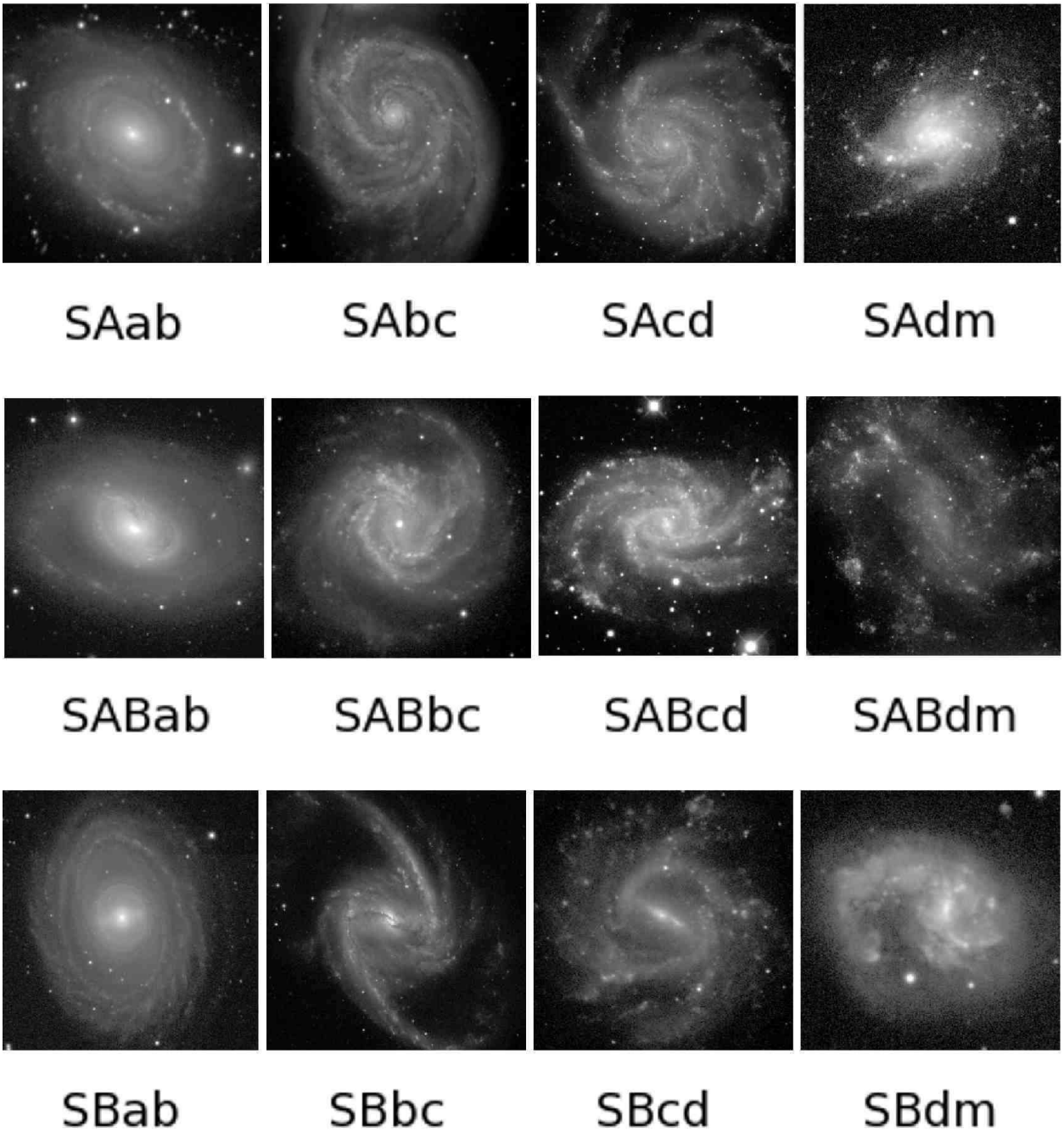

Fig. 9.— Sequences of stages intermediate between the main stages illustrated in Figure 8. The galaxies are (left to right): Row 1 - NGC 2196, 5194, 5457, and 4534; Row 2 - NGC 3368, 4303, 2835, and 4395; Row 3 - NGC 1398, 1365, 1073, and 4027. All images are B-band from the dVA, except for NGC 4534, which is SDSS g-band.

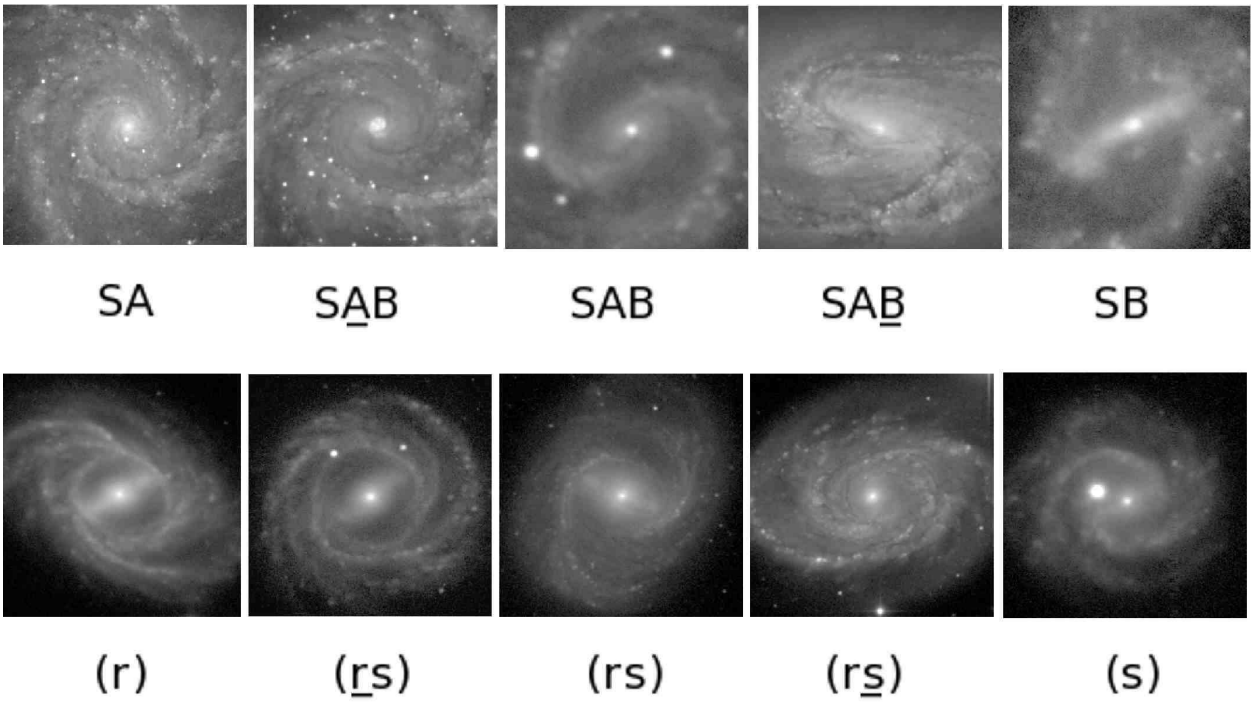

Fig. 10.— The continuity of family and variety characteristics among spiral galaxies, including underline classifications used by de Vaucouleurs (1963). The galaxies are (left to right): Row 1 - NGC 628, 2997, 4535, 3627, and 3513; Row 2 - NGC 2523, 3450, 4548, 5371, and 3507. All images are B-band from the dVA.

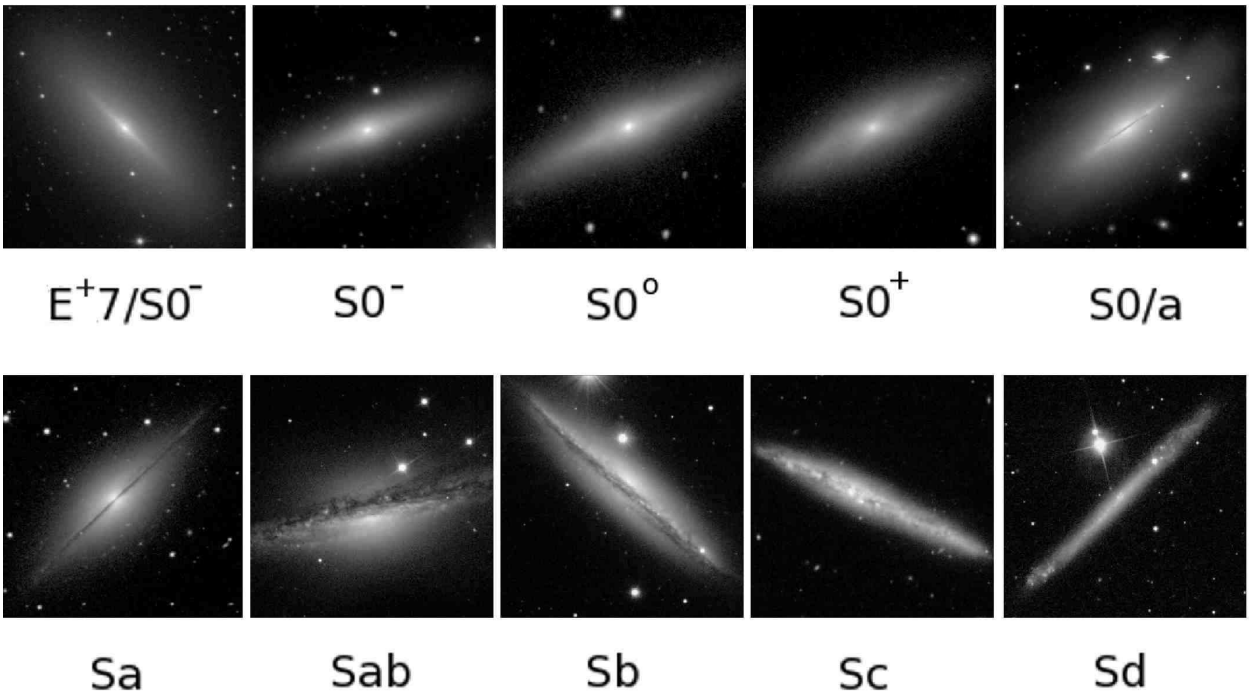

Fig. 11.— Classification of edge-on galaxies by stage. The galaxies are (left to right): Row 1 - NGC 3115, 1596, 7332, 4425, and 5866; Row 2 - NGC 7814, 1055, 4217, 4010, and IC 2233. All images are from the dVA (B and V filters).

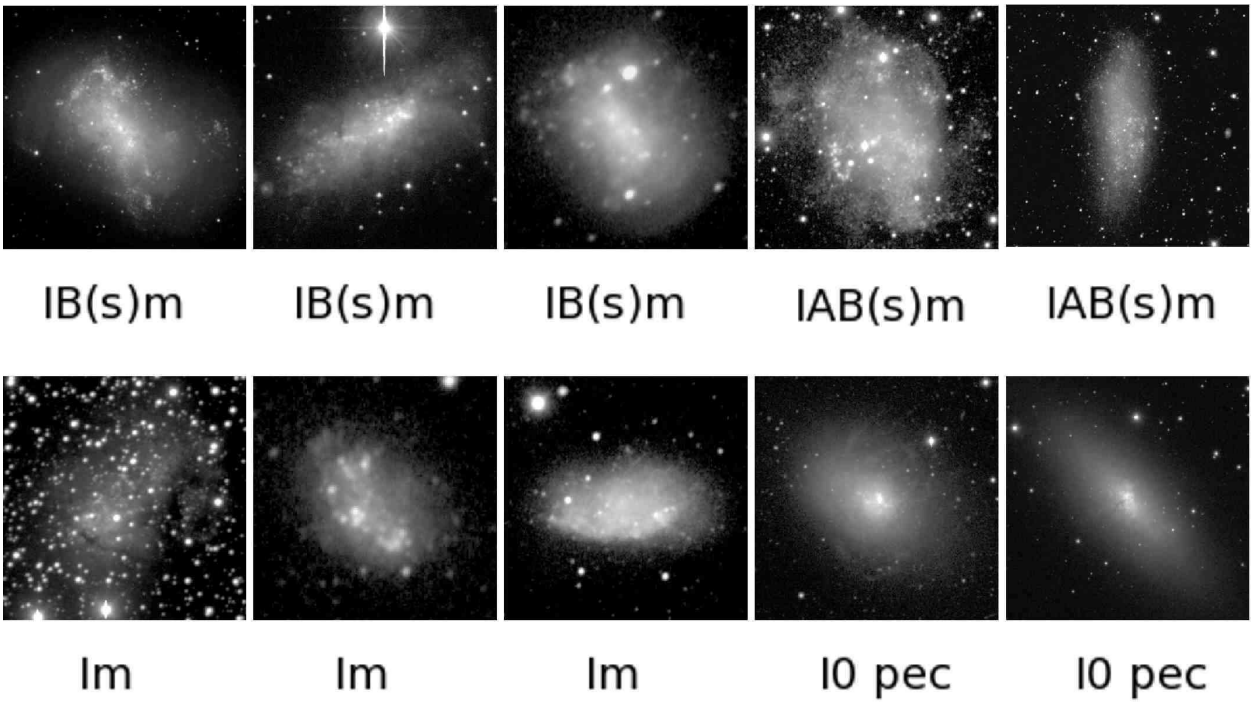

Fig. 12.— Examples of irregular galaxies ranging in absolute blue magnitude from −14 to −18. The galaxies are (left to right): Row 1 - NGC 4449, 1569, 1156, DDO 50, and A2359-15 (WLM galaxy); Row 2 - IC 10, DDO 155, DDO 165, NGC 1705, NGC 5253. The "pec" stands for peculiar. All images are B-band from the dVA.

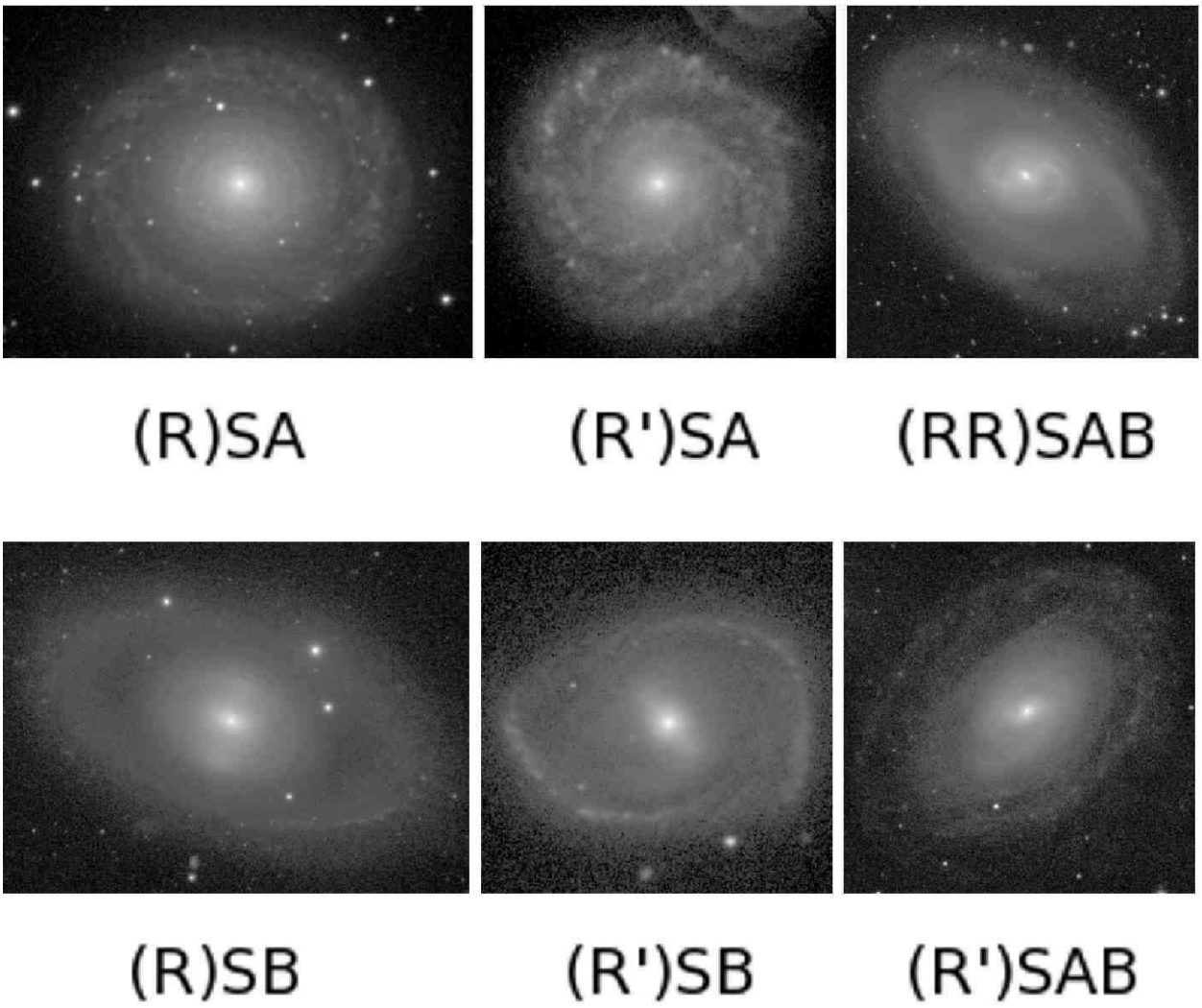

Fig. 13.— Examples of outer rings (R) and outer pseudorings (R′) in barred and nonbarred galaxies. Also shown is a rare example with two largely detached outer rings (RR). The galaxies are (left to right): Row 1 - NGC 7217, IC 1993, and NGC 2273; Row 2 - NGC 3945, NGC 1358, and NGC 1371. All images are from the dVA and are B-band except for NGC 2273, which is r-band.

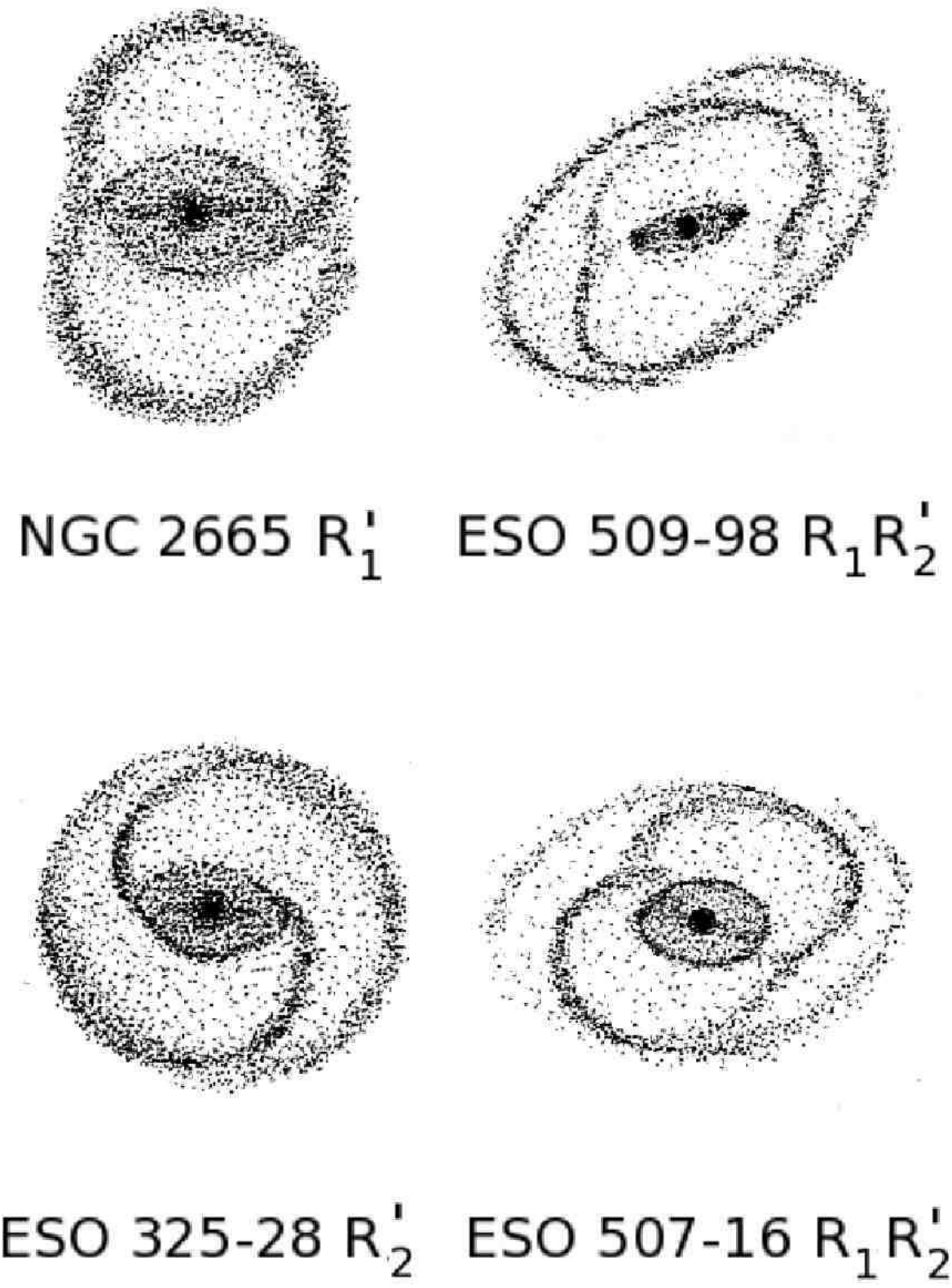

Fig. 14.— Schematic representations of outer Lindblad resonance (OLR) morphologies (Buta & Combes 1996).

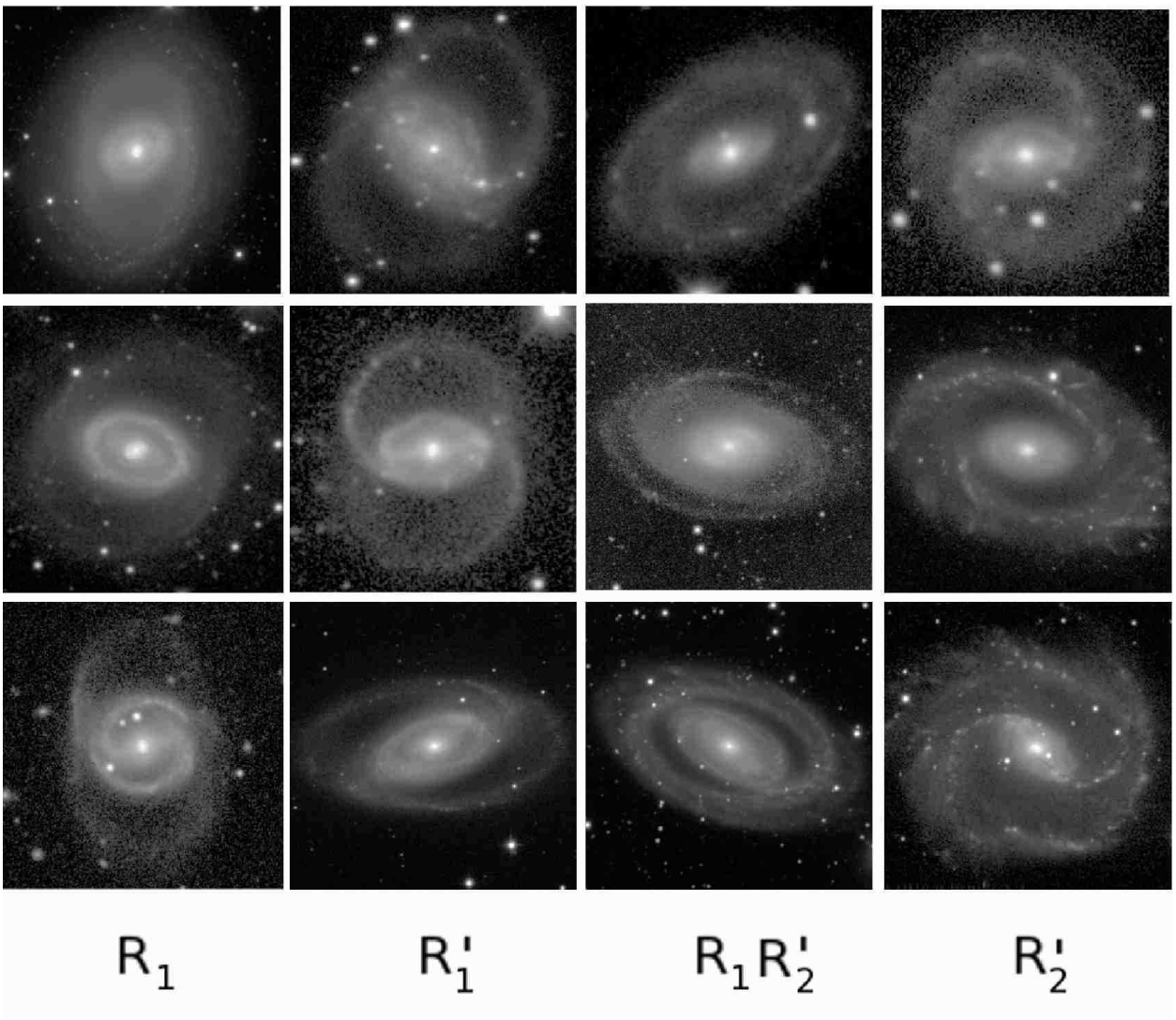

Fig. 15.— Examples of OLR subclasses of outer rings and pseudorings. The galaxies are (left to right): Row 1 - NGC 1326, NGC 2665, ESO 509−98, and ESO 325−28; Row 2 - NGC 3081, UGC 12646, NGC 1079, and NGC 210; Row 3 - NGC 5945, 1350, 7098, and 2935. All images are B-band from the dVA.

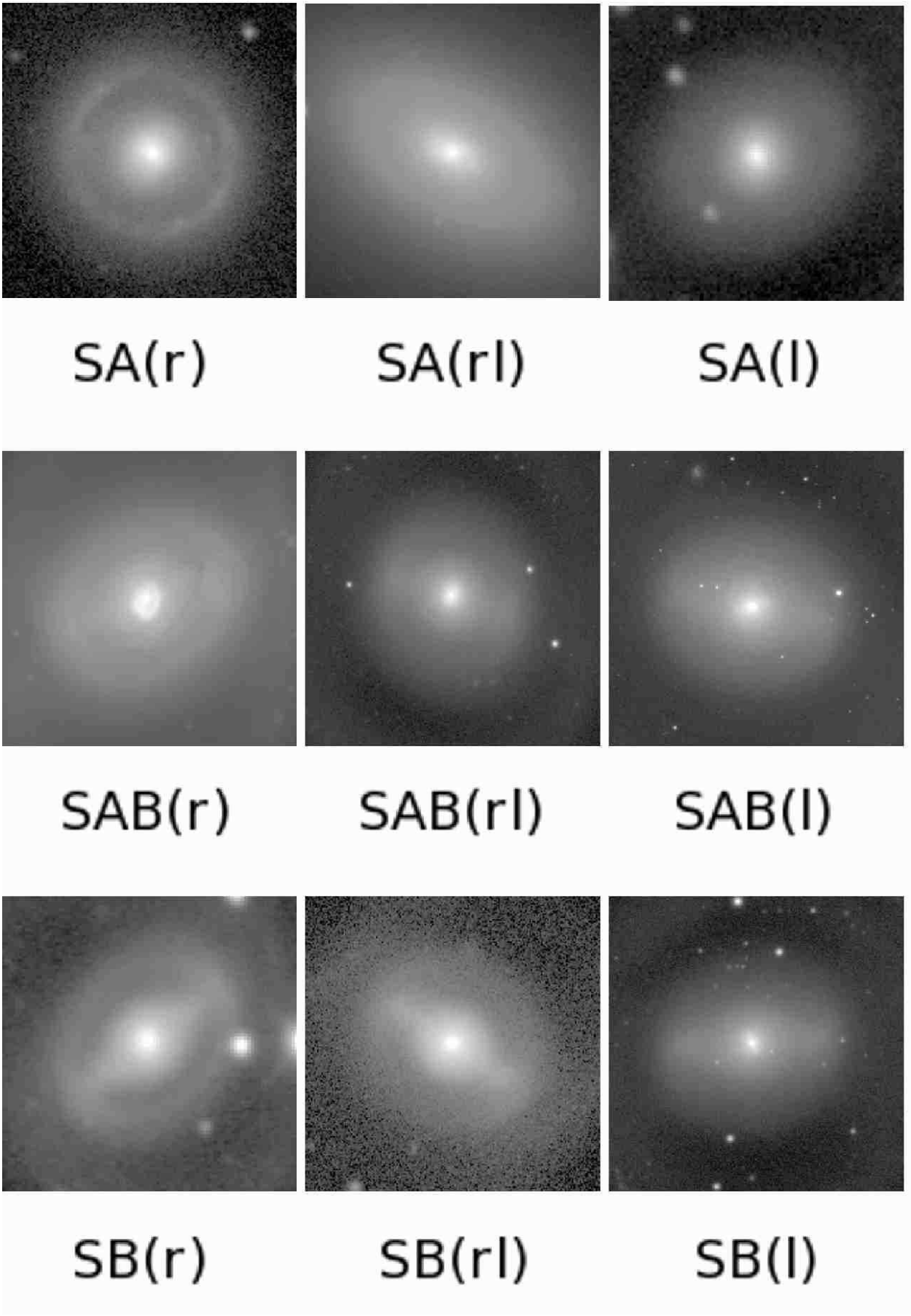

Fig. 16.—

Fig. 16. cont..— Examples showing the continuity of inner rings (r) and lenses (l), for barred and nonbarred galaxies. The galaxies are (left to right): Row 1 - NGC 7187, 1553, and 4909; Row 2 - NGC 1326, 2859, and 1291; Row 3 - ESO 426−2, NGC 1211, NGC 1543. All images are B or g-band from the dVA.

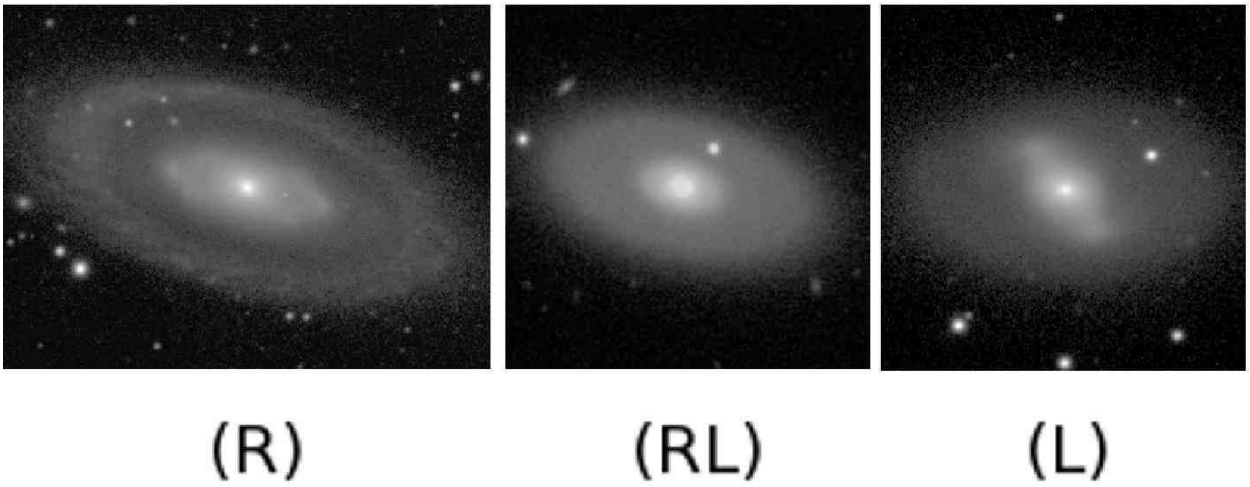

Fig. 17.— Examples showing the continuity of outer rings (R) and lenses (L). The galaxies are (left to right): - NGC 7020 (dVA B), NGC 5602 (SDSS image), and 2983 (dVA B).

nuclear rings (nr)

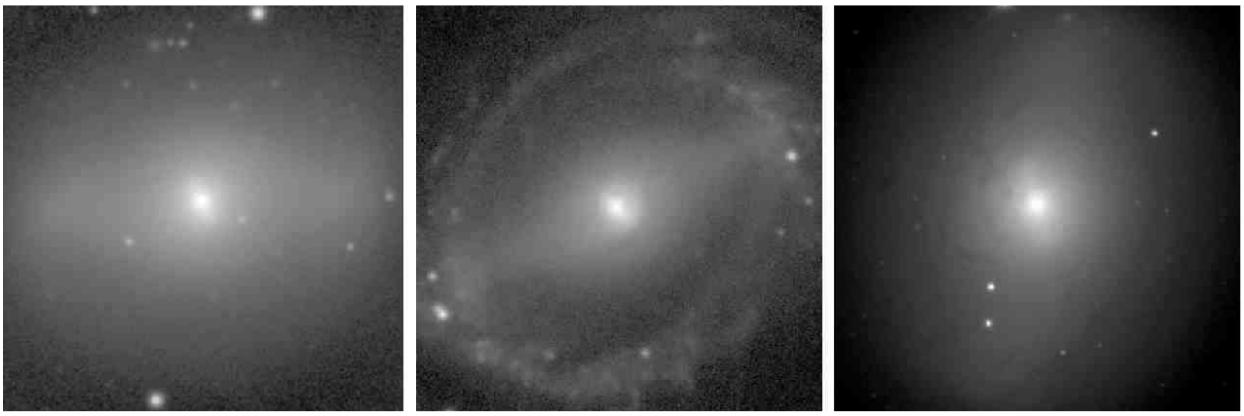

nuclear bars (nb)

Fig. 18.— Examples of nuclear rings and secondary (nuclear) bars. The galaxies are (left to right): Row 1 - NGC 1097, 3351, and 4314; Row 2 - NGC 1543, 5850, and 1291. All images are B-band from the dVA.

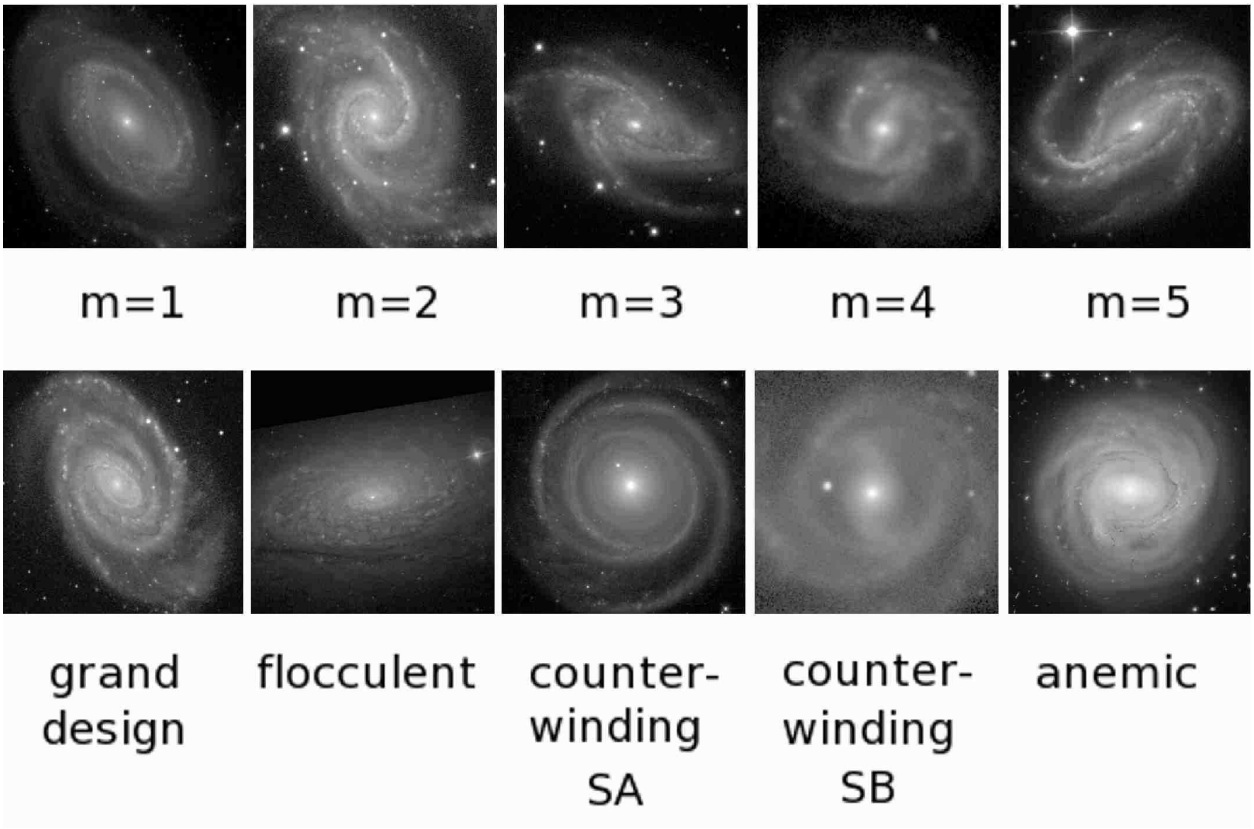

Fig. 19.— Examples showing spiral arm character differences in the form of arm multiplicity, grand design and flocculent spirals, counter-winding spirals, and an anemic spiral. The galaxies are (left to right): Row 1 - NGC 4725, 1566, 5054, ESO 566−24, and NGC 613; Row 2 - NGC 5364, 5055, 4622, 3124, and 4921. All images are B-band from the dVA except NGC 5055, which is SDSS g-band, and NGC 4921, which is from Hubble Heritage.

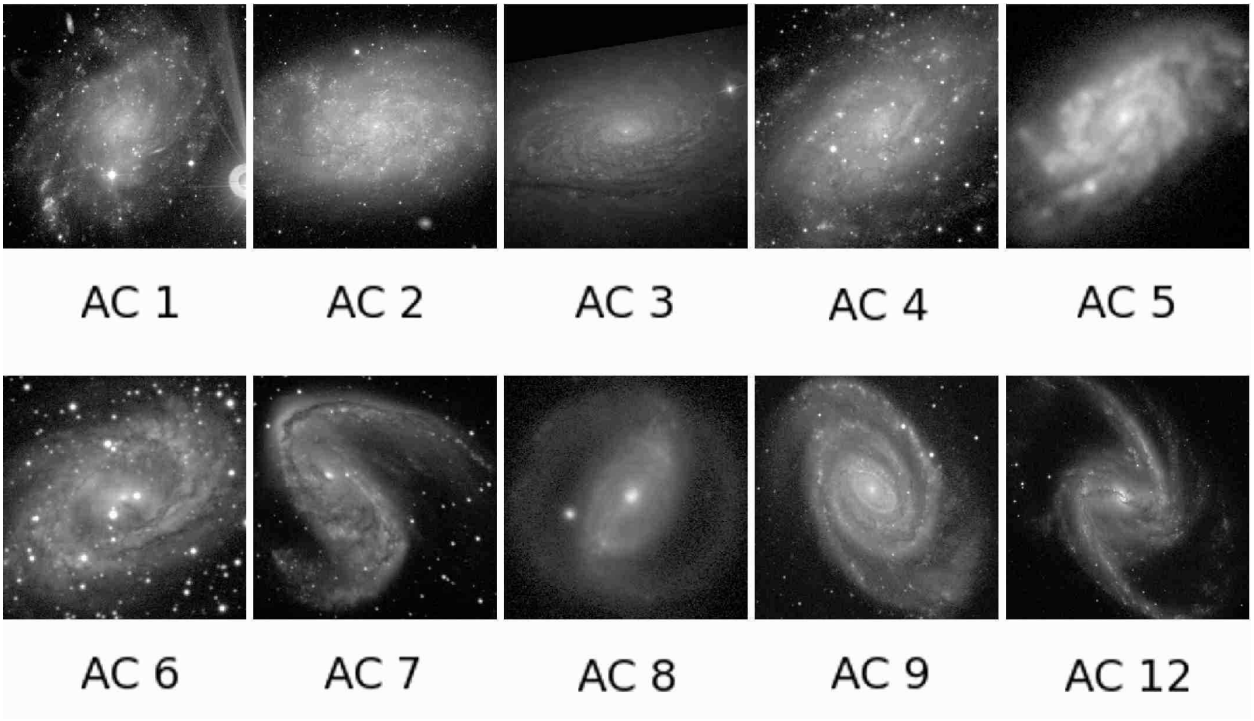

Fig. 20.— Examples showing the spiral arm classes of Elmegeen & Elmegreen (1987). The galaxies are (left to right): Row 1 - NGC 45, 7793, 5055, 2403, and 1084. Row 2: NGC 6300, 2442, 3504, 5364, and 1365. All images are B-band from the dVA, except NGC 5055 which is SDSS g-band.

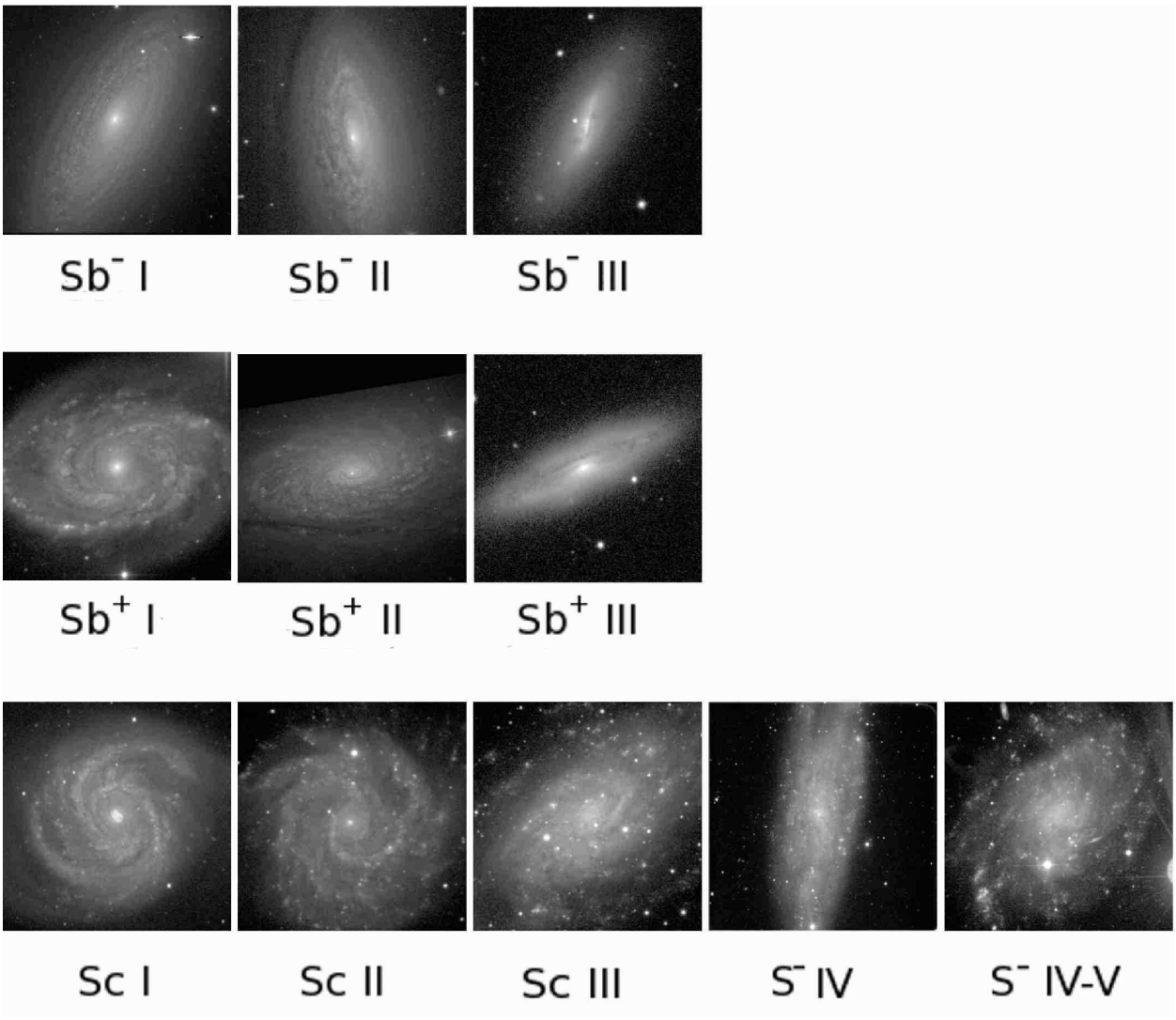

Fig. 21.— Examples showing van den Bergh luminosity classes. The galaxies are (left to right): Row 1 - NGC 2841 (dVA B), 3675 (SDSS g), and 4064 (SDSS g). Row 2: NGC 5371 (dVA B), 5055 (SDSS g), and 4586 (SDSS g). Row 3: NGC 4321, 3184, 2403, 247, and 45 (all dVA B). The classifications are in the van den Bergh system (see van den Bergh 1998).

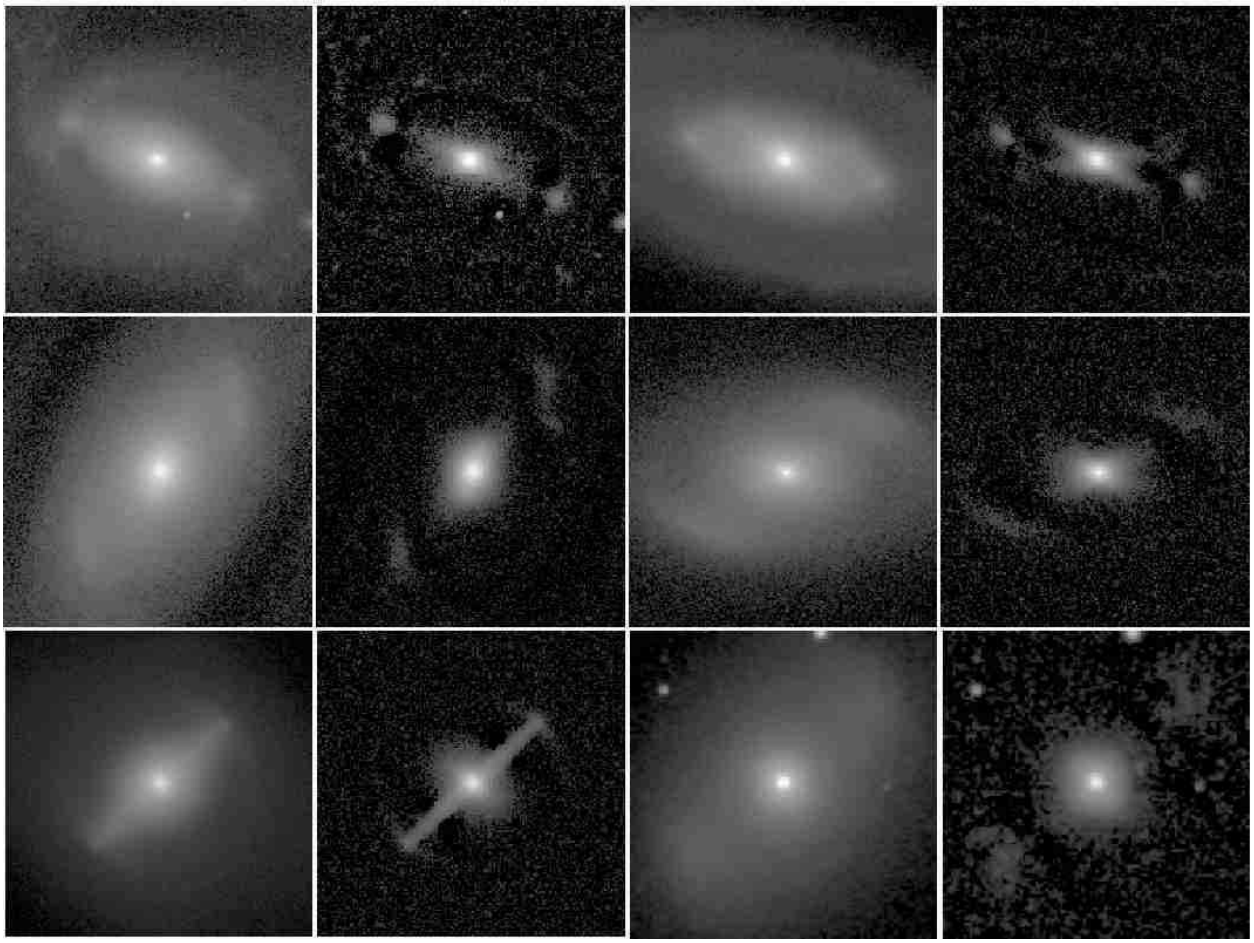

Fig. 22.— Examples showing ansae bar morphologies as compared to one mostly non-ansae bar. For each galaxy, the left frame is the full image while the right frame is an unsharp masked image, both in units of mag arcsec^{-2}. The galaxies are: (left to right): Row 1 - NGC 5375 (SDSS g) and 7020 (I) (both round ansae type); Row 2 - NGC 7098 (I, linear, partly wavy ansae) and NGC 1079 (K_s, curved ansae); Row 3 - NGC 4643 (I, mostly non-ansae type with trace of ring arcs at bar ends) and NGC 4151 (OSUBSGS H, irregular ansae).

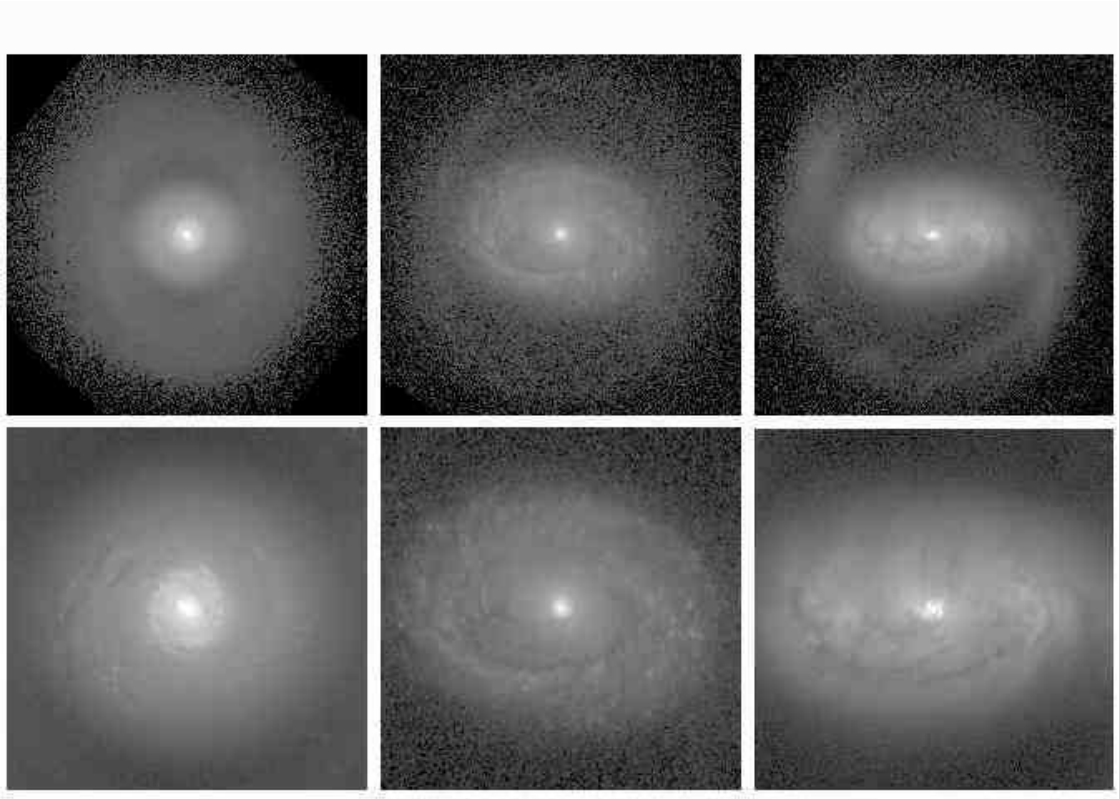

Fig. 23.— Examples of oval disk galaxies. Left to right: NGC 4736 (B), NGC 4941 (B), and NGC 1808 (V). The images are cleaned of foreground and background objects and have been deprojected and rotated so that the major axis of the oval is horizontal. The upper panels show the ovals imbedded within outer rings, while the lower panels focus on the ovals alone.

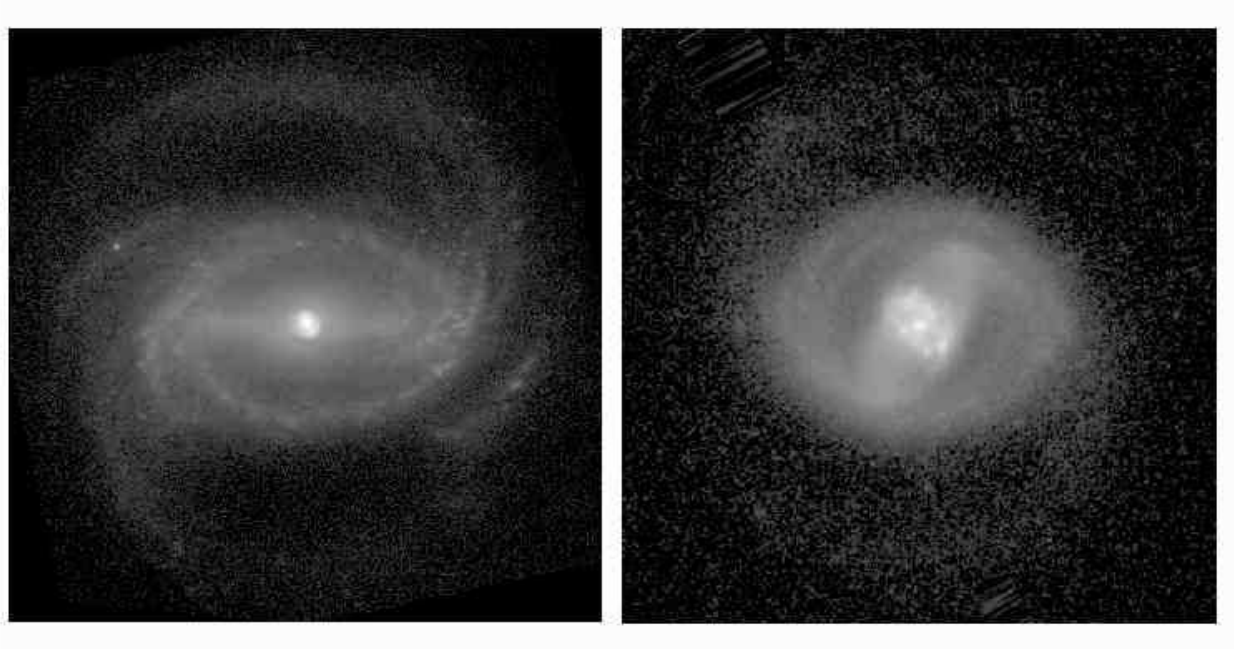

Fig. 24.— Examples of two galaxies having highly a elongated inner ring at the boundary of a broad oval. Left to right: NGC 1433, ESO 565−11 (both B-band). Each galaxy also has a prominent bar which is aligned with the oval and inner ring in NGC 1433, but misaligned with these features in ESO 565−11. ESO 565−11 also has a highly elongated, large nuclear ring of star-forming regions.

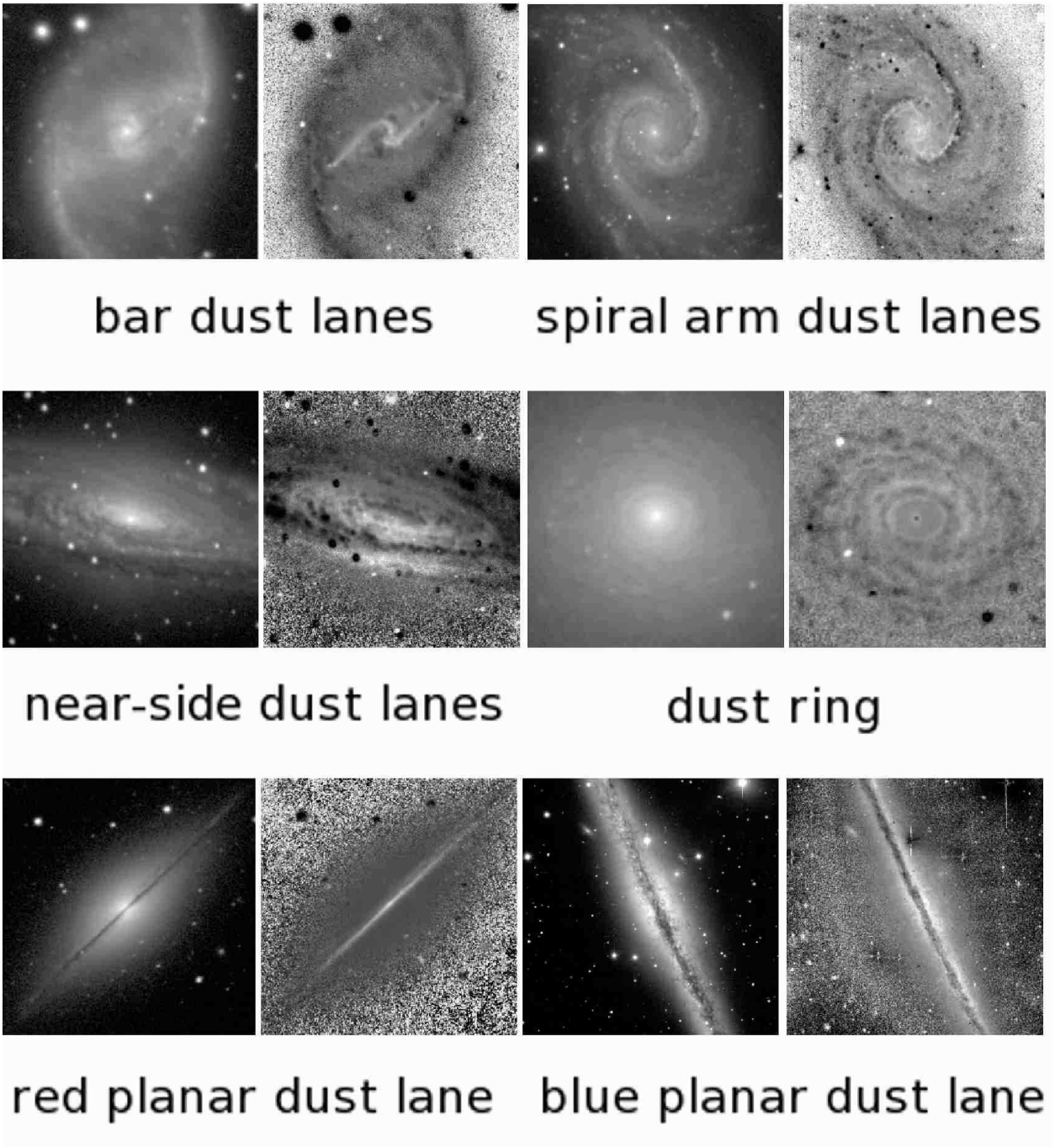

Fig. 25.— Examples showing different classes of dust lanes (left to right) - Row 1 NGC 1530, V-band image and $V - K_s$ color index map; NGC 1566, B-band and $B - K_s$ color index map; Row 2 - NGC 7331, B-band image and $B - I$ color index map; NGC 7217, B-band image and $B - I$ color index map; Row 3 - NGC 7814, B-band image and $B - I$ color index map; NGC 891, B-band and $B - V$ color index map.

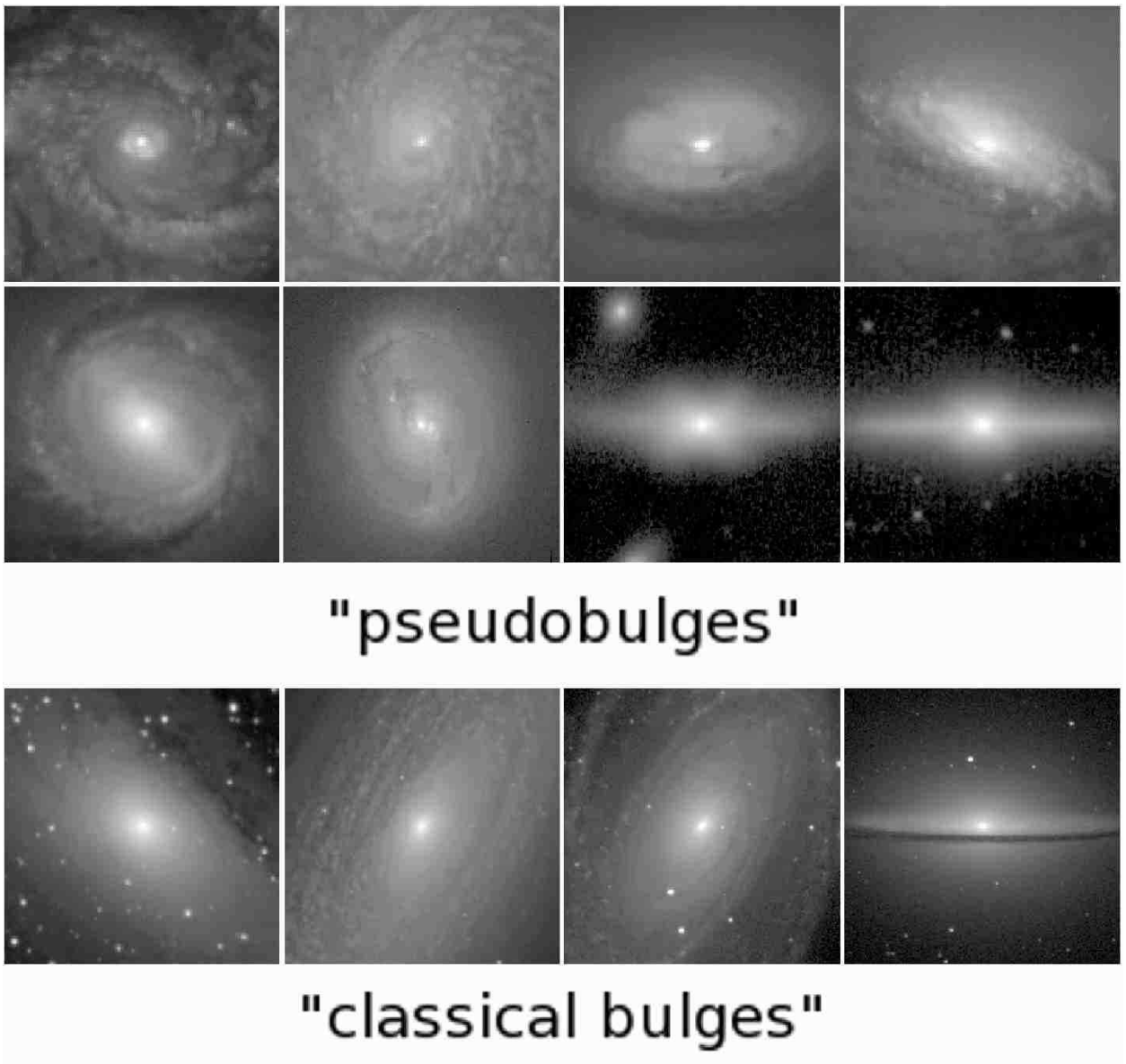

Fig. 26.— Examples of pseudobulges and classical bulges in spiral galaxies (left to right): Row 1: NGC 3177, 4030, 5377, and 1353 (all HST wide V-band filter F606W; KK04); Row 2: NGC 6782 (I-band, F814W), 3081 (wide B, F450W), 128 (K_s), and 1381 (K_s); Row 3: NGC 224 (M31), 2841, 3031 (M81), and 4594 (M104) (all B-band). The images of NGC 128 and 1381 are from Bureau et al. (2006).

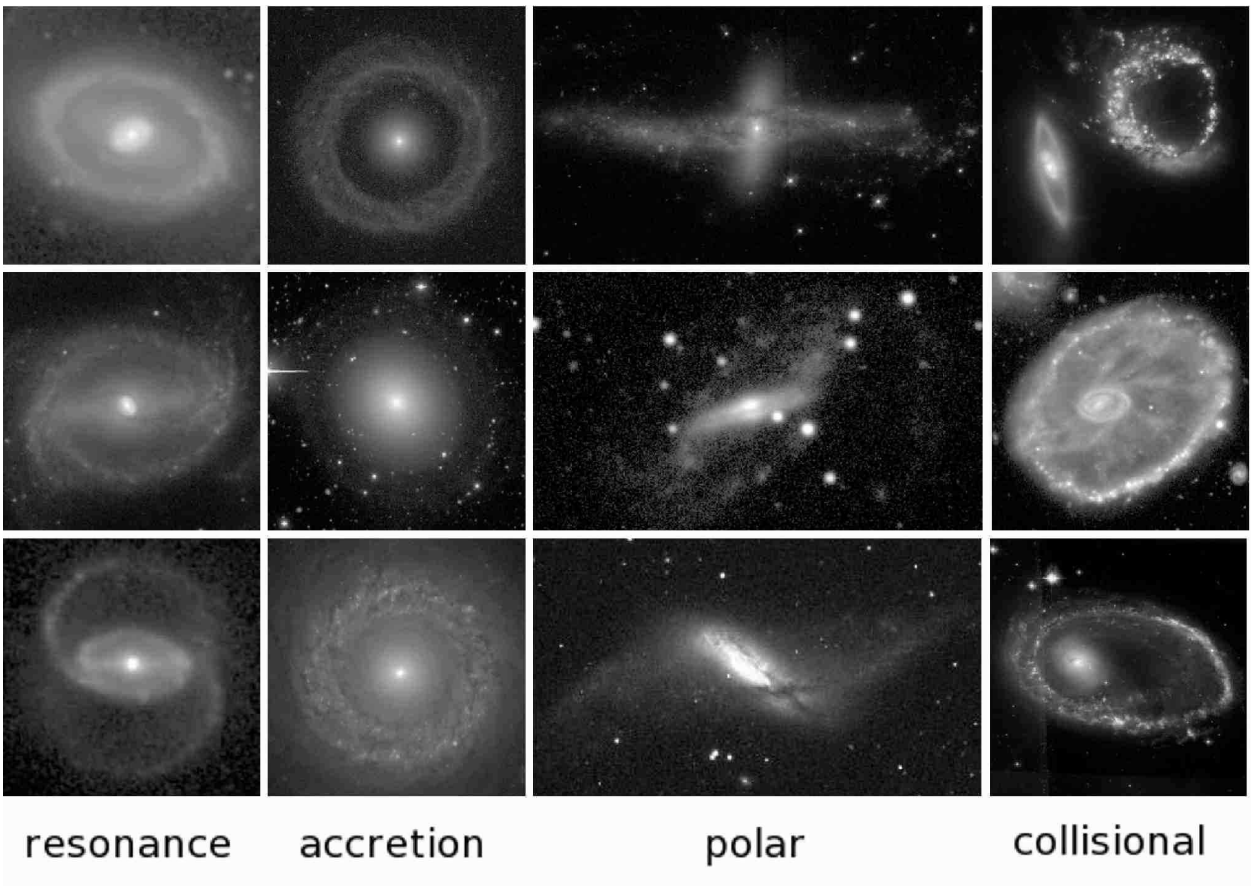

Fig. 27.— Different classes of ring phenomena seen in galaxies (top to bottom): Column 1 - NGC 3081, NGC 1433, and UGC 12646. Column 2 - Hoag's Object, IC 2006, and NGC 7742; Column 3 - NGC 4650A, ESO 235−58, and NGC 660; Column 4 - Arp 147, the Cartwheel, and the Lindsay-Shapley ring. All images are from the dVA except Arp 147.

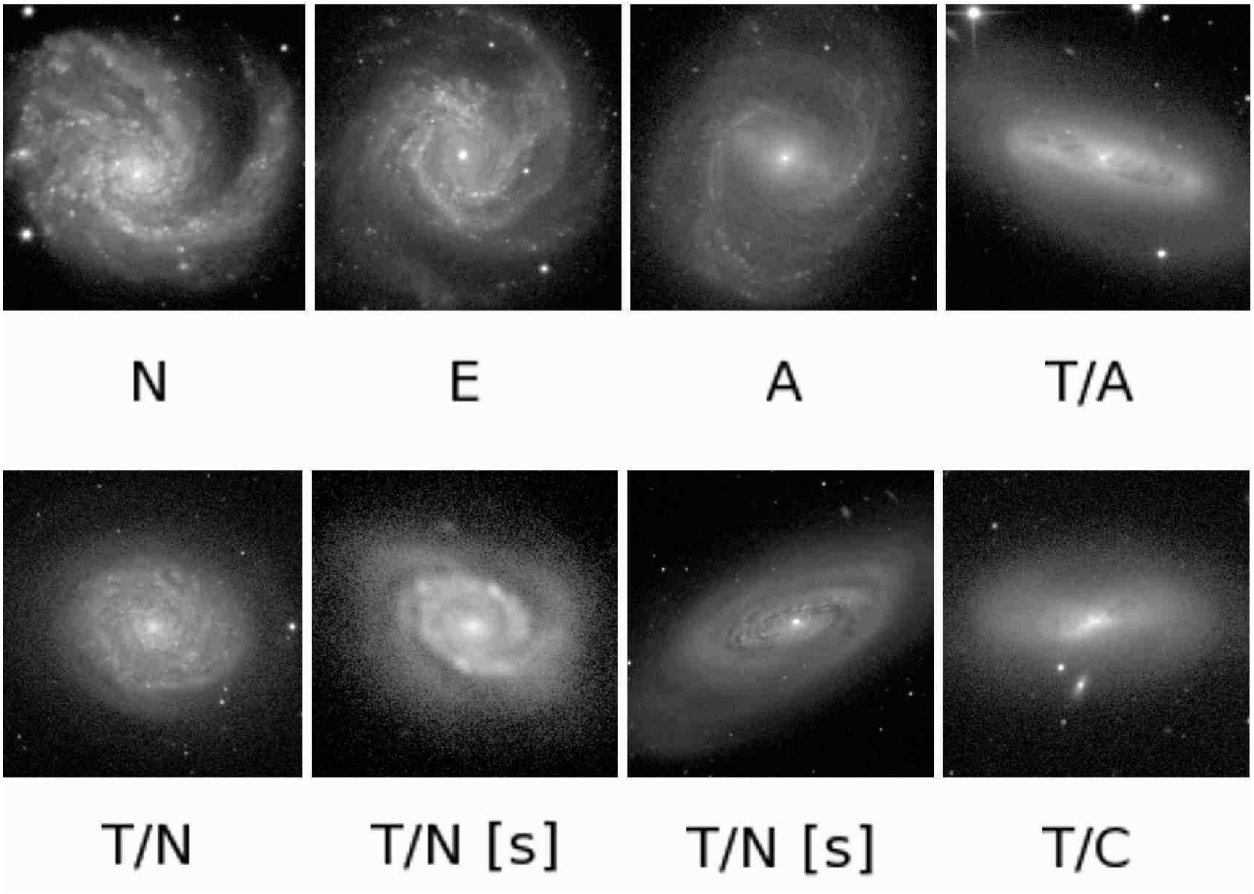

Fig. 28.— Blue light morphologies of eight Virgo Cluster spirals having different Koopmann & Kenney (2004) Hα star formation morphologies. The galaxies are (left to right): Row 1: NGC 4254 (normal N); NGC 4303 (Enhanced E); NGC 4548 (Anemic A); NGC 4293 (Truncated/Anemic T/A); Row 2: NGC 4689 (Truncated/Normal T/N); NGC 4580 and 4569 (Truncated/Normal (severe) T/N [s]); NGC 4424 (Truncated/Compact T/C). Images are dVA B, except for NGC 4424 which is SDSS g.

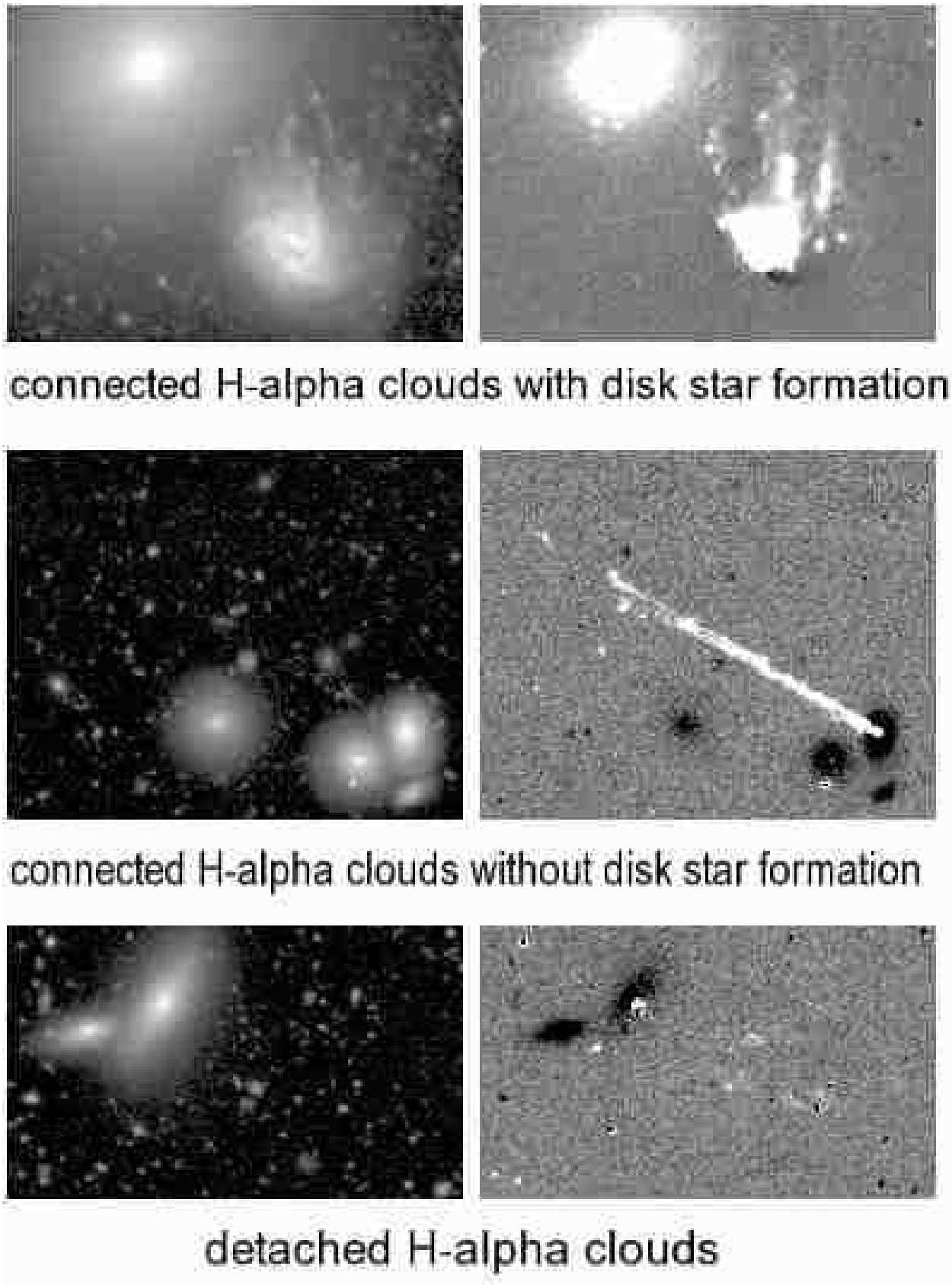
connected H-alpha clouds with disk star formation
connected H-alpha clouds without disk star formation
detached H-alpha clouds

Fig. 29.—

Fig. 29. (cont.).— Three galaxies in a possible evolutionary stripping sequence in the Coma Cluster. The images and categories are from Yagi et al. (2010). The left frames are B-band images in units of mag arcsec^{-2}, while the right frames are net Hα images in linear intensity units (called NB−R by Yagi et al.). From top to bottom, the galaxies are GMP 3816, GMP 2910, and GMP 2923. The idea is that GMP 3816 is in an earlier phase of stripping, such that there is still considerable disk ionized gas; GMP 2910 is in a more advanced phase with still connected clouds but an absence of disk emission; and finally GMP 2923 is in the most advanced phase of the three, showing only scattered HII regions.

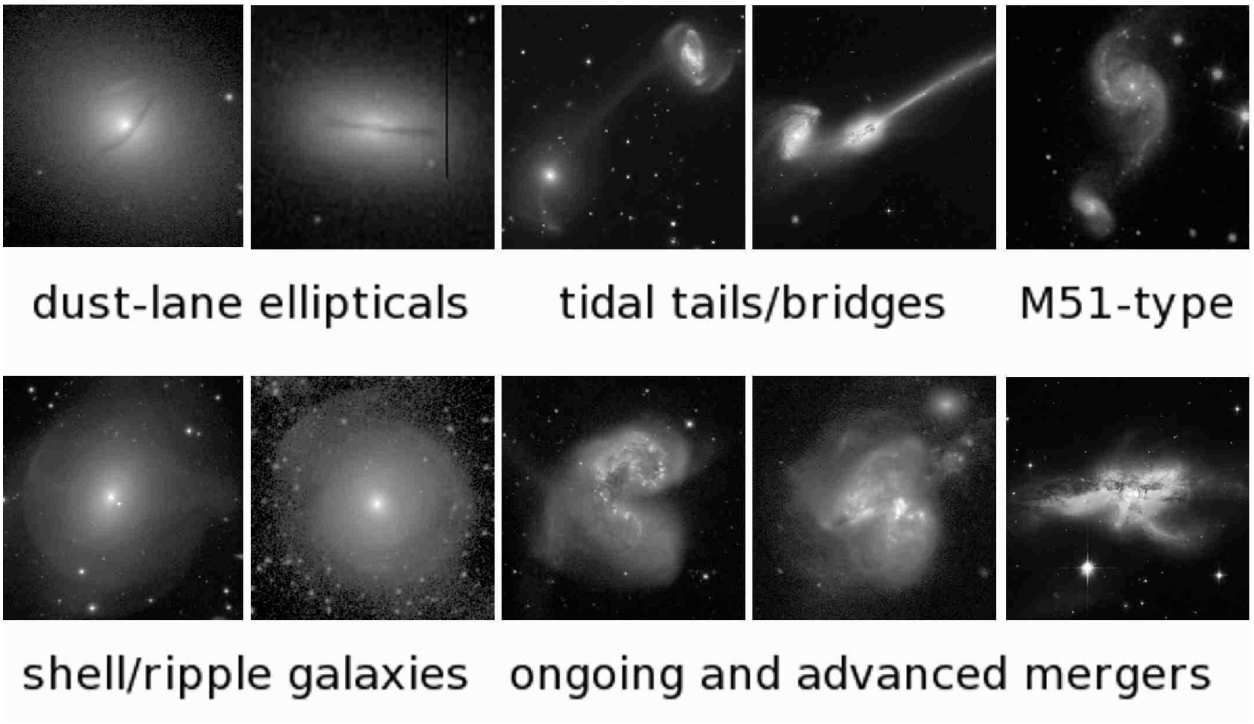

Fig. 30.— Interacting and peculiar galaxies. The galaxies are (left to right): Row 1: NGC 5485 (SDSS), 4370 (SDSS), 5216/18 (A. Block), 4676 (Hubble Heritage), and 2535-6 (SDSS); Row 2: NGC 2865, 474, 4038-9, 3690, and 6240, all B except NGC 474, which is a 3.6μm image (section 12).

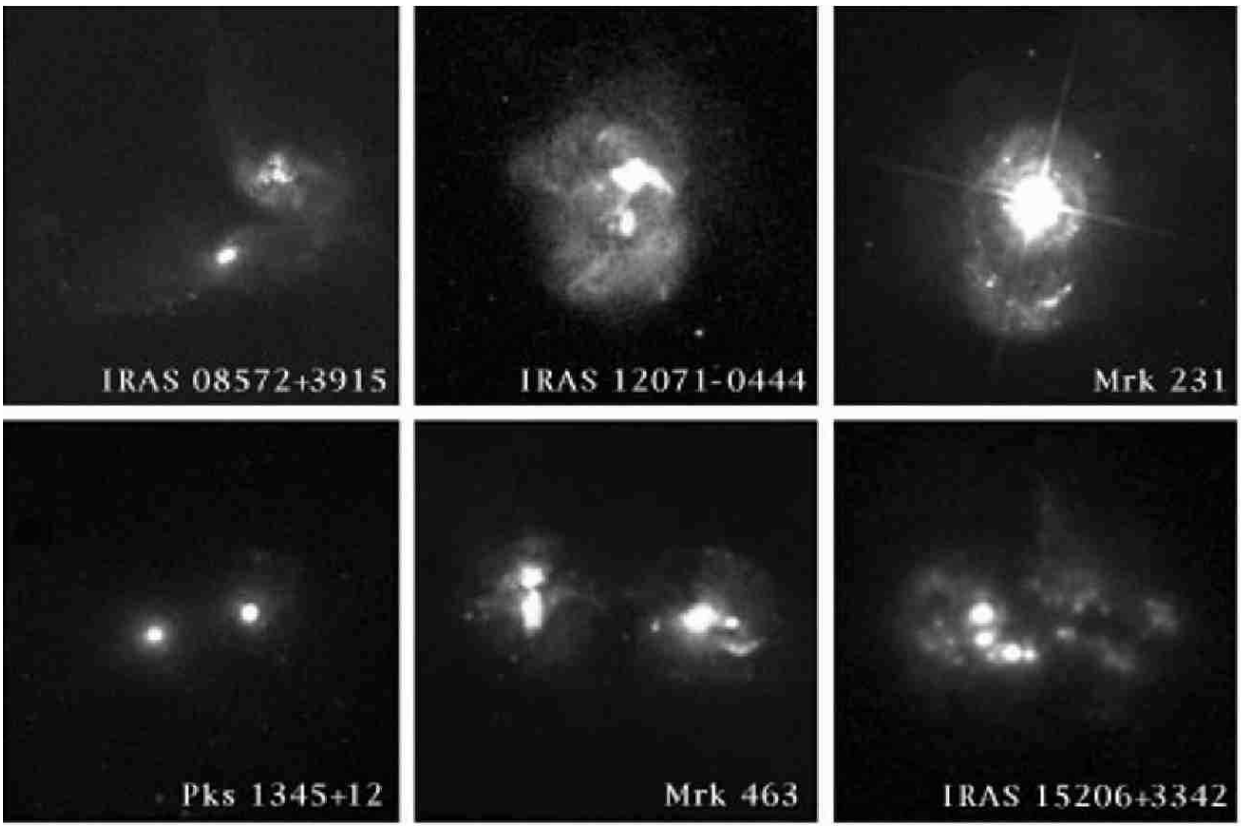

Fig. 31.— The morphologies of six "ultra-luminous infrared galaxies" from HST optical/near-IR imaging (Surace et al. 1998). These images are not in units of mag arcsec^{-2}.

Fig. 32.— Three galaxies showing strong optical disk warping. Left to right: NGC 4762 (B), NGC 4452 (SDSS), UGC 3697 (Internet Encyc. of Science)

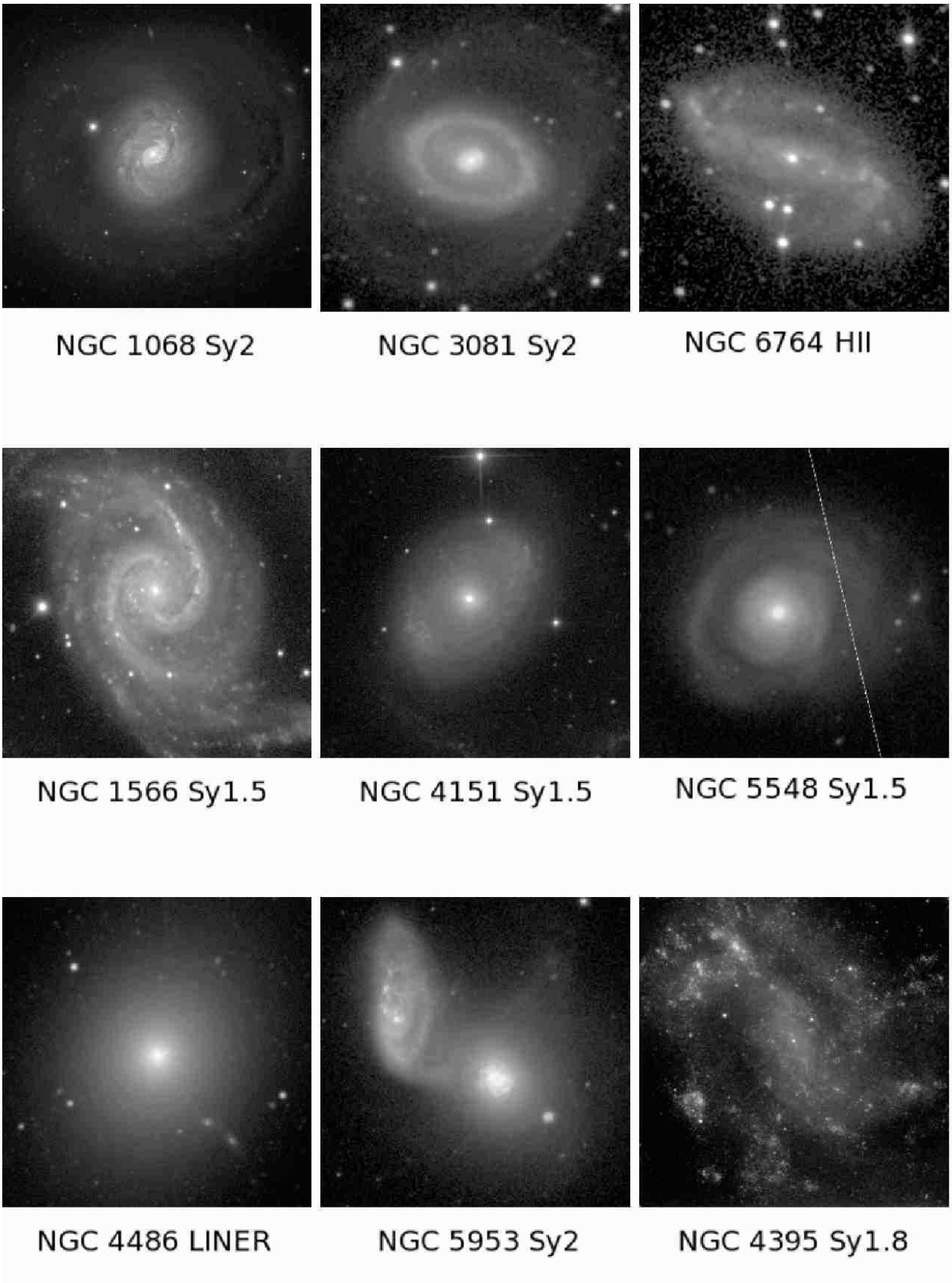

Fig. 33.— Images of nearby active galaxies, dVA B-band except for NGC 5548 and 5953, which are SDSS. The activity classification is from Veron-Cetty & Veron (2006).

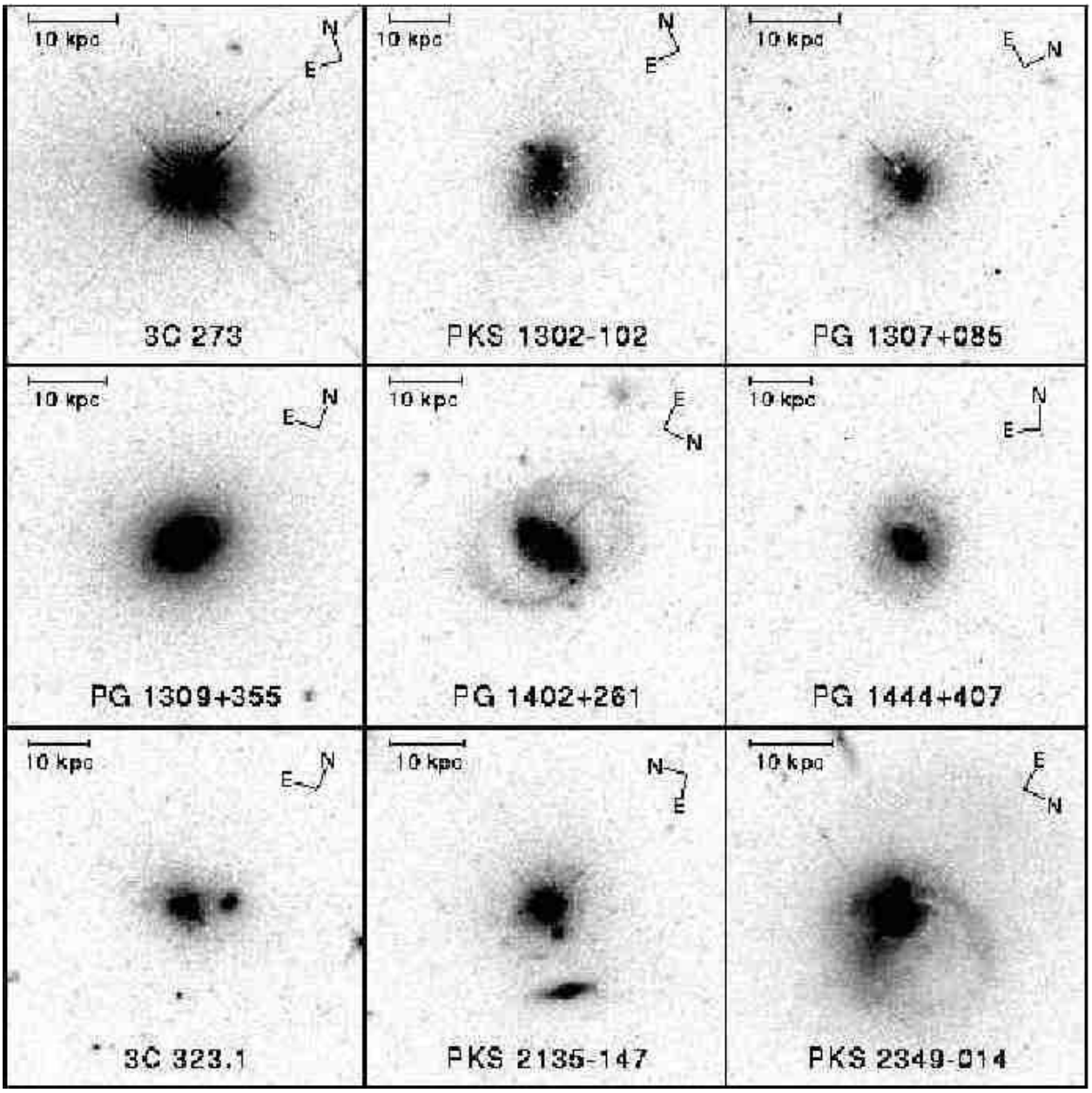

Fig. 34.— The morphologies of the host galaxies of nine nearby quasars, from Bahcall et al. (1997). These images are not in units of mag arcsec^{-2}.

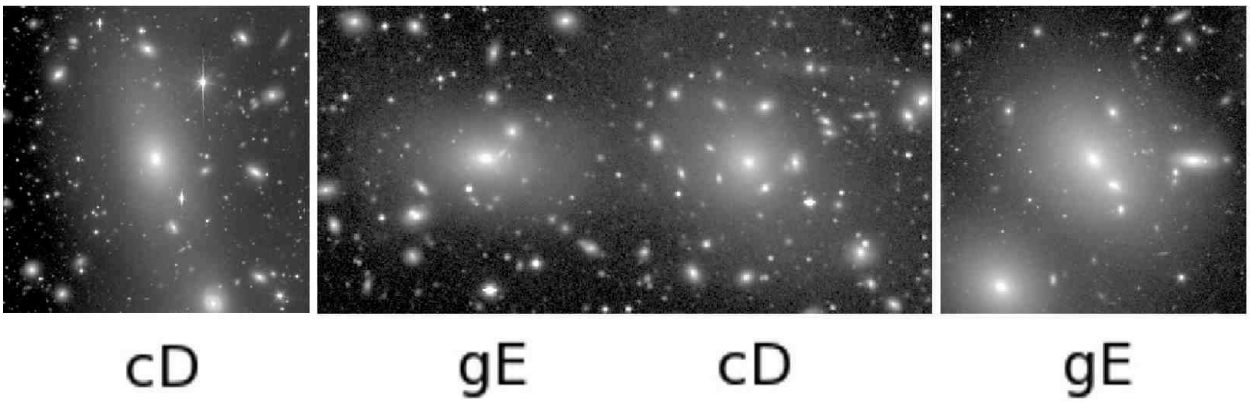

Fig. 35.— Deep images of the brightest members of three rich galaxy clusters (left to right): UGC 10143 in A2152 (R-band), NGC 4889 (left) and 4874 (right) in A1656 (B-band), and NGC 6041 (R-band) in A2151. The images of UGC 10143 and NGC 6041 are from Blakeslee (1999), while that of NGC 4874-89 is from the dVA.

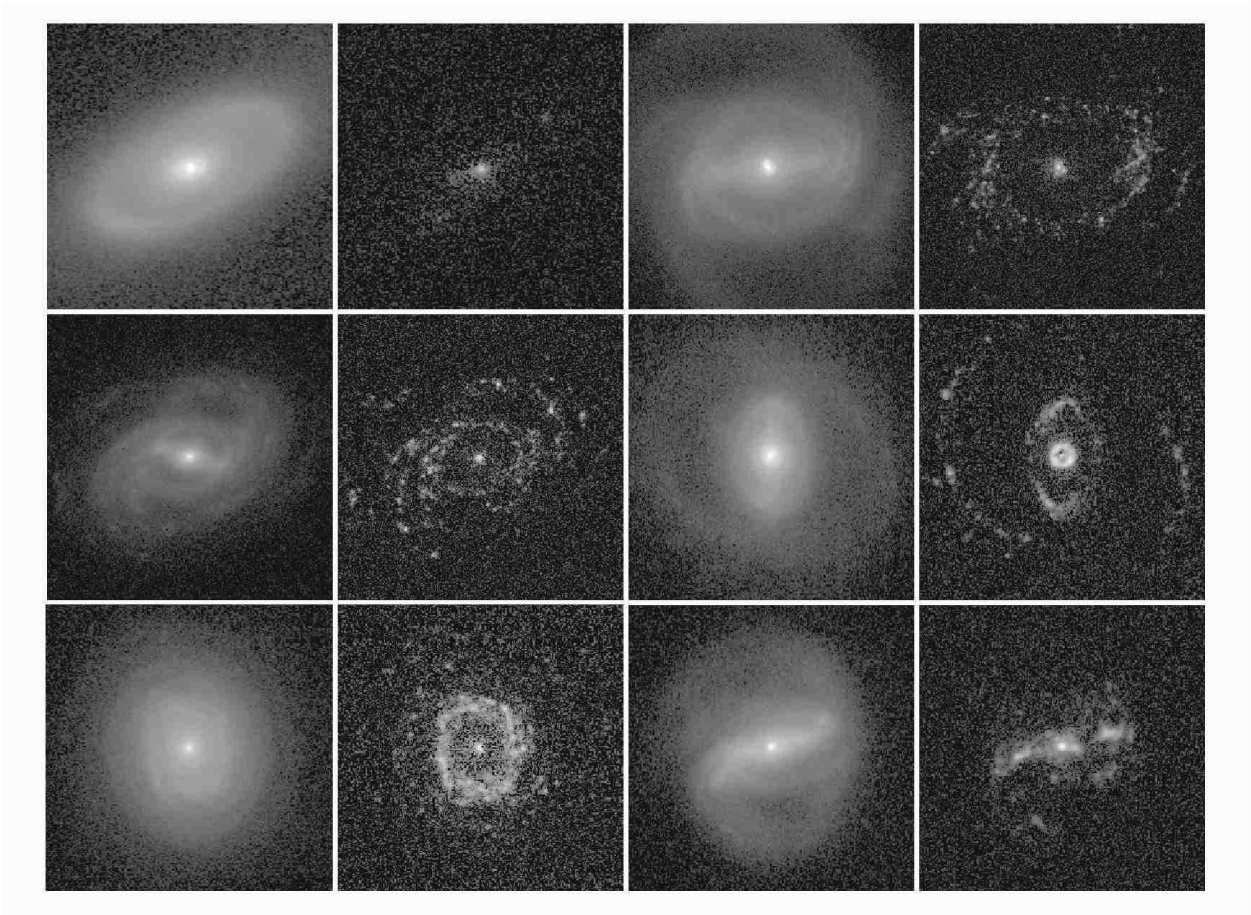

Fig. 36.— Red continuum (left) and net Hα (right) images of six early-to-intermediate-type galaxies. The galaxies are (left to right): top row: NGC 7702, 1433; middle row: NGC 7329, 6782; bottom row: NGC 6935, 7267. From Crocker, Baugus, & Buta (1996).

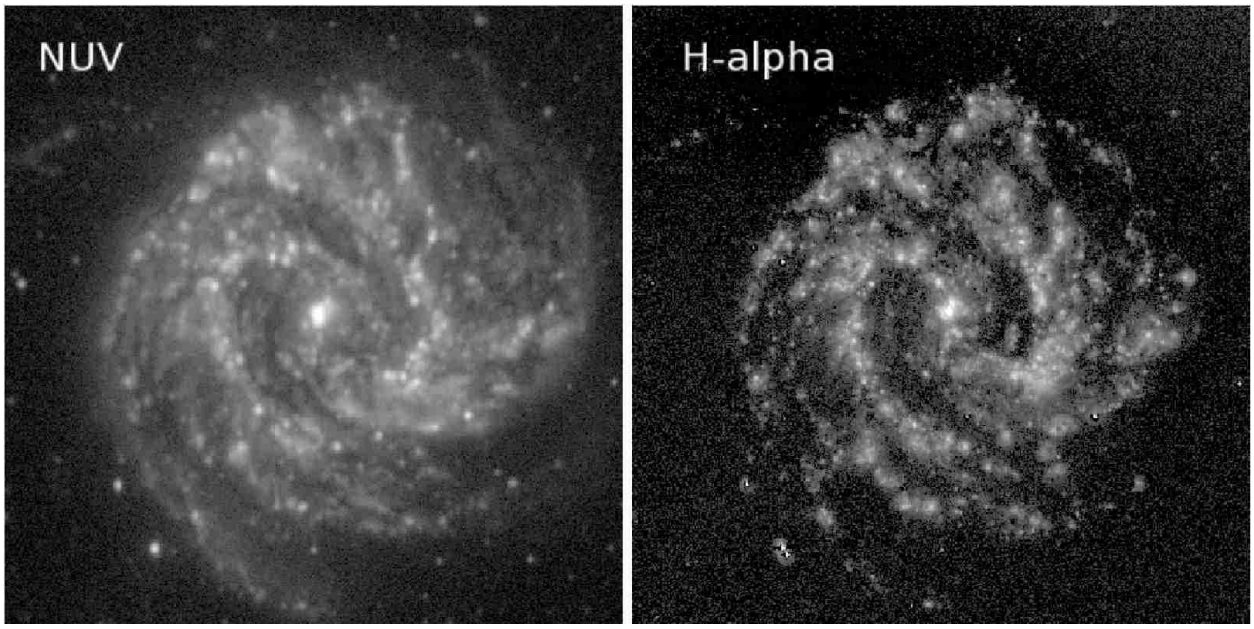

Fig. 37.— Comparison of a near-UV image (0.225μm) with an Hα image for the nearby spiral galaxy M83.

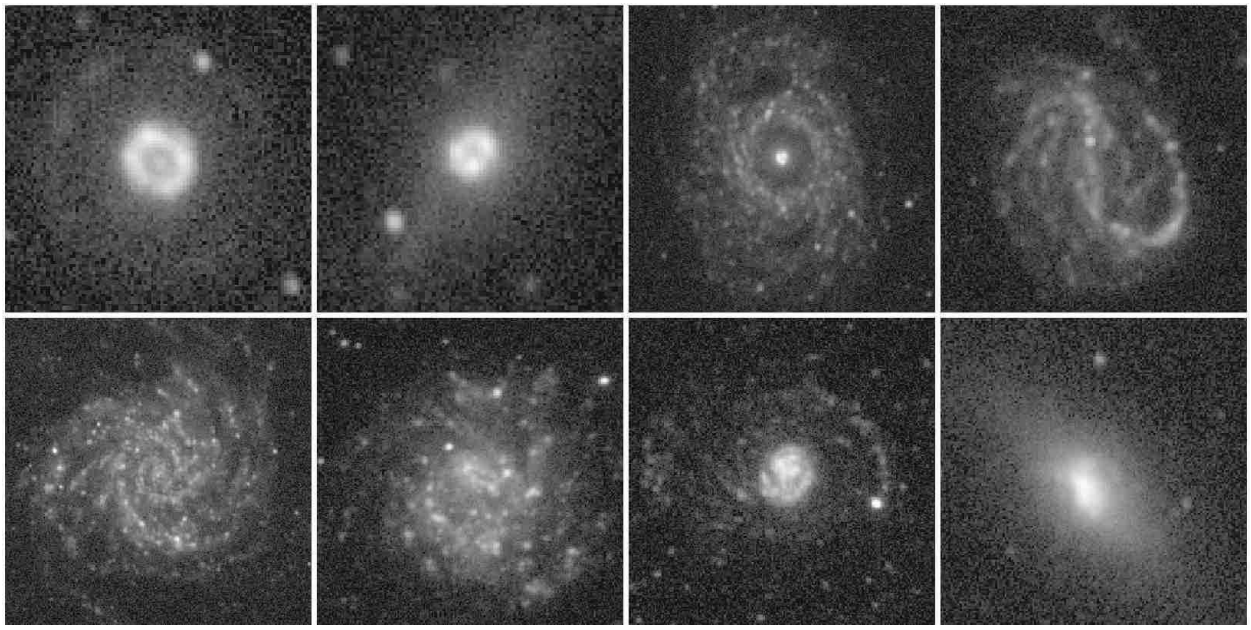

Fig. 38.— GALEX near-UV images of eight galaxies: (left to right) Top row: NGC 1317, 4314, 3351, and 7479; bottom row: NGC 628, 5474, 4625, and 5253

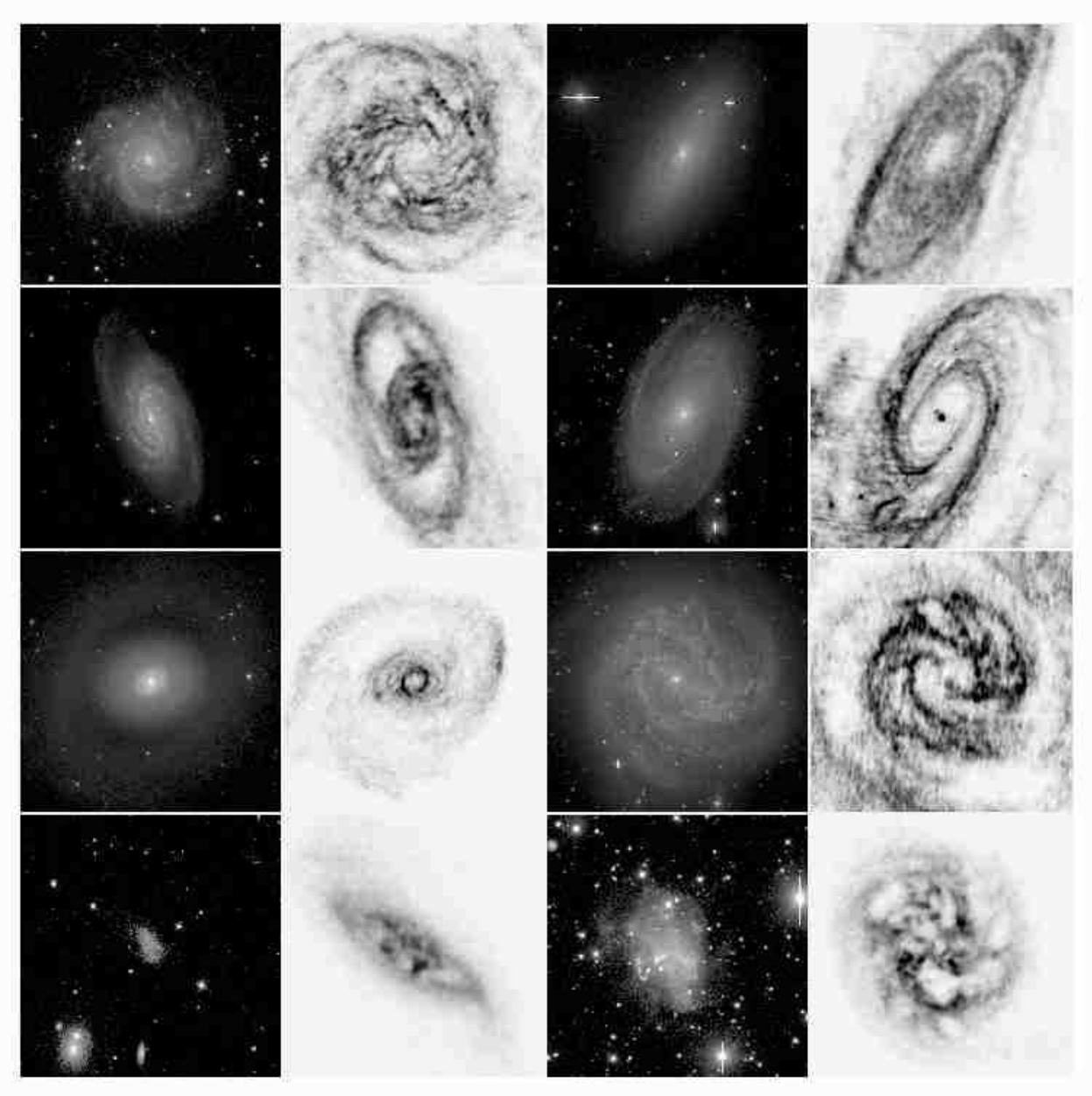

Fig. 39.— HI morphologies (Walter et al. 2008) of eight galaxies as compared to optical *B*-band morphologies. Left panels: NGC 628 (M74), NGC 4258 (M106), NGC 4736 (M94), and DDO 154. Right panels: NGC 2841, NGC 3031 (M81); NGC 5236 (M83), and DDO 50 (Ho II).

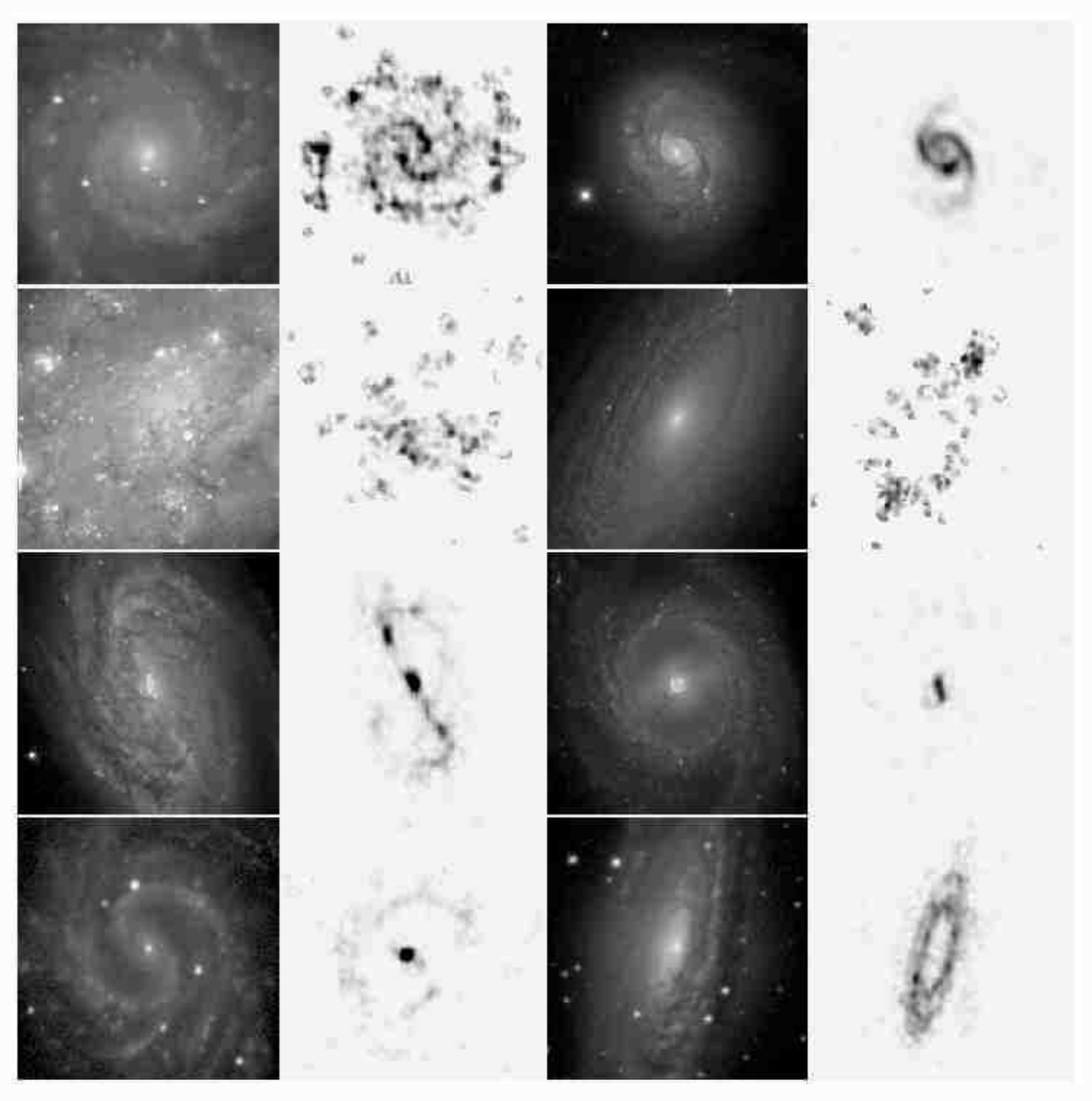

Fig. 40.— CO morphologies (Helfer et al. 2003) of eight galaxies as compared to optical B-band morphologies. Left panels: NGC 628 (M74), NGC 2403, NGC 2903, and NGC 4535. Right panels: NGC 1068 (M77), NGC 2841; NGC 3351 (M95), and NGC 7331.

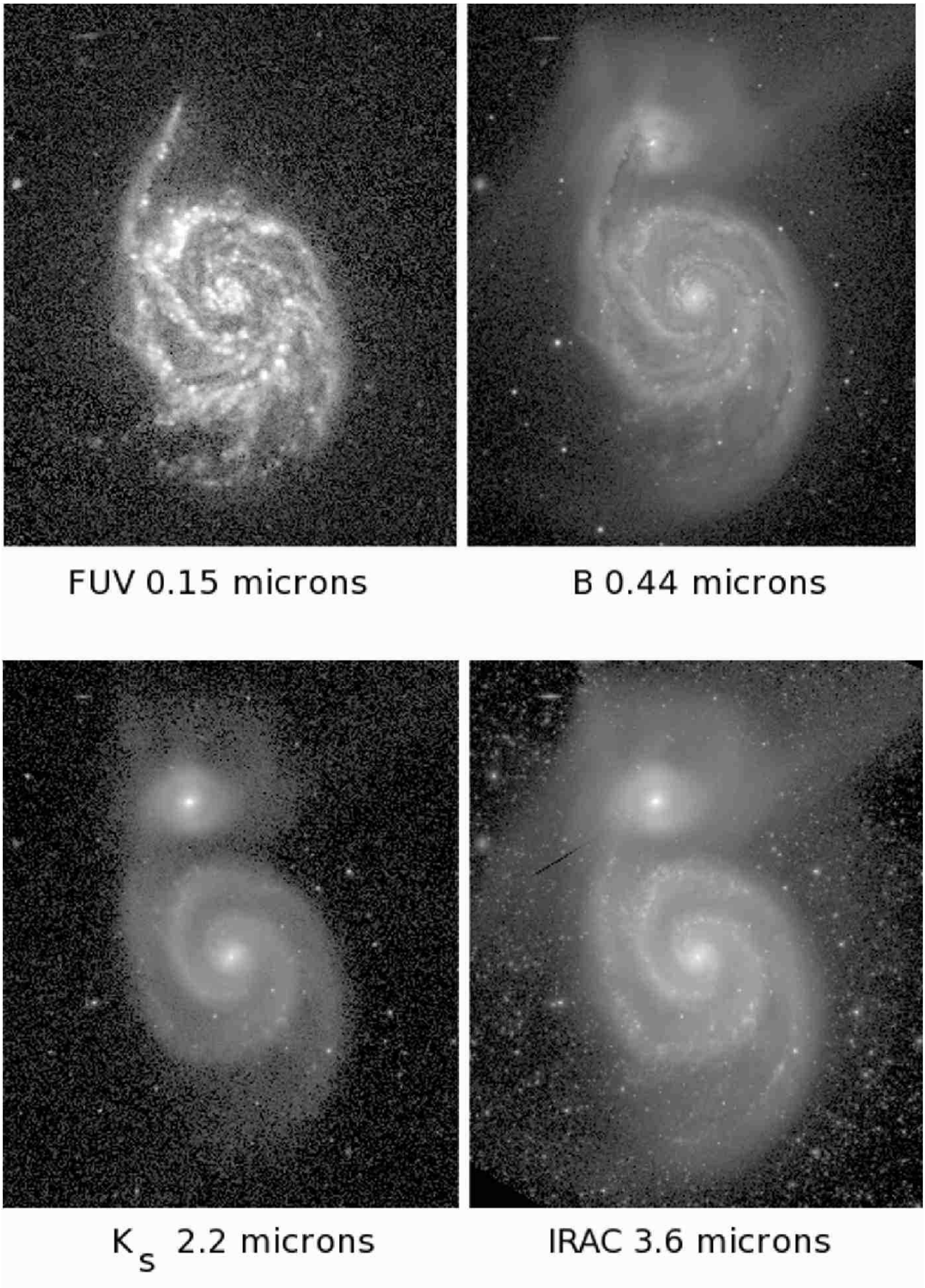

Fig. 41.— Multi-wavelength images of M51.

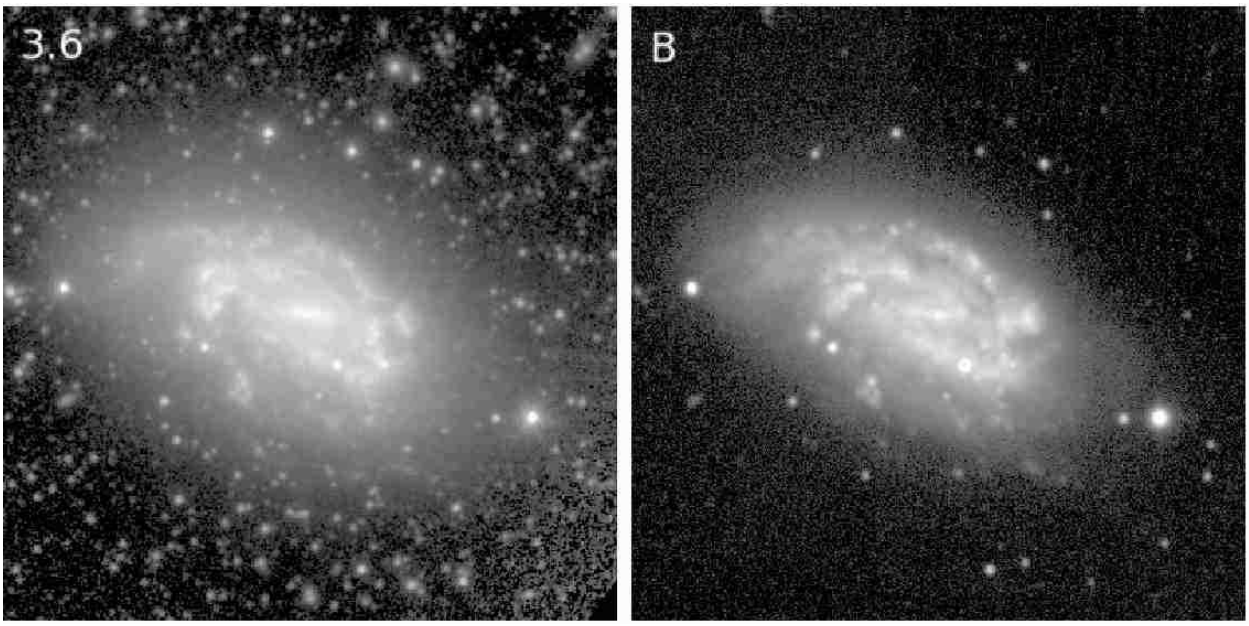

Fig. 42.— Comparison of IRAC 3.6μm image of NGC 1559 (left) with a ground-based B-band image of the same galaxy at right. Note the significant correspondence of features between the two very different wavelength domains in this case.

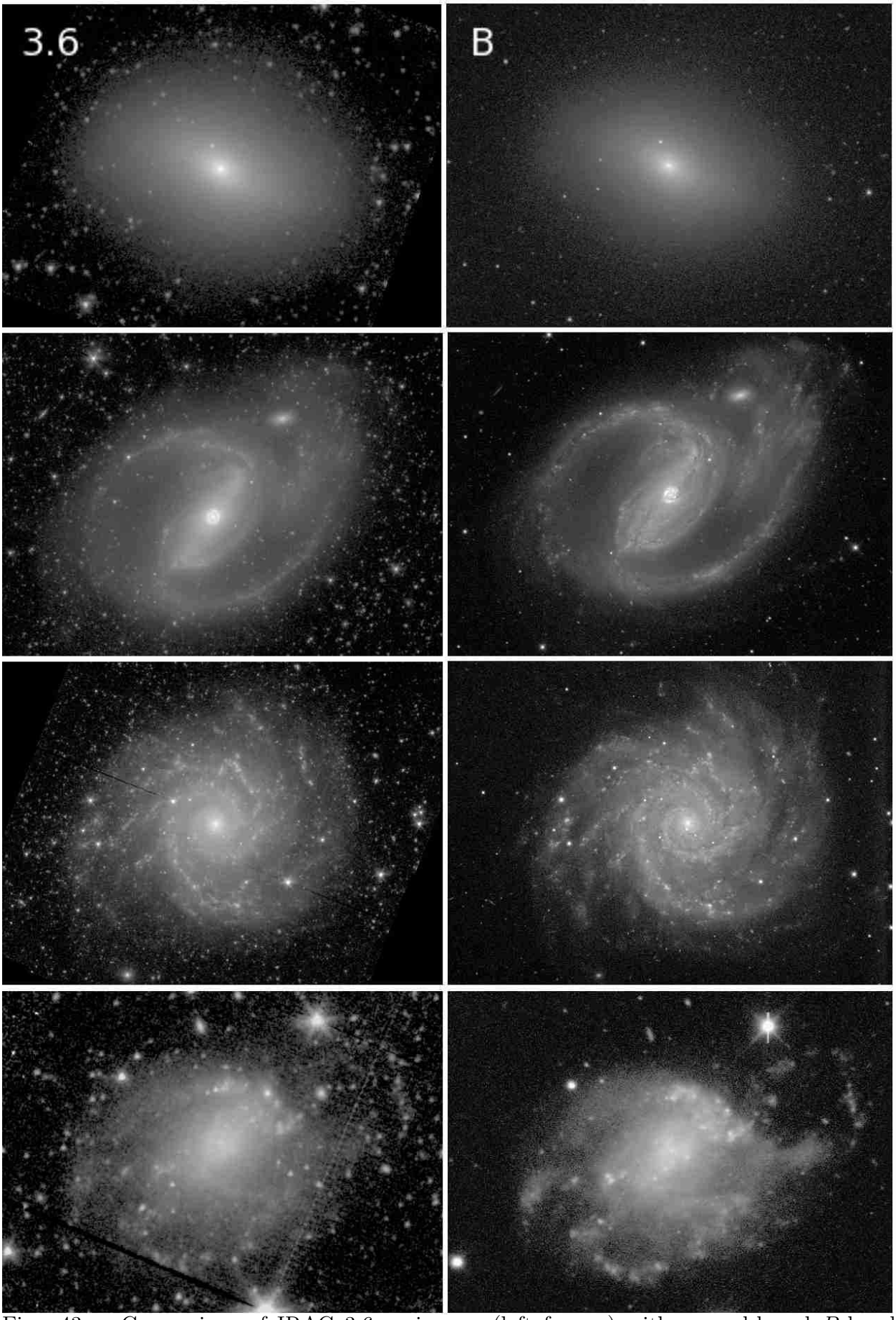

Fig. 43.— Comparison of IRAC 3.6μm images (left frames) with ground-based B-band images for (top to bottom): NGC 584, 1097, 628, and 428.

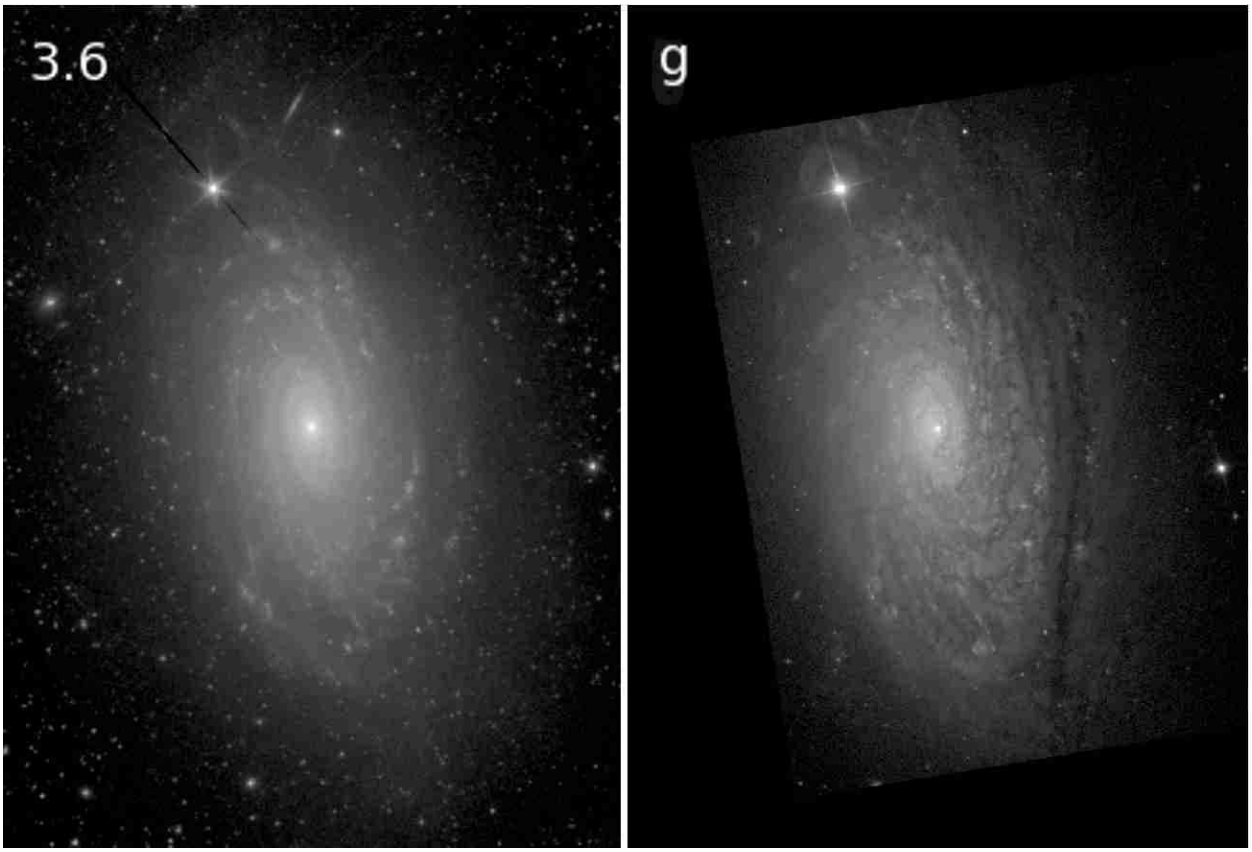

Fig. 44.— Comparison of IRAC 3.6μm and SDSS g-band images of the flocculent spiral galaxy NGC 5055.

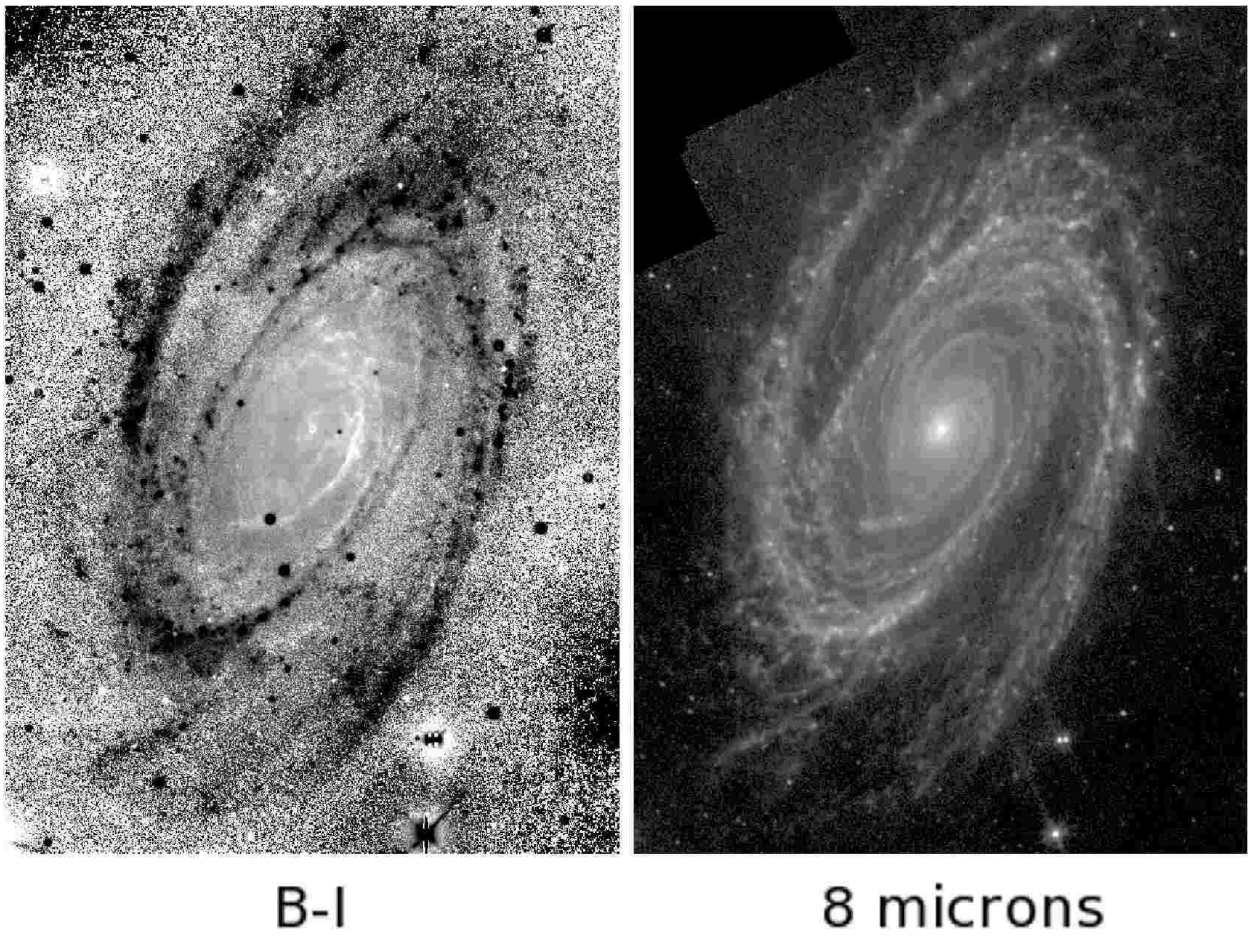

Fig. 45.— A comparison between a $B - I$ color index map and an 8μm dust emission map of the nearby spiral galaxy M81.

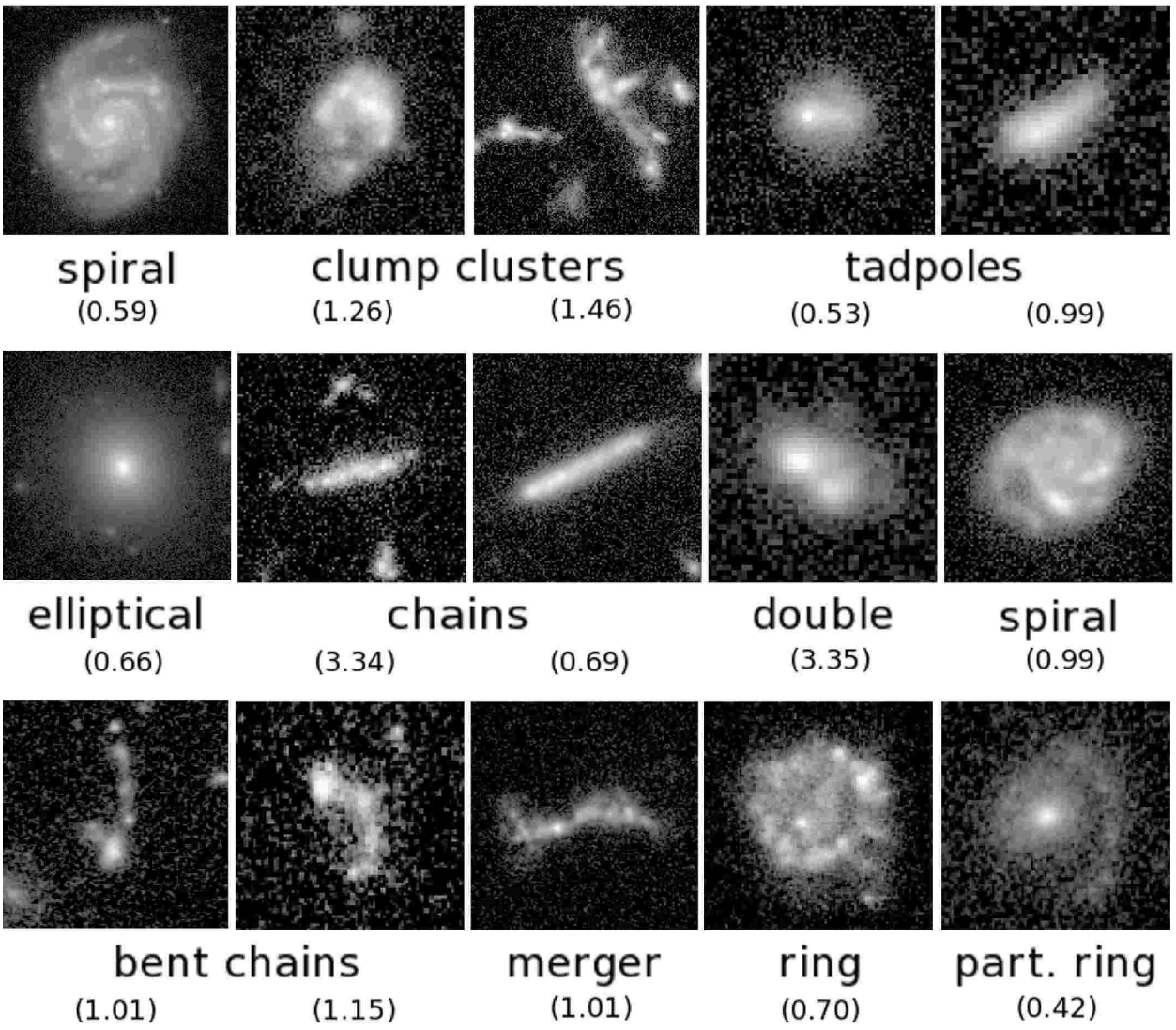

Fig. 46.— Intermediate to high redshift galaxy morphology (V and i-bands). The categories are due to EES04 and EE06. The number in parentheses below each frame is the redshift z of the galaxy shown.

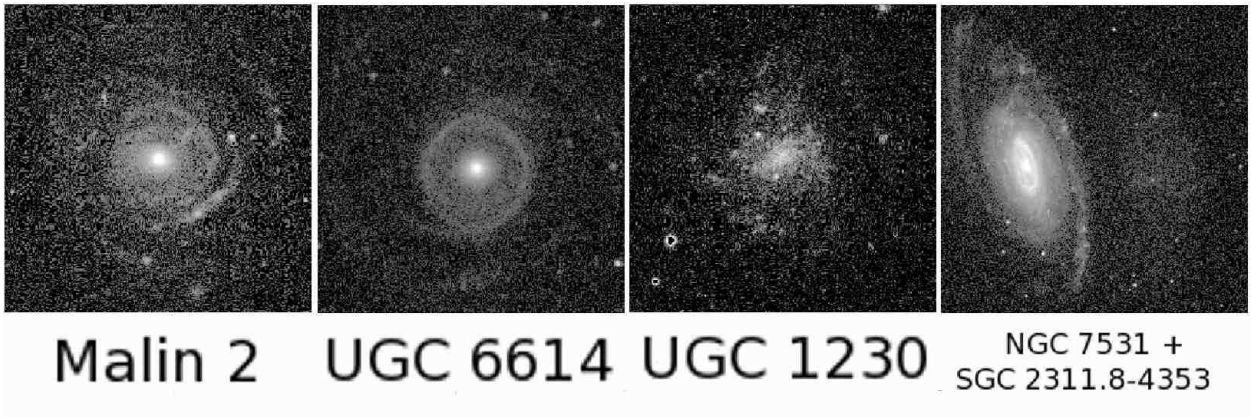

Fig. 47.— Examples of giant or large low surface brightness galaxies. In the far right panel, SGC 2311.8−4353 is the diffuse object to the right of high surface brightness spiral NGC 7531. All of these images are B-band.

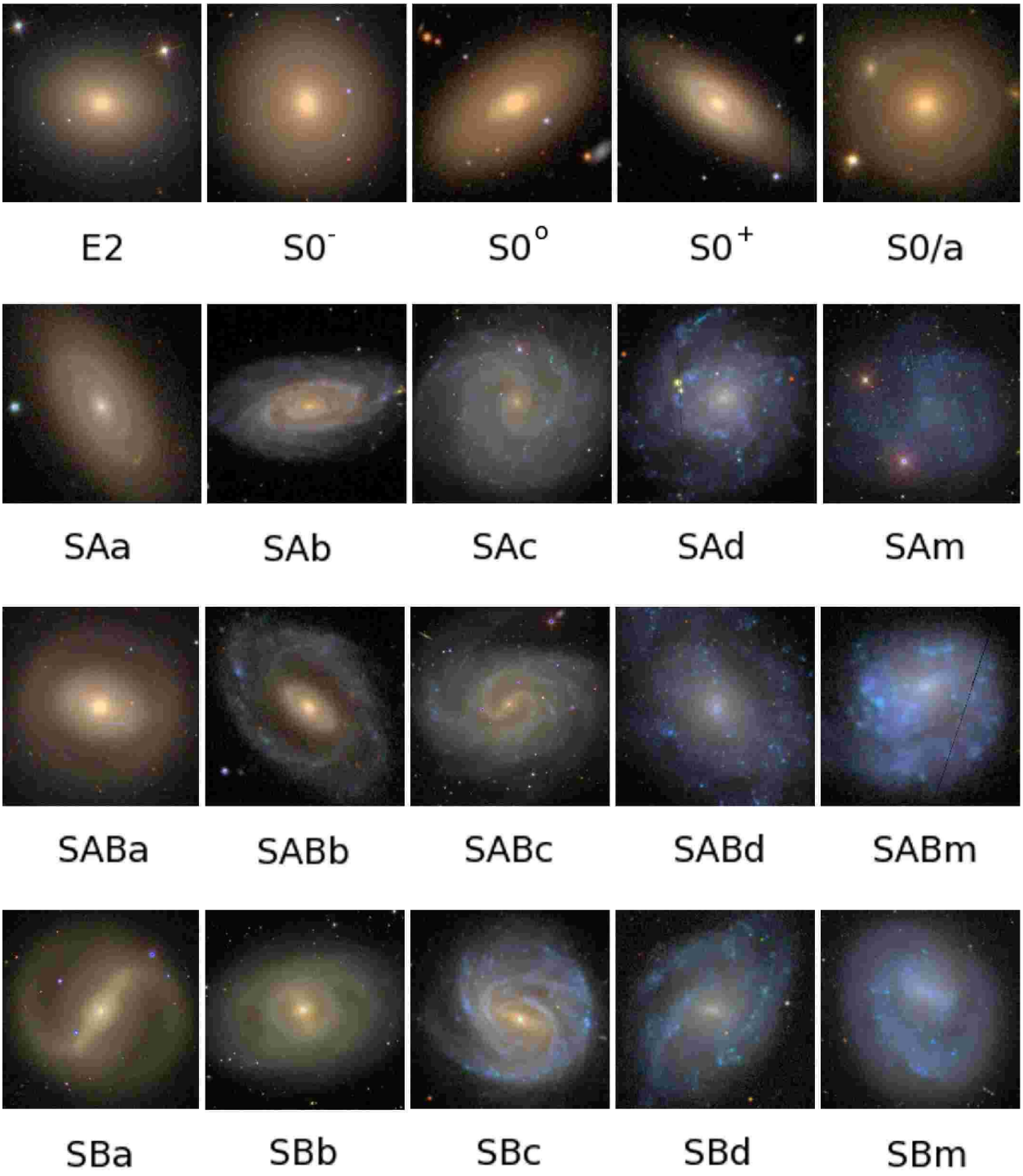

Fig. 48.— The Hubble tuning fork of ellipticals, S0s, and spirals of different bar classifications are shown here using SDSS color images. The galaxies are (left to right): Row 1 - NGC 3608, 4203, 6278, 4324, and 932. Row 2 - NGC 4305, 5351, 3184, 5668, and IC 4182. Row 3 - NGC 4457, 5409, 4535, 5585, and 3445. Row 4 - NGC 4314, 3351, 3367, 4519, and 4618.

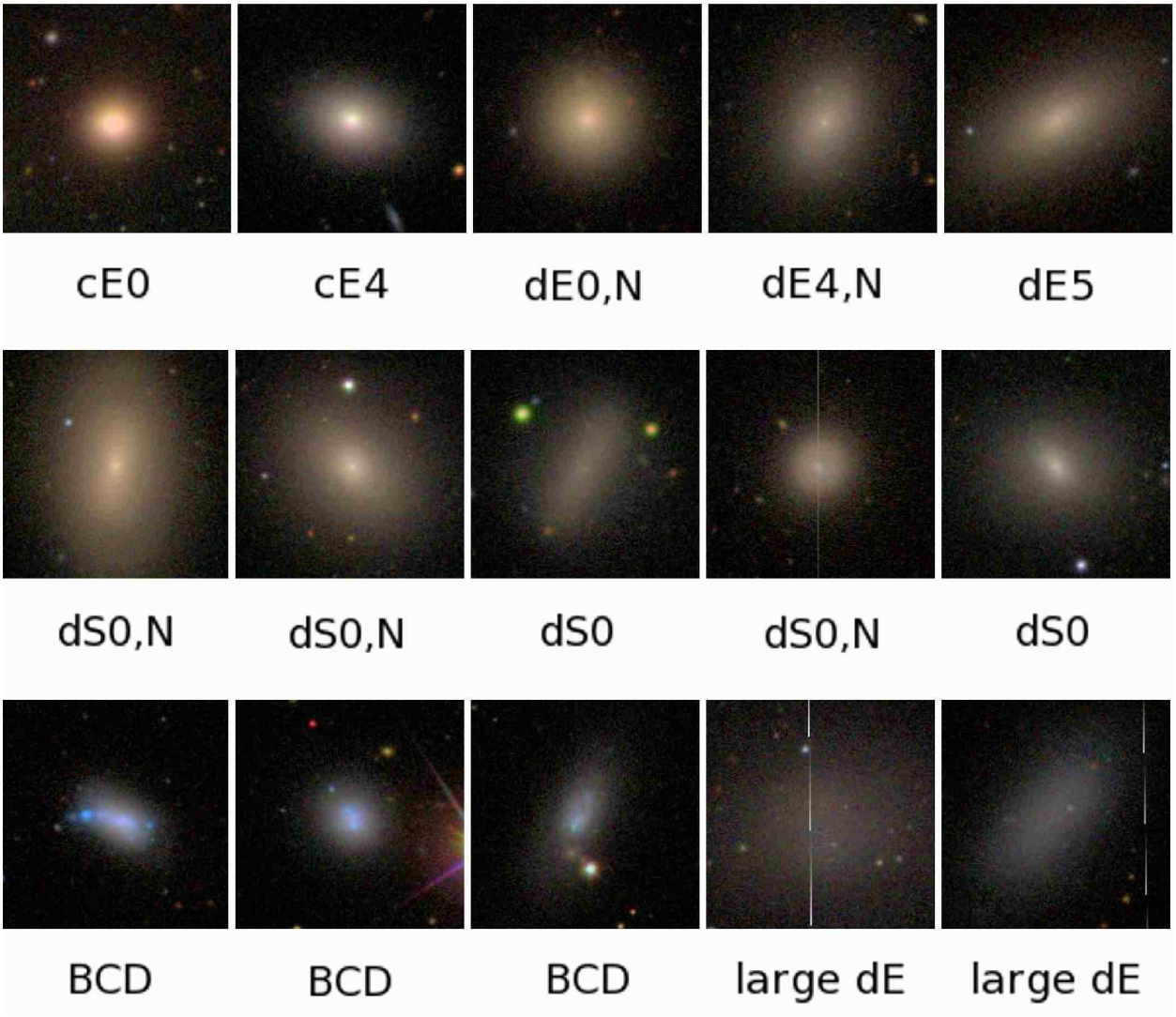

Fig. 49.— Examples of dwarf galaxies in the Virgo Cluster, drawn from the catalogue of Binggeli, Sandage, & Tammann (1985) and highlighted using SDSS color images. The classifications are from the BST catalogue and the galaxies are (left to right): Row 1 - NGC 4486B, IC 767, IC 3470, IC 3735, and UGC 7436. Row 2 - NGC 4431, IC 781, IC 3292, VCC 278, IC 3586. Row 3 - VCC 459, VCC 2033, VCC 841, IC 3475, and IC 3647.

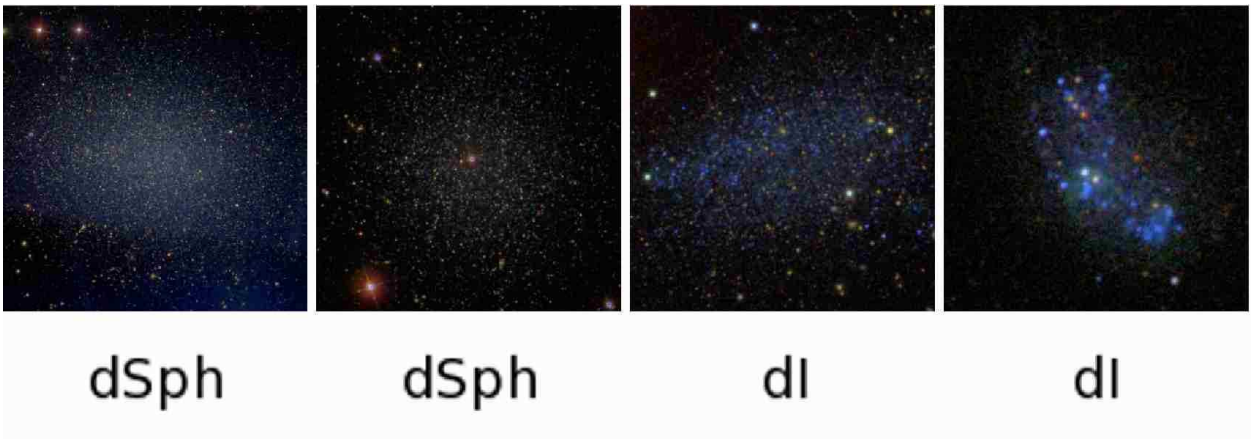

Fig. 50.— Four Local Group dwarfs having $M_V > -12$ (left to right): Leo I, Leo II, Leo A, and DDO 155 (all SDSS color images)

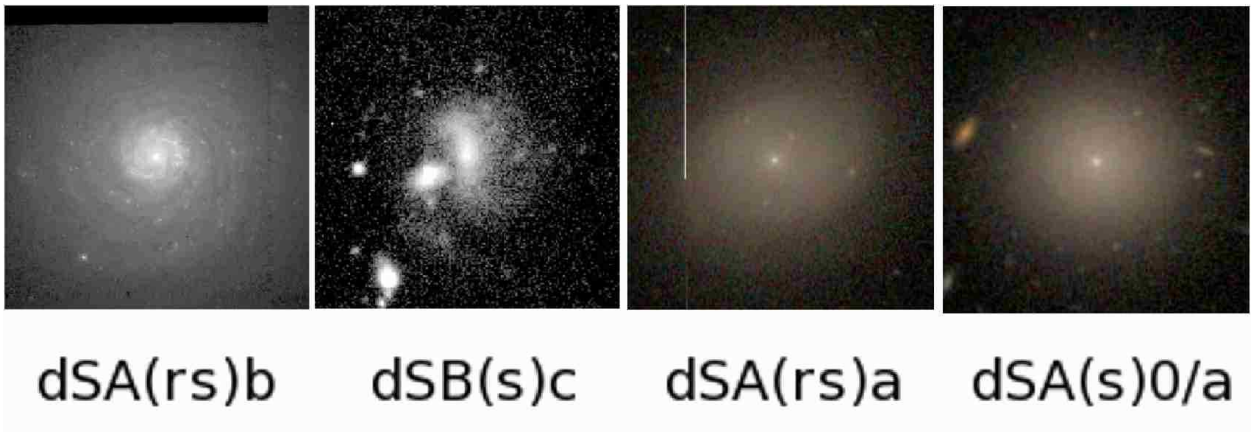

Fig. 51.— Four dwarf spiral galaxies (left to right): NGC 3928, D563−4, IC 783, and IC 3328

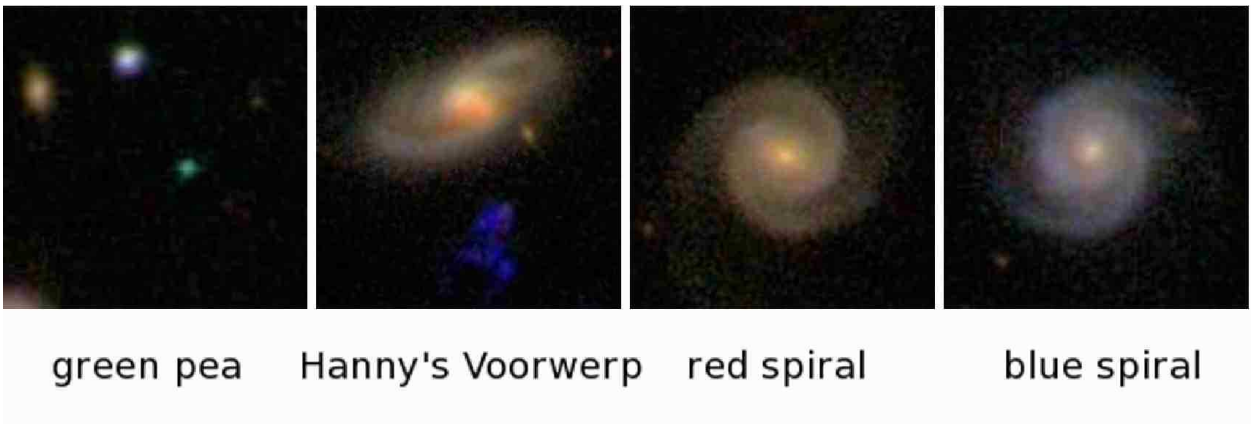

Fig. 52.— Interesting morphologies and color characteristics found by the Galaxy Zoo project team participants. A "green pea" is a star-like galaxy with a high flux in [OIII] 5007. "Hanny's Voorwerp" is a cloud of ionized gas that may be the light echo of a quasar outburst in the nucleus of nearby IC 2497. Red spirals are morphologically similar to blue spirals, but have a lower star formation rate. (All SDSS color images)

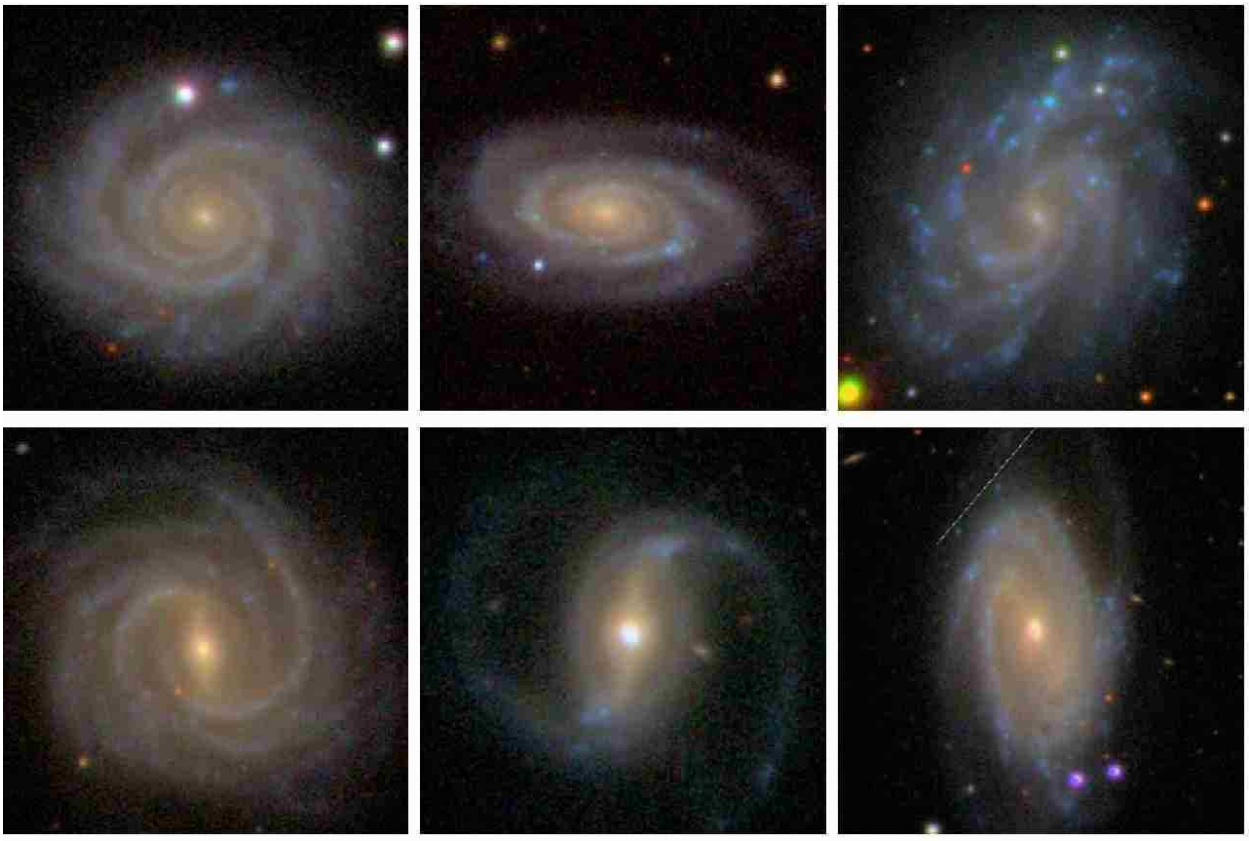

Fig. 53.— SDSS color images of six isolated Sb-Sc galaxies, both barred and nonbarred, from the AMIGA sample, a refined version of the Catalogue of Isolated Galaxies (Karachentseva 1973). The galaxies are (left to right): Row 1: NGC 2649, 5622, and 5584; Row 2: NGC 4662, 4719, and 2712.

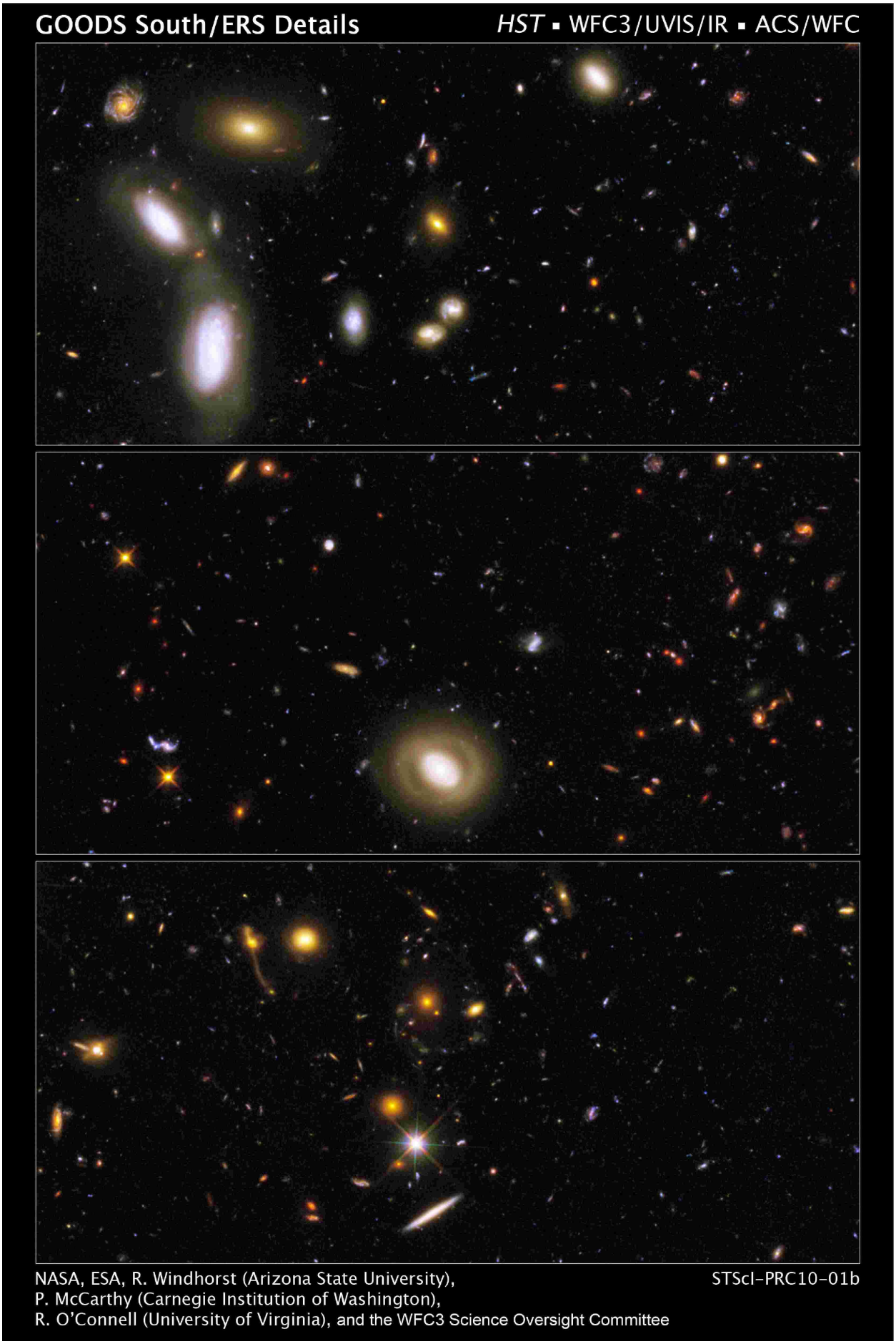
GOODS South/ERS Details
HST ▪ WFC3/UVIS/IR ▪ ACS/WFC
NASA, ESA, R. Windhorst (Arizona State University),
P. McCarthy (Carnegie Institution of Washington),
R. O'Connell (University of Virginia), and the WFC3 Science Oversight Committee
STScI-PRC10-01b

Fig. 54.—

Fig. 54. (cont.).— Three subsections from the WFC3-ERS survey of the GOODS-south field (Windhorst et al. 2010). The colors are based on images obtained with 10 filters ranging from 0.2μm to 2μm.